

University of Tasmania Open Access Repository

Cover sheet

Title

Mapping the progression of non-carious cervical lesions

Author

Grenness, MJ

Bibliographic citation

Grenness, MJ (2008). Mapping the progression of non-carious cervical lesions. University Of Tasmania. Thesis. <https://doi.org/10.25959/23210768.v1>

Is published in:

Copyright information

This version of work is made accessible in the repository with the permission of the copyright holder/s under the following,

Licence.

If you believe that this work infringes copyright, please email details to: oa.repository@utas.edu.au

Downloaded from University of Tasmania Open Access Repository

Please do not remove this coversheet as it contains citation and copyright information.

University of Tasmania Open Access Repository

Library and Cultural Collections

University of Tasmania

Private Bag 3

Hobart, TAS 7005 Australia

E oa.repository@utas.edu.au

CRICOS Provider Code 00586B | ABN 30 764 374 782

utas.edu.au

Mapping the Progression of Non-Carious Cervical Lesions

by

**Malcolm. J. Grenness
B.D.Sc., L.D.S., M.Med.Sc.,
F.R.A.C.D.S.**

**Spatial Information Sciences Group
School of Geography and Environmental Science
(University of Tasmania)**

Submitted in fulfilment of the requirements for the
Degree of Doctor of Philosophy

(June 2008)

Declaration

This thesis contains no material which has been accepted for the award of any other degree or diploma in any tertiary institution, and to the best of my knowledge and belief, contains no material previously published or written by another person, except where due reference is made in the text of the thesis.

Signed:

M.J. Grenness

Disclosure

The author Grenness is named on a patent associated with the use of materials with improved optical texture.

This Thesis may be made available for loan and limited copying in accordance with the *Copyright Act 1968*.

Statement of Co-Authorship

The following people contributed to the publication of the work undertaken as part of this thesis:

Grenness, M.J., Osborn, J.E. and Tyas, M.J., 2005. Stereo-Photogrammetric mapping of tooth replicas incorporating texture. Photogrammetric Record 20 (110), 147-161. (Chapter 5, excluding appendix)

	Candidate (Author 1) , %	Author 2 , %	Author 3 %
Conception	> 90	< 10	< 5
Experimental design	> 90	< 5	< 5
Experimental work	100		
Analysis	100		
Writing	> 95	< 5	< 5

Grenness M.J., Osborn J.E. and Tyas M.J., 2005. Digital very close range photogrammetry of a test object incorporating optical texture. 7th Optical 3D Measurement Techniques, Oct 3-5, Vienna, Austria. (Chapter 6, not refereed)

	Candidate (Author 1) , %	Author 2 , %	Author 3 %
Conception	> 90	< 10	< 5
Experimental design	> 90	< 5	< 5
Experimental work	100		
Analysis	100		
Writing	> 95	< 5	

The undersigned agree with the above stated “proportion of work undertaken” for each of the above published manuscripts contributing to this thesis.

Signed:

M. J. Grenness

School of Geography and Environmental Science
University of Tasmania

Abstract

'Non-carious cervical lesion' (NCCL) is a term used to describe loss of hard tissue in the cervical one-third of teeth. NCCLs are commonly encountered in dental practice and frequently require clinical intervention. There are few reports of high quality mapping and monitoring of NCCLs, and dental practitioners currently have no reliable method for measuring and monitoring their progress. Improved understanding of the underlying causes and progression of NCCLs will rely on reliable and practical methods of mapping their topography and monitoring their progress.

NCCLs on the facial surfaces of teeth can be easily imaged, either directly or on cast replicas, and therefore may be well suited to mapping using a photogrammetric approach. A preliminary investigation led to the development of a casting material that incorporated optical texture so that photogrammetric image-matching techniques could be utilized.

Three-dimensional coordinate data for tooth replicas was successfully generated using the casting material, convergent stereoscopic photography and commercial digital photogrammetric software. Imaging was performed initially using a semi-metric 35 mm film camera, then a high-resolution digital SLR camera, and finally a fixed-base digital SLR stereo camera. The quality of the surface data and the capacity to align tooth surfaces was investigated. Two specific examples of NCCLs were mapped and monitored at baseline, 12 month and 24 month time periods.

For the film camera and the single digital camera, the photogrammetric solutions were not highly stable, with systematic height errors of up to 80 μm attributed to unstable exterior orientation. However, for the fixed-base stereo camera, model precision was shown to be in the order of 13 μm and the accuracy of surfaces derived from automatic measurement was approximately 3 μm . The error associated with aligning independent measurements of tooth surfaces was approximately 17 μm . Change detection

of the two NCCL surfaces was sensitive to 30 μm , with change ranging from 30 to 320 μm per annum for one surface and 30 to 70 μm per annum for the second surface. Different rates of change were clearly evident in different areas of the same surfaces. The replication, stereoimagery, photogrammetric processing, and detection of changes to the surfaces were shown to be reliable and convenient.

The results of this investigation show that stereo-photogrammetric techniques can be applied to the mapping of NCCLs, and that the surfaces can be mapped at sufficient accuracy to enable change to be monitored. The two examples suggest that annual change detection studies will provide a clearer picture of the rate of progression and the geometry of progression and, in combination with other analytical techniques, a more detailed explanation of the natural history of non carious cervical lesions.

Acknowledgments

I wish to express my sincere gratitude to many persons whose generosity and helpfulness have contributed to this thesis.

I am extremely grateful to my supervisors, Dr. Jon Osborn and Professor Martin Tyas, for their invaluable guidance, advice, patience and understanding during the supervision of this thesis. Their deep knowledge and experience in their respective fields have been central to the arrival at an outcome far in excess of my initial expectations.

My thanks to the staff at the School of Geography and Environmental Studies, The University of Tasmania, for their kind support. I owe special thanks to Dr Tony Sprent for his assistance with the design and fabrication of components for the imaging equipment and to Dr. Christopher Watson and Assoc. Prof. Richard Coleman for assistance with MATLAB software programming. I thank Keith Bolton for preparation of photoplots.

I am indebted to John Farrow (School of Fine Art), Jeff Bester (Ash Bester Photographics), Fred Koolhof (Koolhof Enterprises), Alex Nazarov (Hobart Photographic Society) and the staff at Walch Optics (Hobart) for assistance and advice in photography, photographic accessories and lens design and application.

Thanks also go to Jason Birch and Yongru Huang of ADAM Technology P/L, Perth, Australia for technical support and modification of their software products, and to Dr. Harvey Mitchell from University of Newcastle for providing access to DS Match proprietary software.

Finally, I acknowledge my family, Susan, Alasdair and Emily, for their patience and forbearance of the many, many evenings and weekends where I disappeared to conduct the endless hours of modeling and analysis for this thesis.

Table of Contents

Chapter 1	Introduction.....	1
1.1	References.....	3
Chapter 2	Literature Review.....	6
2.1	Non-carious cervical lesions.....	6
	<i>Description, Terminology, Prevalence, Structure of teeth, Mechanisms of tooth surface loss, Experimental methods, Experimental models (Laboratory studies, In situ studies, Computer simulation, Clinical studies), Lesion initiation and progression, Monitoring the progression of non-carious cervical lesions, Discussion.</i>	
2.2	Mapping human teeth and objects of similar size.....	20
	<i>Profile / Silhouette tracing, Measuring Microscopy, Contact stylus, Photogrammetry, Structured light (Tooth surface opaquing), Laser scanning, Confocal Laser Microscopy, Computed Tomography and Magnetic Resonance Imaging, Discussion.</i>	
2.3	Replicating teeth.....	33
	<i>Impression materials, Casting materials, Dimensional accuracy (Linear measurement, Surface matching), Discussion.</i>	
2.4	Conclusion.....	40
2.5	References.....	41
Chapter 3	Aims and objectives	56
Chapter 4	Preliminary investigations into the provision of optical texture on tooth replicas.....	57
4.1	Trials with plaster replicas.....	58
4.2	Trials with epoxy resin.....	63
4.3	Camera systems.....	71
4.4	Conclusion.....	71

Table of Contents

Chapter 5	Stereo-photogrammetric mapping of tooth replicas incorporating texture.....	70
	Abstract	
5.1	Introduction.....	71
5.2	Method.....	73
	<i>Preparation of tooth replicas and photo control, Image acquisition and camera calibration, Image matching and generation of 3D coordinate data, Accuracy and precision testing.</i>	
5.3	Results.....	77
	<i>Camera calibration, Accuracy, Surface models.</i>	
5.4	Discussion.....	83
	<i>Tooth Replicas, Image acquisition and interior orientation, Exterior orientation and model accuracy, Image matching and precision, Surface models.</i>	
5.5	Conclusion.....	91
5.6	References.....	91
5.7	Appendix.....	96
	5.7.1 Film photographic setup.....	96
	5.7.2 Image matching techniques.....	97
Chapter 6	Digital very close range photogrammetry of a test object incorporating optical texture.....	100
	Abstract	
6.1	Introduction.....	101
6.2	Method.....	104
6.3	Results.....	107
6.4	Discussion.....	113
6.5	Conclusion.....	118
6.6	References.....	118

Chapter 7	Calibration of a fixed-base stereo camera for tooth replicas.....	121
7.1	Introduction.....	121
7.2	Method.....	123
	<i>Model generation and accuracy testing, Tooth surface modelling.</i>	
7.3	Results.....	127
	<i>Model accuracy, Model precision, Image and object space errors, Tooth surface modelling.</i>	
7.4	Discussion.....	133
	<i>Target measurement, Parameter set, Object space accuracy.</i>	
7.5	Conclusion.....	136
7.6	References.....	136
Chapter 8	Tooth surface alignment using two methods.....	139
8.1	Introduction.....	139
8.2	Method.....	145
	<i>Data acquisition and sampling, Data alignment, Mapping and alignment precision (DSMatch - Sequential alignment, Varying grid interval and exclusion threshold, Varying exclusion threshold; Polyworks - Sequential alignment, Varying grid interval and exclusion threshold, Varying exclusion threshold upon quality of alignment), Alignment precision (DSMatch, Polyworks).</i>	
8.3	Results.....	151
	<i>Data acquisition and sampling, Mapping and alignment precision (DSMatch – sequential alignment, alignment of unsampled data, varying grid interval and exclusion threshold, varying exclusion threshold; Polyworks – sequential alignment, varying grid interval and exclusion threshold, varying exclusion threshold), Alignment precision (DSMatch, Polyworks).</i>	

Table of Contents

8.4	Discussion.....	167
	<i>Data Acquisition, Data sampling, Data alignment, Mapping and alignment precision, Varying grid interval, Varying exclusion threshold, Alignment precision.</i>	
8.5	Conclusion.....	173
8.6	References.....	173
 Chapter 9 Change detection of non-carious cervical lesions from stereoimagery.....		
		177
9.1	Introduction.....	177
	Surface alignment and change detection	
9.2	Method.....	180
	<i>Replica preparation, Data acquisition, Accuracy and precision of the 3D data acquisition, Precision of 3D data acquisition and alignment, Change detection of NCCLs.</i>	
9.3	Results.....	184
	<i>Accuracy and precision of the 3D data acquisition, Precision of 3D data acquisition and alignment, Precision of replication, 3D data acquisition and alignment, Change detection of NCCLs (Tooth 1, Tooth 2).</i>	
9.4	Discussion.....	193
	<i>Precision of replication, 3D data acquisition and alignment, Change detection of NCCLs.</i>	
9.5	Conclusion.....	197
9.6	References.....	197
 Chapter 10 Conclusion.....		
		199

Chapter 1

Introduction

A variety of physical effects is visible on teeth with the passage of time. In addition to dental caries, hairline cracks, tooth fracture and therapeutic interventions, loss of surface material results from attrition, abrasion and dental erosion (Harris and Gorgas, 1899). The non-carious cervical lesion (NCCL) is a generic term used to describe loss of hard tissue in the cervical one-third of teeth. In a review of cervical lesions, Levitch et al. (1994) concluded that the initiation and progression of these lesions was likely to be multifactorial, hence the generic term, and criteria were suggested to help distinguish between lesions of different aetiology based on the location, shape, the margins and the enamel surface. NCCLs have a wide variety of size, shape, symmetry and location and are commonly encountered in clinical practice, with prevalence ranging from 5 to 85% (Levitch et al., 1994). Such a wide prevalence range suggests that there are deficiencies in the classification and recording of lesions. Lesions may occupy anywhere from a few percent of the surface of a tooth up to complete loss of the surface of a tooth. A clinical case illustrating a wide range of NCCLs appears in Figure 2.1 (pp.7).

Recent studies have focused on a snapshot characterisation of lesions such as height, depth, location, patient age and gender information (Aw et al., 2002). Findings have demonstrated strong correlations with age, dietary acids and toothbrushing (Lussi and Schaffner, 2000), and the presence of lesions in association with occlusal attrition and erosion (Khan et al., 1999). Work is presently being carried out in many centres to further understand the biomechanical factors which are presumed to cause NCCLs. Tooth flexion has been demonstrated (Grippio and Masi, 1991) and strain patterns in cervical enamel of teeth subjected to occlusal loading have been reported

(Palamara et al., 2000). Enamel dissolution has been shown to significantly increase in sites subject to cyclic tensile stress (Palamara et al., 2001). One view is that NCCLs are predominantly caused by acid dissolution with stress distribution within teeth acting as a modifying or amplifying factor (Khan et al., 1999).

However there are few studies that investigate the progression of the destructive process over time. The only recent study followed one case, at four time intervals, over a 14-year period (Pintado et al., 2000). Other studies have monitored erosion on palatal surfaces of teeth (Bartlett et al., 1997) and occlusal wear in young adults (Pintado et al., 1997). In a review of techniques for the measurement of tooth wear and erosion, Azzopardi et al. (2000) concluded that the current methods of quantifying tooth substance loss involving impressions, pouring of models, mechanical or laser digitization and analysis were slow and cumbersome and confined to the laboratory. As a result most investigations have small numbers of subjects, analysis is limited, and there is scarce information about the geometry of progression and rate of progression of NCCLs.

The review by Azzopardi et al. (2000) did not include a consideration of photogrammetric techniques. There have been no relevant research reports in the dental literature for over 15 years and the last review of photogrammetry as a dental research tool was conducted by Chadwick (1992). Photogrammetric techniques have been applied to a variety of biomedical measurement problems, with teeth and dental subjects being a common research application (Chadwick et al., 1991; Clarke et al., 1974; Gruner et al., 1967; Lamb et al., 1987; Mitchell et al., 1989). Precision of 10 μm has been reported (Mitchell et al., 1989). Work conducted at the University of Tasmania has shown the feasibility of mapping the human cornea, which is in the same size range as human teeth (Osborn and Wise, 1996). More recently the use of commercial digital photogrammetric software has been reported for the measurement of small objects photographed through an

optical microscope (Mitchell et al., 1999), although this latter approach was not successful when applied to a human tooth replica due to a lack of targets or optical texture on the surface of the tooth replicas.

There appears, therefore, potential to utilize modern digital photogrammetry to map tooth surfaces and monitor the progression of NCCLs, provided a suitable optical texture is present on the imaged tooth surface. The application of varnishes and curable resins is an everyday occurrence in clinical dental practice, however the inclusion of optical texture into a varnish or curable resin in a clinical environment is an untried concept. The addition of a varnish to the surface of a tooth will change the surface geometry of the tooth with an uncertain impact on the accuracy and precision of surface measurements and may also interfere with the surface being monitored. The application of optical texture onto or into a dental casting material has not been reported and may offer an alternative path to development of a practical technique. Appropriate stereo imaging equipment for macrophotography is not available as an off-the-shelf item, so there is also a need to develop and prototype appropriate imaging equipment and to investigate capacity of a photogrammetric system to meet clinical accuracy requirements.

The studies reported in the following thesis are, therefore, intended to develop a photogrammetric approach to generate surface models of tooth replicas incorporating optical texture of sufficient precision to enable monitoring of the progression of NCCLs.

1.1 References

- Aw, T., Lepe, X., Johnson, G. and Mancl, L., 2002. Characteristics of non-carious cervical lesions. *Journal of the American Dental Association*, 133: 725-733.
- Azzopardi, A., Bartlett, D., Watson, T. and Smith, B., 2000. A Literature Review of the Techniques to Measure Tooth Wear and Erosion.

- European Journal of Prosthodontics and Restorative Dentistry, 8 (3): 93-97.
- Bartlett, D., Blunt, L. and Smith, B., 1997. Measurement of tooth wear in patients with palatal erosion. *British Dental Journal*, 182 (5): 179-184.
- Bell, E.J., Kaidonis, J., Townsend, G.C. and Richards, L.C., 1998. Comparison of exposed dentinal surfaces resulting from abrasion and erosion. *Australian Dental Journal*, 43 (5): 362-366.
- Chadwick, R., 1992. Close range photogrammetry--a clinical dental research tool. *Journal of Dentistry*, 20 (4): 235-239.
- Chadwick, R., McCabe, J., Walls, A., Mitchell, H. and Storer, R., 1991. Comparison of a novel photogrammetric technique and modified USPHS criteria to monitor the wear of restorations. *Journal of Dentistry*, 19 (1): 39-45.
- Clarke, C., Flinn, R., Atkinson, K. and Wickens, E., 1974. The measurement and comparison of tooth shape using photogrammetry. *Photogrammetric Record*, 8 (44): 217-221.
- Grippio, J. and Masi, J., 1991. Role of biodental engineering factors (BEF) in the etiology of root caries. *Journal of Esthetic Dentistry*, 3 (2): 71-76.
- Gruner, H., Zulqar-Nain, J. and Zander, H., 1967. A short-range system for dental surgery. *Photogrammetric Engineering*, 33 (11): 1240-1245.
- Harris, C. and Gorgas, F., 1899. A dictionary of dental science. 6th Edition. P. Blakiston's & Son, Philadelphia.
- Khan, F., Young, W., Shahabi, S. and Daley, T., 1999. Dental cervical lesions associated with occlusal erosion and attrition. *Australian Dental Journal*, 44 (3): 176-186.
- Lamb, R., McGarrah, H. and Eick, J., 1987. Close-range photogrammetry with computer interface in dental research. *Photogrammetric Engineering and Remote Sensing*, 53 (12): 1685-1689.
- Levitch, L., Bader, J., Shugars, D. and Heymann, H., 1994. Non-carious cervical lesions. *Journal of Dentistry*, 22 (4): 195-207.

- Lussi, A. and Schaffner, M., 2000. Progression of and risk factors for dental erosion and wedge-shaped defects over a 6-year period. *Caries Research*, 34 (2): 182-187.
- Mitchell, H., Chadwick, R. and McCabe, J., 1989. Stereo microscope photogrammetry for the measurement of small objects. *Photogrammetric Record*, 13 (74): 289-299.
- Mitchell, H., Kniest, H. and Oh, W.-J., 1999. Digital photogrammetry and microscope photographs. *Photogrammetric Record*, 16 (94): 695-704.
- Osborn, J. and Wise, G., 1996. Stereophotogrammetric mapping of the anterior surface of the human cornea. *International Archives of Photogrammetry and Remote Sensing*, 31 (B5): 443-449.
- Palamara, D., Palamara, J., Tyas, M. and Messer, H., 2000. Strain patterns in cervical enamel of teeth subjected to occlusal loading. *Dental Materials*, 16 (6): 412-419.
- Palamara, D., Palamara, J., Tyas, M., Pintado, M. and Messer, H., 2001. Effects of stress on acid dissolution of enamel. *Dental Materials*, 17 (2): 109-115.
- Pintado, M., Anderson, G., DeLong, R. and Douglas, W., 1997. Variation in tooth wear in young adults over a two-year period. *Journal of Prosthetic Dentistry*, 77 (3): 313-320.
- Pintado, M., DeLong, R., Ko, C.-C., Sakaguchi, R. and Douglas, W., 2000. Correlation of non-carious cervical lesion size and occlusal wear in a single adult over a 14 year time span. *Journal of Prosthetic Dentistry*, 84 (4): 436 - 443.

Chapter 2

Literature Review

The objective of this chapter is to review:

- i) the description, aetiology and progression of NCCLs,
- ii) the mapping of human teeth and small objects of similar size, and
- iii) the replication of teeth.

A condensed review of methods of mapping teeth appears in the introduction to Chapter 5. Concise reviews of very close range photogrammetric applications, photogrammetric calibration methods, tooth surface data alignment, and tooth surface change detection appear in the introductions to Chapters 6, 7, 8 and 9.

2.1 Non-carious Cervical Lesions

2.1.1 Description

'Non-carious cervical lesion' (NCCL) is a generic term used to describe loss of hard tissue at the cemento-enamel junction (CEJ) in the cervical one-third of teeth. NCCLs have been defined as any non-carious loss of hard tissue at the cervix of the tooth, identified visually or tactilely. For smaller lesions, the classification challenge is differentiation of a detected change in contour due to disease, from change in contour due to normal cemento-enamel junction morphology. In these instances, differentiation is based on comparison with the morphology of the same area on adjacent and contralateral teeth (Bader et al., 1996). NCCLs have a wide variety of size, shape, symmetry and location. They occur predominantly on the buccal surfaces of teeth, but may also occur on the lingual and/or approximal surfaces (Levitch et al., 1994). NCCLs on the buccal surfaces of teeth can be imaged directly. Premolars

from both arches are the commonly affected teeth (Borcic et al., 2004; Xhonga and Valdmanis, 1983). It has been proposed that the shape of lesions may be related to aetiology (Levitch et al., 1994; Sognnaes et al., 1972), however this has not been confirmed experimentally or clinically (Bartlett and Shah, 2006).

The initial stage of the lesion may be characterized by a wave-like or corrugated pattern in the disruption of the cervical surface enamel. Lesions may contain two separate individual wedge shape defects (Braem et al., 1992). Figure 2.1 shows the lower left quadrant of a female patient, aged 81 years, with NCCLs of varying sizes affecting all teeth (black arrows); attrition and erosion is also apparent affecting the occlusal/incisal surfaces of all teeth.

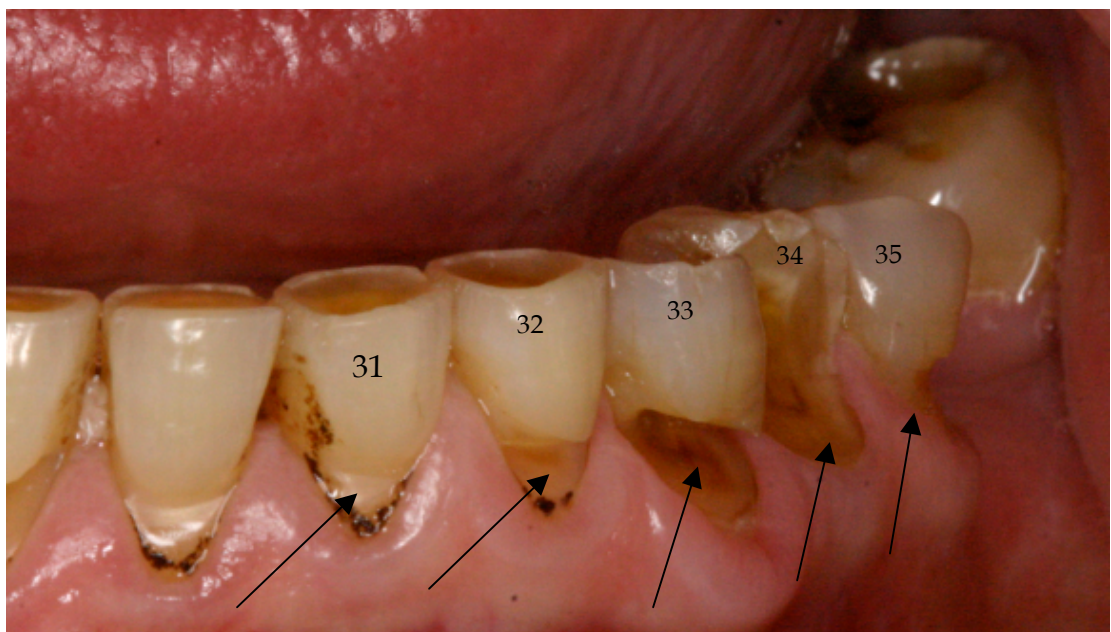


Figure 2.1. Lower left quadrant of a female patient aged 81 years with NCCLs affecting all teeth (black arrows); 33 lesion extending into pulp chamber now filled with reparative dentine; 34 shows bulk loss of buccal enamel and dentine. Erosion affecting occlusal/incisal surfaces with dentine 'cupping' affecting all teeth.

2.1.2 Terminology

The term NCCL arose in the early 1990s with recognition that the origin of these lesions is multifactorial and that the existing terms used to describe them were based on individual aetiological factors (Bader et al., 1993; Levitch et al., 1994). The aetiological factors are reported as dental erosion (the non-bacterial chemical dissolution of tooth structure) and abrasion (pathological wear as a result of abnormal processes, habits, or use of abrasive substances). A third type of surface loss, the stress-induced cervical lesion (also known as abfraction), has been attributed to stress originating at the occlusal surface and results in micro-cracking and subsequent loss of tooth material in the cervical region (Lee and Eakle, 1984). Grippo and Masi (1991) considered the factors operating at the tooth surface and extended the concept of erosion by classifying acid dissolution of tooth substance in the presence of static loads as 'stress corrosion', and dissolution in the presence of cyclic tensile loads as 'fatigue corrosion'. Dental erosion was originally described as 'an affectation of the teeth characterised by a loss of substance occurring without an apparent cause' (Harris and Gorgas, 1899). By the 1950s, the cause of erosion was well known as a chemical process without action of bacteria (Thoma and Robinson, 1955). Thus erosion was differentiated from dental caries, which is now described as a bacterial infection moderated by diet.

2.1.3 Prevalence

These lesions are commonly encountered in clinical practice, with prevalence ranging from 5 to 85% (Levitch et al., 1994). A lack of clear diagnostic criteria makes comparison of prevalence data difficult and may account for the wide range of rates reported. More recent prevalence studies have examined cervical lesions alone and found that enamel loss is common and that dentine loss ranges from 2 to 6% (Bartlett et al., 1998; Smith and Robb, 1996). However, in a sample of 1002 patients with 18,555 teeth, the prevalence and severity increased with age from 4 % up to 26 years of age, to 33.3 % over 65 years of age; the number of restorations and other anomalies in the cervical

region also increased with age (Borcic et al., 2004). Clearly, the maximum number of teeth in this sample could have been over 30,000, therefore a large number of teeth was missing or lost during the patient life, affecting the prevalence data in this study (Table 2.1).

Age range	% teeth with lesions	% teeth restored
Up to 26 years	4.0	1
26 – 35 years	11.2	13.8
36 – 45 years	18.7	11
46 – 55 years	25.6	12.7
56 – 65 years	25.6	9.1
Over 65 years	33.3	14.6

Table 2.1. Distribution of total number of lesions as a percentage of the total number of teeth (18,555 teeth), in the six age groups (Borcic et al., 2004).

Several clinical studies have been conducted to record the presence of NCCLs in association with other dental conditions such as occlusal wear facets (Pegoraro et al., 2005), occlusal erosion and attrition (Khan et al., 1999), occlusal parameters such as jaw relationship, occlusal guidance, wear facets and mobility (Aw et al., 2002), dietary factors and toothbrushing (Lussi and Schaffner, 2000) and the thickness of salivary pellicle (film) on various tooth surfaces (Amaechi et al., 1999c).

2.1.4 Structure of teeth

The major part of a tooth surface is covered with enamel, which is composed of about 96% mineral in the form of calcium hydroxyapatite crystals arranged as rods or prisms. Crystal diameters in sound enamel are typically 50-100 nm (Frazier, 1968). At the edges of enamel prisms, crystal diameters can grow to 120-150 nm, presumed to be as a result of remineralisation and crystal growth. Water is present in enamel as a hydration shell surrounding the crystallites (Gwinnett, 1992), enabling permeation of water and ions and ionic exchange, either demineralisation or remineralisation. The pathways of

fluid penetration are through defects and around the borders of enamel rods (Charbeneau et al., 1981). Reduced mineral content leads to reduced hardness and increased susceptibility to abrasion. Reduced mineral content also leads to greater fluid content available for ionic exchange. Saliva present in the mouth has a physiological pH of 7.4 and is supersaturated with calcium and phosphate ions, which are the main natural source of ions able to remineralise dental hard tissues, provided a residual crystalline framework is present. The solubility product (the pH above or below which remineralisation or demineralisation respectively occur) for hydroxyapatite is 5.5; the solubility product for fluor-hydroxyapatite (where fluoride ions have replaced some of the hydroxide ions in the crystalline structure) is 4.5. At eruption, the enamel may be up to 2.3 mm thick over the cusps of human teeth, reducing to 1 to 1.3 mm thick over the facial and lingual surface (Boyde, 1989).

The white colour of human enamel in recently erupted teeth is only relative and depends on its light-scattering properties, which reduces translucency. Translucency increases with age as the mineral content of the enamel increases (known as maturation). At the macroscopic level, teeth may exhibit imbrication lines (known as perikymata) on the smooth surfaces, becoming more common towards the cervical region. Some perikymata may be deep enough to form grooves and pits. The cervical margin of the enamel is generally a smoothly curved line with only minor excrescences. Close examination through the enamel surface reveals bands at approximately 100 μm intervals known as Hunter-Schreger bands. Other features which may appear at the surface of mature teeth are fissures, brochs, surface overlapping projections and isolated deep pits. At the light microscopic level, the fundamental visible unit, the enamel prism, is of the order of 6 to 7 μm . Much of the contrast originating from ordinary illumination of transmitted light is dependent upon reflection, or scattering, of light at interfaces of prism boundaries. Under dark field illuminating conditions, all features seen are essentially self luminous but lie within the entire thickness range of the

enamel (Boyde, 1989). During clinical adhesive restorative procedures enamel is etched by the application of acid. Acid etching removes mineral predominantly from prism boundaries to a depth of approximately 5 to 25 μm (Gwinnett, 1971). The etching of enamel renders the surface dull as the surface becomes less translucent and reflective to light (Boyde, 1989).

Where enamel is not present in the cervical part of the tooth, exposed dentine, a less heavily mineralised tissue, is more susceptible to an increased rate of surface loss. Dentine consists of 20% w/w organic matter, 10% w/w water and 70% w/w inorganic material. The organic substrate mainly consists of collagen fibrils (35 – 120 nm diameter), arranged in a random network, and a ground substrate of mucopolysaccharides. The inorganic component consists of hydroxyapatite crystals, which are plate shaped and much smaller than the hydroxyapatite crystals in enamel (36 nm mean length and 10 nm mean thickness), and are deposited on the collagen fibres (Frank and Nalbandian, 1989). Fluid filled dentinal tubules traverse the dentine from the pulp to the dentino-enamel junction (DEJ), with a diameter from 1 to 5 μm and a density of tubules varying from 15,000 to 65,000 tubules/ mm^2 (Garberoglio and Brännström, 1976). The dentine immediately around the tubules, known as peritubular dentine, is more highly mineralised than the intertubular dentine. Whereas dentine may be demineralised due to exposure to acids, the collagen component may be degraded by exposure to acids and lost due to abrasion. The organic content of dentine also allows elastic flexion, while the overlying enamel provides some resistance to this flexion (Frank and Nalbandian, 1989).

Dentine is typically opaque and featureless at the macroscopic level. Microscopically several features are described. Mantle dentine is the first layer of dentine formed adjacent to the dentine-enamel junction and has larger collagen fibrils of 100 to 200 nm diameter (Avery, 1992). Mantle dentine is approximately 150 μm thick and would be the first type of dentine exposed in the cervical region. Below this, areas of globular dentine (also

known as interglobular dentine) are present. Globular dentine is less heavily mineralised. There are age related changes in dentine such as reparative dentine, dead tracts and sclerotic dentine (Bhaskar, 1990). Sclerotic dentine is translucent and results from obliteration of the tubules by calcified material which has a similar refractive index to that of the rest of the dentine. Dentine sclerosis commences at the root tip and extends teeth linearly with age towards the crown tip (Frank and Nalbandian, 1989).

Where enamel and dentine meet, at the dentino-enamel junction (DEJ), consolidation of collagen in the dentine gives rise to micro-scallops between neighboring coarse collagen fibrils, which has the effect of increasing the effective surface area between the two main contiguous tissues (Lin et al. 1993). There is less scalloping in the cervical region of teeth and the enamel rods are irregular and lack definition around the cemento-enamel junction (CEJ) (Fernandes and Chevitarese, 1991). Therefore the DEJ in the cervical region of teeth is not as strong as in other areas, such as the occlusal surface, and may be at increased risk of bulk loss of enamel.

2.1.5 Mechanisms of tooth surface loss

Many elements come together to form the micro environment at the tooth surface. These include:

- i) the tooth ultrastructure (observed by electron microscopy),
- ii) the presence of internal stresses associated with functional (mastication, swallowing and speech) and parafunctional (bruxism and clenching) tooth contacts,
- iii) the gingival tissues from which the tooth emerges and the crevicular fluid which emanates from the gingival crevice,
- iv) the mucosal surfaces of the cheeks, lips and tongue which come into contact with teeth and influence and control the movement of material within the oral cavity,

- v) the saliva which arises from several sources around the mouth and the salivary pellicle (film) that accumulates on a tooth surface shortly after cleaning,
- vi) the oral microflora which populates the saliva, the salivary pellicle to form dental plaque, and mucosal surfaces,
- vii) ingested foods and fluids and their breakdown products,
- viii) gastric juices which may reflux into the oral cavity,
- ix) factors associated with human habits and behaviours such as toothbrushing and nail biting, and
- x) environmental exposures to noxious agents that find their way into the oral cavity.

The weakening effect of cavity preparation, via the mechanism of increased tooth flexion, may also contribute to the development of NCCLs (Rees, 1998). Stress distribution and concentration, as a result of occlusal function, throughout a tooth has the potential to affect the ultra structure of the tooth.

However it has been noted that occlusal functional relationships change over time and the presence of wear facets might only provide historical information of uncertain currency (Bader et al., 1996). Chemical dissolution (erosion) of the mineral content of enamel and dentine occurs as a result of the presence of intrinsic and extrinsic acids which exceed the immediate buffering, diluting and clearing effects of saliva, and proteolytic degradation of the organic component of dentine. Mechanical breakdown of enamel and dentine occur as a result of fracture, scratching and/or rubbing with abrasive agents (abrasion). Surface loss due to erosion and abrasion is permanent as there are no physiologic mechanisms to 'regrow' lost tooth surface.

Subsurface loss of mineral due to erosion is reversible provided sufficient matrix remains for remineralisation. These mechanisms may act separately or together, influenced by the micro-environment at the tooth surface. The concept that wear associated with abrasion was accelerated with acid softening of tooth surfaces arose around 1980 (Davis and Winter, 1980).

2.1.6 Experimental methods

A number of methods is currently used for the study of NCCLs. These include:

- i) qualitative characterization of shape and distribution of lesions within the dentition (e.g. Aw et al., 2002; Bader et al., 1996; Borcic et al., 2004),
- ii) ultrastructural characterization of tooth surfaces using scanning electron microscopy to identify the presence of demineralization and hard tissue defects such as enamel cracking and collagen degradation in dentine (e.g. Bell et al., 1998; Khan et al., 1998),
- iii) microradiography of sections of enamel and dentine to determine volume loss and partial mineral loss (Amaechi et al., 2003; Amaechi et al., 1999c),
- iv) confocal microscope measurement of curable film and salivary pellicle thickness (Azzopardi et al., 2004),
- v) profilometry measurement of curable film and surface loss in the laboratory and *in situ* (Attin et al., 2004; Azzopardi et al., 2004; Hooper et al., 2003; Vanuspong et al., 2002),
- vi) finite element analysis (FEA) modelling (computer simulation) to study patterns of stress distribution within teeth (Borcic et al., 2005; Palamara et al., 2000; Palamara et al., 2006),
- vii) cyclic occlusal loading of teeth in association with acid exposure (Palamara et al., 2001), and cyclic loading of teeth in association with toothbrushing (Litonjua et al., 2004),
- viii) identifying the presence of lesions in association with other occlusal factors on the same tooth such as wear facets, occlusal attrition and erosion (Khan et al., 1999; Pegoraro et al., 2005; Piotrowski et al., 2001),
- ix) identifying the presence of extrinsic and intrinsic acid exposure and saliva quality, quantity and distribution (Amaechi et al., 1999b), and
- x) identifying the presence of patient behavioral factors such as diet, other occupational exposures and toothbrushing habits (Lussi et al., 1991).

2.1.7 Experimental models

Three experimental models are available to recreate intra-oral (clinical) conditions. These are laboratory, *in situ*, and computer simulation.

2.1.7.1 Laboratory studies

Numerous laboratory studies have been conducted to establish the causal links between the aetiological factors and the development of lesions. There was a large number of studies in the 1960s and 1970s examining effects associated with tooth brushing, such as force of brushing, orientation of brushing, prolonged contact time, bristle hardness and toothpaste abrasiveness. These have been recently reviewed, with the conclusion that there is little evidence to suggest that cervical wear lesions are solely caused by tooth brush abrasion (Bartlett and Shah, 2006).

Numerous laboratory studies have reproduced erosion of tooth enamel using acidic beverages and other solutions (Amaechi et al., 1999a; Bartlett and Coward, 2001; Kaidonis et al., 2003; Phelan and Rees, 2003; White et al., 2001). Salivary pellicle has been shown to provide some protection from acid exposure (Nekrashevych and Stosser, 2003), and the protective capacity of a curable film to tooth surfaces has been demonstrated (Azzopardi et al., 2001).

A smaller number of laboratory investigations of erosion of dentine has been conducted. These have shown that dentine is susceptible to erosion at higher pH (> 6) than enamel and has little propensity to remineralise (Vanuspong et al., 2002). For studies involving artificial saliva and salivary pellicle, differences in results have been noted between laboratory and clinical studies (Hannig et al., 2005).

Laboratory studies have demonstrated tooth flexion and increased erosion under static loading (stress corrosion) (Grippio and Masi, 1991). Strain patterns in cervical enamel of natural teeth, when subjected to occlusal loading, have been measured. The magnitude, direction and character of strains are highly dependent on patterns of loading (Palamara et al., 2000;

Palamara et al., 2006). Cyclic occlusal loading of teeth has been found to increase acid dissolution in the gingival third of teeth (fatigue corrosion), with a complex pattern of dissolution in teeth subject to load (Palamara et al., 2001). However occlusal stress did not increase the rate of toothbrush abrasion (Litonjua et al., 2004).

2.1.7.2 *In situ* studies

In recent *in situ* investigations, small pieces of enamel or dentine have been fixed to natural tooth surfaces to investigate site specificity of saliva pellicle thickness (Amaechi et al., 1999c), or fixed to removable appliances to investigate tooth surface loss as a result of toothpaste abrasivity (Hannig and Balz, 2001; Hooper et al., 2003), the protective effect of curable films (Azzopardi et al., 2004), and tooth surface loss as result of abrasion from the tongue and cheeks (Amaechi et al., 1999c). Erosion increased the susceptibility of enamel to toothbrush abrasion (Hooper et al., 2003). An *in situ* experimental model for the investigation of occlusal parameters, related to stresses within teeth and their association with progression of NCCLs, has yet to be devised.

Dentine is considerably more susceptible than enamel to erosion and abrasion alone or combined (Hooper et al., 2003). A 30-minute period of remineralisation of dentine intra-orally, following an acid challenge and prior to toothbrushing resulted in no significant wear compared to unbrushed controls (Attin et al., 2004).

2.1.7.3 Computer simulation

Computer simulation using finite element analysis (FEA) modelling has been used to study patterns of stress distribution within teeth presumed to have an association with NCCLs (Boric et al., 2005; Palamara et al., 2000; Palamara et al., 2006). FEA has also been used to model stress distribution within jaws (Vollmer et al., 2000), and as a result of loading teeth (Korionth

and Hannan, 1994) and loading endosseous dental implants (Benzing et al., 1995).

2.1.7.4 Clinical studies

There are no true clinical studies that study the effect of variables on the initiation and progression of cervical lesions. At the present time, the closest examples are those that have monitored NCCLs clinically by taking impressions and/or pouring casts, and a small number of similar studies has been applied to palatal erosion. These are reviewed below.

2.1.8 Lesion initiation and progression

There may be more than one type of lesion, each possibly associated with a different aetiology. Further, factors associated with the initiation of lesions may be different from factors associated with their progression (Bader et al., 1996).

As noted above, tooth surface loss may simply be a consequence of acid erosion and mechanical abrasion, with different rates of loss in enamel and dentine. However, in a review of the biomechanics of abfraction, Rees (2000) noted that one theory suggests that tooth loss is initiated in the cervical enamel as a result of micro-cracking associated with concentration of stresses originating at the occlusal surface; another theory is that erosion preferentially removes cervical dentine, undermining the enamel, leaving it unsupported and more prone to failure.

In prevalence studies, the significant factors for the progression of wedge-shaped defects were identified to be frequency of tooth brushing and age, explaining 21% of the variability of the progression of wedge-shaped defects (Lussi and Schaffner, 2000). In a study to correlate the presence of NCCLs with occlusal erosion and occlusal attrition, Khan et al. (1999) found that occlusal erosion was the more significant factor suggesting that acid erosion was the more significant causative factor in the development of NCCLs and

that occlusal strains may be have an amplifying effect on their progression. Mayhew et al. (1998) concluded that the multifactorial concept continued to be the most useful model and that, ultimately, longitudinal clinical trials will be necessary to determine the effectiveness and desirability of treatment interventions, such as alteration of occlusion or restoration of lesions.

2.1.9 Monitoring the progression of non-carious cervical lesions

There are few quantitative studies on the progression of NCCLs. Xhonga et al. (1972) selected 14 patients with 113 cervical 'erosion-like' lesions and monitored them for 5 months (measurement method below). The average progress of lesions was 1 μm per day, 31 μm per month and (155 ± 19) μm over 5 months. Some individuals showed a wide range of progression, from undetectable progress to a maximum of 150 μm a month for the same person. Pintado et al. (2000) measured NCCL size and occlusal wear in one patient over a 14-year period and found that there was a direct correlation between occlusal wear and enlargement of NCCLs. They measured volume loss and mean depth of three lesions in the lower first and second premolars and the lower first molar. From the data given, it can be calculated that mean annual increase in depth was in the order of 30 $\mu\text{m}/\text{y}$ for the premolar lesions and was in the order of 55 $\mu\text{m}/\text{y}$ for the molar lesion.

Qualitative studies utilizing a tooth wear index (Smith and Knight, 1984) have been devised and used to measure occlusal wear and NCCLs at the individual and community levels (Table 2.2). This index has been used intra-orally (Poynter and Wright, 1990), and on study casts (Bartlett, 2003). Bartlett (2003) concluded that tooth wear indices remain the only reliable method of assessing wear over long periods, but the Smith and Knight (1984) index did not discriminate wear particularly well once dentine was exposed. In a more recent report, the use of study casts remained the most convenient method to assess progression of lesions, however compliance of patients and dentists in taking and keeping casts was poor (Bartlett et al., 2005).

TWI Score	Criterion
0	No change in contour
1	Minimal loss of contour
2	Defect <1 mm deep
3	Defect 1-2 mm deep
4	Defect >2 mm, or pulp exposure or exposure of secondary dentine

Table 2.2 Tooth wear index (TWI) for cervical lesions
(Smith and Knight, 1984).

In studies of erosion on other surfaces Bartlett et al., (1997) measured the amount of erosion on the palatal surfaces of central incisor teeth and reported mean wear of 36.5 μm in the 6 months of the study period (measurement method below) and Chadwick et al. (2005) reported measurement of palatal erosion of central incisor teeth and use an index modified from Ryge and Snyder (1973). In this latter study, quantitative surface loss was reported as a percentage of the surface area of the tooth that had undergone change. Pintado et al. (1997) investigated occlusal tooth wear in a group of young adults and measured a steady wear rate of 0.04 mm^3 per year by volume and 10.7 μm per year by depth, averaged over all teeth, over two consecutive years.

2.1.10 Discussion

NCCLs have a multifactorial aetiology. There are very few clinical studies characterising and monitoring lesions, their risk to patients, and the effectiveness of treatments. There is a lack of quantitative studies that elucidate the natural history of NCCLs. NCCLs on the facial surfaces of teeth can be easily imaged directly or on study casts.

2.2 Mapping human teeth and objects of similar size

The review of mapping methods in chapter 4 is largely limited to teeth. In the life sciences there is a variety of measurement applications that require accurate mapping of biological surfaces. This section focuses upon measurement and modelling of teeth and objects of a similar size, the resolution and accuracy of applicable measurement systems, and some of the design parameters.

Quantitative measurement systems have traditionally been classified according to the principle by which data are collected, such as contact or non-contact, surface topography or silhouette tracing. The methods reviewed below are:

- i) profile/silhouette tracing,
- ii) measuring microscopy,
- iii) contact stylus,
- iv) photogrammetry
- v) structured light,
- vi) laser scanning,
- vii) confocal microscopy, and
- viii) computed tomography and magnetic resonance imaging.

2.2.1 Profile / Silhouette tracing

Profile tracing methods have been applied to a wide variety of dental research topics. These include the 3D reconstruction of tooth replicas (Han et al., 1998), root canal morphology (Gale et al., 1994), and the tracing of magnetic resonance images of the temporo-mandibular joint (Chu et al., 1995). The object or replica is sectioned at regular intervals, typically 1 mm, then hand traced, photographed or video recorded. In the case of video recording the outline may be enhanced to aid the sampling process. The profile is then sampled for 2D coordinates. Serial profiles can be stacked to build 3D volumetric models. High accuracy is generally not achieved due to

the thickness of the sections. This method may require destruction of the object or replica being measured.

The progression of NCCLs has been monitored using this method by obtaining profile tracings of silicone (Dow Corning, Alhambra, CA) replicas of teeth (Xhonga et al., 1972). Subsequent replicas were orientated manually to the initial replica, and three slices, 1 mm thick, were cut through the lesions, parallel to the long axis of the tooth. Profile tracings and measurements of the replicas were obtained at 20x magnification; the slices procured between time intervals were superimposed using the average of three measurements of the lesions of each tooth replica. No accuracy information was reported. In a subsequent study, the above technique was modified by taking the profile tracings at 40x magnification, then trimming lead foil to the shape of the surface change. The lead foils were weighed individually, and the amount of tooth destruction was determined by the weight of each slice of lead foil (Xhonga and Sognnaes, 1973).

2.2.2 Measuring Microscopy

Measuring microscopes consist of a stereo microscope with an internal mark, cross-hair or graticule to view an object mounted on an x, y stage. The internal mark is used to locate the x and y coordinates of a point or feature visualised through the microscope. The plane of focus can be used to determine the z coordinate where an appropriate recording mechanism is included in the instrument. Height accuracy is increased with increasing magnification, which also narrows the depth of field. A measuring microscope has been used to measure selected points on tooth replicas to a reported accuracy of 1 μm at a magnification of 250x (Lambrechts et al., 1984). Replicas and master casts have been compared with linear measurements taken with measuring microscopes (Hung et al., 1992; Price et al., 1991). Elastomeric impression materials have been measured directly with a measuring microscope (Clancy et al., 1983).

A similar instrument, the Standard Reflex Microscope is a stereo microscope with a floating mark, introduced into the field of view via a split mirror, focussed onto the surface of the object to obtain the z (height) coordinate (Scott, 1981). The observer views the object through an ordinary stereoscopic microscope. The accuracy of the Standard Reflex Microscope in the z axis is reported as 4 μm (Speculand et al., 1988). The Standard Reflex Microscope has been used for a number of dental research applications: to measure the dimensions of the glenoid fossa (Owen et al., 1992), to measure areas of dental caries in teeth (Neilson and Pitt, 1993); to measure the cement thickness of porcelain crowns (Shearer et al., 1996); to measure tooth morphology and wear in two small animals (Bezzobs and Sanson, 1997); to measure tooth movement on sequential casts during orthodontic treatment (Battagel and Ryan, 1998); and to measure palatal cleft defects (Owman-Moll et al., 1998).

Both these instruments require individual point recording by an operator. Typically, 20 points per minute can be recorded when the measurement routine consists of recording points on an ordered grid and the x-y stage automatically advances to the next point. This type of instrument is well suited to objects where the density of points to be recorded is not great and where the number of objects to be mapped are both small.

A newer type of measurement system, marketed as 'video measurement' (e.g. Starlite 250/300; Optical Gaging Products Inc. Rochester, NY, USA), has been used for measurement of a calibration artefact in Chapter 7 of this thesis. No reports of this system have appeared in the dental literature. This system consists of a video camera with calibrated zoom lens and x, y stage. In common with a measuring microscope, the object is moved within the field of view to allow visualisation of a point or feature, alignment with a measurement mark for determination of X and Y coordinates, and determination of the Z coordinate by location of the centre of the depth of field. Point and feature measurement is enhanced with through-the-lens

illumination, and image processing capabilities such as edge detection and sub-pixel centroiding. Varying levels of automation are available and video measurement equipment can be complimented with contact styli and laser sensors for autofocus and scanning (Mason, 2001).

2.2.3 Contact stylus

Contact stylus systems have been designed and built in a number of different centres (Chadwick et al., 1997; DeLong and Douglas, 1983; Roulet et al., 1983; Stinson and Lawton, 1989). Tooth replicas are typically profiled one at a time with measurement routines taking several hours.

DeLong and co-workers (DeLong and Douglas, 1983; DeLong et al., 1985) designed and built a closed-loop servo-hydraulic profilometer to measure occlusal profiles. Sequential profiles of the same tooth showed reproducibility of $\pm 7 \mu\text{m}$. A large number of profiles may be assembled into an image of the tooth's surface (Peters et al., 1999). This profiling system has been used to evaluate factors affecting the accuracy of impressions (Lee et al., 1995). In that study the accuracy of the measuring system was determined by comparing 40 sequential digital images of a master model, on $50 \times 100 \mu\text{m}$ grid, with the mean of the root mean square (rms) of the differences between measured points being $(3.6 \pm 0.5) \mu\text{m}$. A CAD/CAM method for ceramic restoration fabrication (Procera; Nobel Biocare AB, Gothenburg, Sweden) utilizes a mechanical contact stylus to scan prepared tooth replicas, with a accuracy of $10 \mu\text{m}$ (Persson et al., 1995).

Three methods of determining when the stylus is in contact with the surface of the object have been used. The probe may be attached to a micro-switch, which is actuated following a small deflection when touching the surface of the object, and the 3D location of the probe tip is recorded (Roulet et al., 1983; Stinson and Lawton, 1989). The second method utilizes a closed-loop system employing strain gauges (DeLong and Douglas, 1983) and the third method is suitable for electro-conductive objects such as dental casts poured with an

electroconductive medium (Chadwick et al., 1997). In this case, the contact stylus probe forms part of a feedback loop such that on coming into close proximity with an electrically conductive specimen, the electrical current passes and the position of the tip is recorded. The positioning and measurement resolution in the X, Y and Z axes has been reported at 2.5 μm (Chadwick et al., 2002).

In recent years commercial contact stylus measurement systems have become commonly available and their use is being reported in the dental literature. Whilst they are typically referred to as 'profilometers', they come under the general classification of coordinate measurement machines (CMM) and often have nanometre accuracy. Individual product models are designed to measure objects within a specified size range. Typically, the smaller the CMM, the greater the accuracy within the limits of the measurement range. One example used for an *in situ* study of enamel erosion (Nekrashevych and Stosser, 2003), has measurement specifications reported by the manufacturer as range/resolution of $\pm 80/0.01 \mu\text{m}$, and $\pm 320/0.04 \mu\text{m}$ (Hommel Tester T1000; Hommelwerke GmbH, Germany). These ranges are not suitable for mapping entire tooth surfaces. Use of other commercial systems in similar *in situ* studies have also been reported (Attin et al., 2004; Vanuspong et al., 2002).

There are no reports of contact systems being used directly on teeth in the mouth and few upon elastomeric impressions. One report used a contact probe system on cadaveric ear impressions using three-part light industrial silicone, with a setting time of several hours (Stinson and Lawton, 1989). However, dental elastomeric impressions are subject to deformation during contact measurement and as such have not been used in this manner. Contact stylus systems are now fully automatic, and while the measurement procedure may take several hours, it does not require actual operator time. However for best results, teeth surfaces need to be mapped individually, requiring that replicas have to be individually prepared.

2.2.4 Photogrammetry

At its broadest, photogrammetry is the taking measurements from images to generate 2D and 3D data. Measurements are taken from natural features appearing in the images or targets placed into the scene. The mathematical algorithms and software processing are scale independent, however, like other approaches, imaging equipment is scale dependent. Traditionally, photography was the means of non-contact imaging and found its major application in aerial based land mapping (aerial photogrammetry) utilizing single, very large format (230 mm x 230 mm) cameras and to a lesser extent land based mapping of architectural and engineered structures (non-topographic, terrestrial or close range photogrammetry) utilizing single or stereo large format (e.g. 100 mm x 150 mm) cameras. Between the late 1960s (Gruner et al., 1967) and late 1980s (Lamb et al., 1987; Mitchell et al., 1989) the use of small format (35 mm) cameras was explored for very close range photogrammetry with dental applications being a major research area. Very close range photogrammetry applications are reviewed in Chapter 6 and imaging options and calibration methods are reviewed in Chapter 7.

The investigation of the potential of electronic sensors to replace film photography for photogrammetry commenced in the 1980s. The calibration of a charge injection device (CID) array camera, 128 x 128 pixels, was reported for dental use (Curry et al., 1986), however there were no follow-up clinical reports. The low resolution of the early sensor arrays was a severe limitation when applied to traditional photogrammetric methods.

The advent of desktop computers in the 1980s aided the development of digital photogrammetry. Digital photogrammetric systems (DPS) follow a sequential process in which either hard-copy photographs are digitised or the images are directly acquired by digital cameras, then automatic matching takes place, where images are compared digitally, the small differences (parallaxes) automatically calculated, and 3D coordinate data generated. Photogrammetry has the significant advantage over all other methods that

3D data acquisition can be instantaneous, given simultaneous acquisition of images from different directions. In recent years there have been numerous reports on the use of high resolution digital SLR and compact cameras for close range photogrammetry (e.g. Chandler et al., 2000; Fraser, 1998; Mills et al., 2003; Shortis et al., 1998). However, the only very close range photogrammetry report is that of (Mitchell et al., 1999) who applied automatic digital photogrammetric software to microscope photographs of several objects. Precision of a small number of measured points of around 10 μm was reported, provided a suitably textured object was chosen. A piece of fractured concrete 10 mm x 20 mm in size was successfully mapped, however a gypsum replica of a tooth did not contain suitable texture for successful mapping.

2.2.5 Structured light

An alternative approach, known as structured light or active pattern projection, employs a light stripe or grid pattern of known geometry projected onto the object surface and photographed. Methods of pattern projection have included a light stripe combined with object movement through the stripe, Moiré fringe projection, grey-coded pattern projection, laser beam matrix projection and transparent liquid crystal pattern projection (Ahlers and Lu, 1989). The structured light approach has been used for a number of biomedical applications (Mitchell and Newton, 2002) including face mapping (Fricker, 1985). In recent years complex patterns (unstructured light) have been used in combination with two or more cameras (D'Apuzza, 2002; Thomas et al., 1996).

A proprietary structured light system for intra-oral mapping of teeth was developed in 1985 (CEREC; Siemens AG, Bensheim, Germany). It consists of a 3D tooth-scanning camera, integrated image processing, computer-aided design software and milling machine. This enables 3D scanning, at a single visit, of prepared cavities in teeth and the milling of a ceramic or composite polymer block to the shape of the required restoration, which is then

cemented into the prepared cavity. The camera consisted of a Charged Coupled Device (CCD) sensor, 680 x 480 pixels, and pixel size 25 x 29 μm . An infrared, polarised light source (840 nm) projects a striated line pattern onto the tooth surface. Four images are taken of the tooth surface in 0.133 s. The 3D model is achieved by active triangulation at an angle of 4° over a measurement volume of 18 x 14 x 12 mm. It has a reported measurement accuracy of $\pm 25 \mu\text{m}$ (Pfeiffer, 1999). However, there is a significant discrepancy between reported accuracy and the accuracy of restorations machined by the system with the average internal gap of posterior crowns created with this process being 100 to 200 μm (Mou et al., 2002) compared to the 50 – 100 μm gap generally recommended (Leinfelder et al., 1989).

The CEREC system was not developed as a research tool and at present there is no easy method of recovering raw data from the system. The CEREC system presents a potential clinical method for mapping NCCLs, however its reported measurement accuracy of 25 μm does not match that of contact stylus systems. Further, the reported accuracy is diminished by the need to render the surface of the tooth opaque prior to imaging (see section 2.2.5.1). It has the advantage of being fully automatic and 3D reconstruction occurs in a matter of seconds.

A structured light digitizing system utilising Moiré fringe projection (Comet 100; Steinbichler Optical Technologies, Neubeuern, Germany) has been used to scan vinyl polysiloxane impression materials (DeLong et al., 2001), evaluate impression accuracy (Brosky et al., 2002), and to scan dental casts and interocclusal records (DeLong et al., 2002). The XYZ measurement volume was 85 x 65 x 80 mm, an accuracy of 40 μm , and a resolution of 130 μm in the X and Y directions and 5 μm in the Z direction (parallel to the line of sight of the beam).

2.2.5.1 Tooth surface opaquing

Prior to taking optical impressions with the CEREC camera, the tooth surface needs to be made opaque for two reasons. Firstly, active triangulation is always impeded by reflective surfaces, because the camera is then not imaging a point on the object surface. Secondly, opaquing of the object is important because the reflected pattern may include components backscattered from different depths within the tooth. The resulting value calculated for the surface of the tooth would thus not correspond to its actual position, but would give a layer somewhere within the tooth, below the surface. Coating the tooth helps, because this backscatters nearly all radiation within 20 μm and thus clearly defines the surface of the tooth (Pfeiffer, 1999).

Clinically, tooth opaquing is achieved by wetting the tooth surface with an imaging liquid and blowing titanium dioxide powder (Cerec powder; Vita Zahnfabrik, Bad Säckingen, Germany) onto the tooth surface and air drying (Beutell, 1998). Powdering techniques are subject to the formation of lumps and clouds of dust; excessive powder falsifies the surface and powdered surfaces are sensitive to humidity. The error due to powder application has been reported as a minimum of 20 μm (Pfeiffer, 1999), 20 to 40 μm (Mou et al., 2002), and 100 μm (DeLong et al., 2001), although this source of error does not appear to have been rigorously investigated.

2.2.6 Laser scanning

The improved directionality of laser light has been exploited to improve structured light mapping systems, with methods including double-axis laser scanning, telecentric scanning, laser strip projection, optical radar and time-of-flight laser rangefinders (Ahlers and Lu, 1989). For dental tooth mapping applications, acquisition times range from a couple of seconds (Mehl et al., 1997) to minutes (Bartlett et al., 1997), during which time a person/object must remain stationary. As with other approaches to mapping, systems are typically scale dependent with examples being developed for the face with accuracies in the order of 1 mm (Coward et al., 1997; Wilson et al., 1997).

Systems for full dental casts have reported accuracies in the order of 50 μm (Commer et al., 2000; Kusnoto and Evans, 2002; Lu et al., 2000; Quick and Holtan, 1991; Sohmura et al., 2000). The Computer Integrated Ceramic Reconstruction (CICERO) system (CICERO Dental Systems B.V, Hoorn, The Netherlands) uses laser-stripe scanning of prepared tooth replicas and interocclusal records with scanning accuracy claimed to be 10 μm (van der Zel et al., 2001).

A small number of authors has reported utilisation of laser scanning systems for mapping teeth. A contacting laser point profilometer (Rank Taylor Hobson, Leicester, England) has been used to measure tooth wear on the impressions of the palatal surfaces of incisor teeth. The profilometer had a 6 mm range of vertical movement and a resolution of 10 nm. Each impression was scanned over a 5 mm² area, comprising of 164 profiles (30 μm apart) and each took an hour to complete (Bartlett et al., 1997).

A non-contacting profilometer with a laser line and CCD camera at an angle of 25° was developed to measure tooth wear (Mehl et al., 1997). The light line full width at half maximum (FWHM) was 22 μm and 512 surface points were measured in one video cycle. A step motor advanced the model in the y direction. The tooth surface was scanned at an interval 25 μm between points in x and y directions (250,000 points) in 20 to 40 seconds. Accuracy of $(6.0 \pm 0.6) \mu\text{m}$ was reported and precision was $(2.9 \pm 0.5) \mu\text{m}$. Further work with a related system utilising a triangulation angle of 30° (Laser Scan 3D; Willytec GmbH, Munich, Germany) has been reported for mapping human teeth (Perry et al., 2000) and another model (Surveyor 500 and RPS 450 laser; Laser Design Inc., Minneapolis, MN) used to map molars of *G. gorilla* (Ungar and Williamson, 2000).

A non-contacting laser profilometer (Keyence LC-2450 Series Laser displacement meter; UBM Messtechnik, Germany) with a maximum resolution of 0.5 μm has been used in the laboratory to measure 20 tooth surfaces with erosion and abrasion (Azzopardi et al., 2001). The

measurement range and accuracy of this system was $\pm 8 \text{ mm} \pm 0.031 \text{ mm}$ (www.keyence.co.uk/products/vision/laser/lc/lc_specifications_1, accessed 20 July, 2007).

An experimental laser stripe scanner (3Shape A/S, Copenhagen, Denmark) has been compared to the contact stylus system used for the Procera system (Nobel Biocare AB, Gothenburg, Sweden) with relative accuracy for both systems of $6 \text{ }\mu\text{m}$ (Persson et al., 2006).

2.2.7 Confocal Laser Microscopy

Confocal microscopy generates a common focal plane for both illumination and imaging and generates optical tomograms, giving thin slices ($>1 \text{ }\mu\text{m}$) up to $100 \text{ }\mu\text{m}$ below the surface of enamel and dentine (Watson, 1997). Slices may be obtained by reflection or fluorescence, subjected to image analysis, such as silhouette tracing to generate 2D data, and then combined to generate 3D data.

The use of laser confocal microscopy in the study of mammalian dental morphology has been reported (Evans et al., 2001; Jernvall and Selanne, 1999). Jernvall and Selanne (1999) reported using a maximum scanning window of $12.8 \text{ mm} \times 10.2 \text{ mm}$ at $2.5\times$ magnification and $3.2 \text{ mm} \times 2.5 \text{ mm}$ at $10\times$ magnification. Larger teeth could be scanned in several overlapping scan windows. The quality of 3D models was shown to deteriorate visibly when the teeth were scanned at $200 \text{ }\mu\text{m}$ intervals. No accuracy information was given. They concluded that the confocal scanning method was suitable for large samples of small teeth and other small fossils. Evans et al. (2001) reported on laser confocal microscopy by reflection and fluorescence. Reflection imaging of the natural teeth was found to result in excessive reflection in many areas, mostly likely due to enamel prisms or small sections of tooth surface perpendicular to the laser source causing significantly more reflection than the rest of the surface. This led to the misrepresentation of the surface position at these points. Staining the surface

of a replica with fluorescent eosin gave the strongest signal compared to the low amount of autofluorescence exhibited by natural teeth and was shown to be more accurate than depositing a layer of eosin dissolved in oil on the surface.

Confocal microscopy has been used to measure the thickness of curable resin films and the thickness of salivary pellicle in *in situ* studies (Azzopardi et al., 2004). The transparent nature of both the salivary pellicle and some resin films rendered them suitable for this technique, and peak-to-trough (Z height) measurements were taken.

2.2.8 Computed Tomography and Magnetic Resonance Imaging

Computed tomography (CT) utilizes x-radiation to produce 2D sections through the body or radiosensitive material. Conventional CT typically records slices 1 to 2 mm in thickness. Two-dimensional slices are assembled to build 3D models. Magnetic Resonance Imaging (MRI) involves applying magnetic fields to tissues under investigation and recording the differential resonance emitted by different tissue components.

A recent study testing the resolution of MRI on the human cadaver brain has reported spatial resolution of 195 μm in x and y and approximately 100 μm in z (Dashner et al., 2004). Magnetic Resonance Microscopy (MRM) has permitted clinical studies down to 50 μm , and laboratory studies where there was an absence of motion, down to 10 μm and has been used to produce isotropic data sets of live, developing rat embryos (Johnson et al., 1993). MRM has been used to identify brain regions and localisation of lesions in fixed rat brains (Lester et al., 1999). Early investigations of MRM with 112 μm slices have been undertaken on teeth with dental caries (Loyd et al., 2000).

Microscale CT has been applied to an extracted maxillary premolar, fixed in an acrylic glass tube, and placed in a μCT scanner (Scanco MicroCT; Sanco Medical) (Verdonschot et al., 2001). A scan grid of 1024 x 1024 was selected with a resolution of 13 μm and a scan slice thickness of 25 μm . The premolar

was scanned with 770 slices, and the exposure time was set at 10 ms. No dimensional accuracy testing was reported. Similar data has also been recently reported by Magne (2007).

2.2.9 Discussion

In summary, profile and silhouette tracing can be applied to the mapping of tooth surfaces provided high accuracy is not required. Systems such as measuring microscopes and video measurement are most suitable where target identification is important and the number of points to be measured is small. Contact stylus profilometry is very slow and remains a technique limited to the laboratory. Modern digital photogrammetry has potential but has not been successfully applied to teeth. The utility of structured light systems for high resolution single tooth mapping has not been shown. Laser scanning of replicas has become more common since the late 1990s with precision in the range of 1 to 10 μm being reported. Confocal microscopy has been used on specially prepared small animal tooth replicas with reported precision of a few micrometres. Computed tomography is in an early phase of study and its future utility is uncertain.

2.3 Replicating teeth

This section focuses upon the methods and materials involved in tooth replication. The principal issues are the accuracy and dimensional stability of materials used and their suitability for the various methods of measurement reviewed above. Tooth replication consists of two methods and materials:

- i) impressions,
- ii) casting.

2.3.1 Impression materials

Dental impression materials can be classified into non-elastic materials (impression plaster, impression compound, zinc oxide/eugenol and some waxes) which have limited use, predominantly for dental soft tissue (edentulous) areas; and elastic impression materials (the elastomers and hydrocolloids) which are widely used for both soft and hard (teeth) tissue areas. There are the *reversible hydrocolloid* materials, based on *agar*, an extract from the cell walls of certain red seaweeds; and the *irreversible hydrocolloid* (alginate) materials, based on *alginic acid*, an extract from certain species of seaweed, particularly brown algae. Alginates are predominantly used for preliminary casts, diagnostic or study casts (referred to in section 2.1.8) and master casts for partial dentures in many cases. They are not considered accurate enough for master casts for high quality indirect cast restorations (crowns and bridges). Alginates suffer from evaporation and syneresis of their water content, are not stable at room temperature for extended periods of time, and casts must be poured shortly after the material has reached its full set. Reversible hydrocolloid is suitable for all dental applications, but is generally limited to crown and bridge work due its more complex handling requirements (Bell, 1990).

Elastomers are polymers, consisting of larger organic molecules built up by repetition of smaller simpler chemical units called *mers*. Repetition of *mers* can be linear similar to a chain, or branched or interconnected to form three-dimensional networks. The *degree of polymerisation* (DP) is specified by the

number of repeat units in a chain. The control of DP allows tailoring of properties as the larger chains become materials of increased strength and dimensional stability, thereby allowing a given named polymer to range from liquids with low DP to very rigid solids of high DP. Polymers have much lower moduli of elasticity than, say, metals, strongly related to the fact that the macro molecules of polymers are weakly bound together. In some cases, as stress is applied to the polymer, the combined occurrences of chain straightening, chain lengthening and slip between chains, produce very large elastic deformations per unit of applied stress, leading to the term *elastomer* being applied to such polymers. The flow, brittleness and softening point of a polymer may be altered with the addition of *plasticizers*, compounds that should be miscible, compatible and permanent. *Fillers* may be added to enhance dimensional stability, impact resistance, tensile and compressive strengths, abrasion resistance and thermal stability. Colourants of soluble dye or insoluble pigments can change the colour, transparency and refractive index on polymers (Greener et al., 1972).

Elastomers used in dentistry are derived from *polysulphide rubber*, used from the mid 1950s, *condensation silicones*, used from the 1960s, *addition-cured silicones*, introduced in the 1970s, and *polyether polymers*, produced from the late 1960s. Addition-cured silicones, based on the *siloxane* chain with terminal vinyl groups, have become the preferred material used for taking impressions of dental hard tissues (vinyl polysiloxanes). Siloxane is thickened with a finely divided filler such as *silica*, a cross-linking agent such as alkyl silicate, and mixed with a catalyst paste containing a cross-linking agent such as organohydrogen siloxane, a platinum salt activator and a dye designed to assist with uniform mixing. There is no by-product from the setting reaction, which improves the accuracy of these materials, but a slight polymerisation shrinkage may occur (Bell, 1990). Dimensional accuracy of elastomers is discussed below in section 2.3.3 below.

In recent years *automix* systems have become the norm for the use of vinyl polysiloxanes and the inclusion of a dye for manual mixing purposes is no longer required. Vinyl polysiloxanes are naturally clear and are available commercially (for example, Monet – clearbite 2; Erskine Products Pty Ltd, Macksville, Australia) although the overwhelming majority of materials is still coloured for presentation. DeLong et al. (2001) reported on factors affecting the optical scanning of vinyl polysiloxanes and proposed that enhanced colouring of impression materials would assist with scanning.

2.3.2 Casting materials

Casting materials are selected for their functional ability to fill a mould, undergo a physical or chemical change, and result in a product of proper shape and properties. The most commonly used casting materials are gypsum products, in the form of *plaster of Paris* and *dental stones*, used for making life sized models from impressions, mould making and investments for the making of dental appliances. Dental plaster and stone are products of low heat calcination of gypsum, a naturally occurring mineral form of *calcium sulphate dihydrate*. The resulting β -*hemihydrate* (plaster, Type II) and α -*hemihydrate* (unimproved stone, Type III) are then re-combined with water to form solid masses of the hydrous form. The main difference between dental plaster and stone is the amount of water required to make a workable mix, with the final set product from dental stone being denser, harder and stronger than that formed from plaster. Improved (Type IV) stone, produced by removing the crystallisation water with boiling in a 30% calcium chloride solution, is the most dense of the four types of dental stone. Most gypsum materials exhibit an overall linear setting expansion up to 0.2 to 0.25% due to the outward thrust of growing gypsum crystals and creation of internal voids (Greener et al., 1972). Gypsum die materials have been reported to exhibit setting expansion of 0.01 to 0.1 % (Hollenback and Smith, 1976; Toreskog et al., 1966). Die stone is routinely used for the production of high quality replicas of individual teeth and partial and full arch dental casts in

both clinical and research environments. Die stone is dimensionally very stable and resistant to scratching.

Various modifications to the use of gypsum products have been described, such as the use of electro-deposition of copper into elastomeric impressions prior to back filling with diestone (Lambrechts et al., 1981), and the application of electro-conductive paints prior to backfilling with die stone (Chadwick et al., 1997).

Epoxy resins have also been used to produce positive replicas of teeth. These materials are dimensionally stable and resistant to scratching. Many epoxy resins have setting shrinkages of 0.01 % (Evans et al., 2001). The original patent covering epoxy resin suggested its use as a denture base material. It was found unsuitable for this application but has achieved great industrial importance because of its adhesive strength, chemical resistance and dimensional stability (Greener et al., 1972).

2.3.3 Dimensional accuracy

2.3.3.1 Linear measurement

Modern silicone dental impression materials have been extensively studied and compared, alone and in combination with both diestones and epoxy resins. Many testing regimens have been applied, but they are generally based on the International Standard ISO 4823 (1984) which involves taking an impression of a stainless steel block bearing engraved markings which provide reference points for measurements over a normal gauge length of 25 mm. As the engraved markings are fine, varying from 25 to 75 μm in width, the test also gives an assessment of the ability of an impression material to reproduce fine detail. For determination of linear dimensional changes on storage, the distance separating the gauge marks is measured with a travelling microscope and a contraction over 24 hours of not more than 0.4% is allowed under the standard. The standard also includes a compression test to test elastic recovery (Lear and Earnshaw, 1985). The

revised American Dental Association specification No. 19 for non-aqueous, elastomeric dental impression materials (1977) provides for a similar test.

For example, two addition silicone elastomeric dental materials were tested according to the standard and found to have dimensional accuracy (contraction) at 24 hours and at seven days of 0.2 per cent ($0.2\% \times 25 \text{ mm} = 0.05 \text{ mm}$) (Lear and Earnshaw, 1985). Many authors have modified the test procedure to use a test object that more closely resembles dental clinical conditions. In a recent example, the procedure was modified by assembling customised posts, with retentive elements, set into an arch form with distances on a plane between 25 and 47 mm, to evaluate the dimensional accuracy of several polyether and addition-cured silicone impression materials. A measuring microscope was used to take linear measurements. Dimensional changes (reduction) ranged from 11 to 19 μm (equivalent to a maximum of - 0.04 %) for the 25 mm dimension; changes ranged up to 0.1 % for 47 mm dimension and up to +0.15 % for a second 25 mm dimension (Piwowarczyk et al., 2002).

From these and other studies, it is clear that setting contraction is a complex phenomenon. Many influences are at play, including the use of various viscosity materials in the same impression, the impression tray, use of adhesive or other retentive elements, material thickness and temperature, as well as the effects of disinfection. In the studies referred to above, where dimensional change in more than one direction has been measured, greatly varying results in either quantum or sign have occurred for measurements in different directions. This is also a feature of the first study referred to below.

ISO 4823 only measures one linear distance, not three dimensions, and in the clinical setting, impression materials are combined with casting materials to produce a cast or model. Many authors have modified the test procedure to include the pouring of a model and taken measurements from the master die and the model in three dimensions. Price et al. (1991) reported on the dimensional accuracy of four elastomeric impression materials and three

type IV die stones; their reported measurement errors were 0.21 % at most. They fabricated a molar tooth die with four dimples (circular depressions) to create a width of 3.965 mm , a length of 3.754 mm, and a height of 1.548 mm. When replicas were compared with the master die using a measuring microscope, the mean increases in all dimensions were 27.2 μm (0.68%), 10.3 μm (0.27%) and 10.3 μm (0.67%) with a range for each increase no greater than 9 μm . All stone die distances were larger than on the master die and no one combination consistently produced the smallest or largest die in the three measured dimensions. Price et al. (1991) noted that the level of surface detail reproduction (that is, the dimples) ranged from at best 20 μm . This was in agreement with Gerrow and Schneider (1987) who found that the level of surface detail reproduction ranges from at best 20 μm to 50 μm for the combinations used their study. This severely limits studies looking for dimensional changes of less than 20 μm in stone dies (Gerrow and Schneider, 1987). The study of Price et al. (1991) with replication error of 9 μm is commonly referred to in the literature (Azzopardi et al., 2000; Mehl et al., 1997). However, as noted above, the value of 9 μm is a precision measure with absolute error values for ranging from 10 μm (0.27%) to 27 μm (0.68%) for the three dimensions measured.

The edges of geometric tooth sized dies have been measured with a measuring microscope and used to compare five silicone impression materials, and the one-step and two-step putty silicone impression techniques (Hung et al., 1992). For all materials tested, an error of +30.0 μm over a height of 9.6 mm, an error of +28 μm over a length of 10.1 mm, and an error of +188.4 μm over a length of 29.0 mm was reported, equating to an increased replica size of a maximum of 0.36 %. Chaffee et al. (1997) fabricated a geometric tooth abutment sized die with dimples (length 6.3 mm, width 6.4 mm and height 10.3 mm) to study the accuracy of type IV dental stone and epoxy resin die, poured from impressions of a master die, and found that dimensional changes (reduction) for both materials were similar and up to 30 μm , or less than 0.3 %. The authors noted that the manufacturers of the die

material reported a shrinkage of 0.05 % for the epoxy resin and an expansion of 0.09 % for the dental stone.

2.3.3.2 Surface matching

Several reports have appeared which utilise surface mapping and alignment algorithms to evaluate dimensional changes in impression materials and /or casting materials. Lee et al. (1995) used a contact stylus system upon a single cast tooth surface to evaluate impression tray movement during setting of impressions with one-step and a two-step techniques, and found no effect upon impression accuracy. However it was determined that the mean rms difference between 2500 points measured on 60 casts was $(21.5 \pm 6.6) \mu\text{m}$ (measurement error of $3.6 \mu\text{m}$), equating to a 0.30 % distortion.

Brosky et al. (2002) used a structured light system (see section 2.2.5) to map a master die and casts poured from impressions of a geometric dental arch form (same arch form as Quick and Holtan (1991)). The effects of cast fabrication and impression technique were tested for accuracy with distances between cross hairs and heights being measured. When gross outliers were removed, the median rms of errors between cross hairs was $103.2 \mu\text{m}$, and the median rms of errors for the height was $19.3 \mu\text{m}$. No data on percentage errors were provided, however using the height dimensions provided in Quick and Holtan (1991) it would appear that height rms errors were 0.24 %.

Luthardt et al. (2003) used an optical scanning device to scan a metal master die (prepared tooth form) and replica dies poured from type IV dental stone. Eight views of the dies, taken from different directions, were combined to generate a solid CAD model . Best-fit registration of stones dies to the master die CAD model showed enlargement of the type IV die stone dies over time with a mean deviation of $+10 \mu\text{m}$, with a maximum deviation up to $100 \mu\text{m}$.

2.3.4 Discussion

Based on single tooth surface mapping and surface alignment methods, the replication process introduces errors for individual teeth in the order of

20 μm . Elastomeric material setting and contraction is a complex phenomenon in three dimensions and all test regimes introduce variables into the evaluation process. Enhanced colouring of impression materials may enhance their imaging potential with structured light and laser scanners (DeLong et al., 2001). The application of metal and paint films can be used to enhance the surface properties of tooth replicas (e.g. Chadwick et al., 2002; Lambrechts et al., 1981). The incorporation of optical texture into impression materials or casting has not been reported.

2.4 Conclusions

Many aspects of NCCLs need to be further investigated to aid understanding of the development and progression of NCCLs. There are measurement methods currently in use, predominantly on tooth replicas, to measure tooth wear and erosion. Measurement systems report accuracy and precision of tooth surfaces under 10 μm , however the small number of studies that have performed change detection of models poured from impressions of teeth have reported errors up to 20 μm . They remain confined to the laboratory and no clear path to the development of a clinical method has been identified. There are few reports utilizing current digital stereophotogrammetry, which offers an alternative approach with the advantage of instantaneous data acquisition, provided a suitable surface with optical texture can be provided. The surface properties of tooth replicas can be enhanced to aid mapping however the incorporation of optical texture into casting materials has not been reported. A laboratory method could be developed with suitable targets or optical texture present on, or incorporated into, the surface of tooth replicas.

2.5 References

- Ahlers, R.-J. and Lu, J., 1989. Stereoscopic vision - an application oriented overview. In: Svetkoff DJ (Ed.), Optics, Illumination, and image sensing for machine vision IV, SPIE - The International Society for Optical Engineering, Philadelphia, Pennsylvania, pp. 298-307.
- Amaechi, B., Higham, S. and Edgar, W., 1999a. Factors influencing the development of dental erosion in vitro: enamel type, temperature and exposure time. *Journal of Oral Rehabilitation*, 26: 624-630.
- Amaechi, B., Higham, S. and Edgar, W., 1999b. Techniques for the production of dental erosions in vitro. *Journal of Oral Rehabilitation*, 26: 97-102.
- Amaechi, B., Higham, S. and Edgar, W., 2003. Influence of abrasion in clinical manifestation of human dental erosion. *Journal of Oral Rehabilitation*, 30 (4): 407-413.
- Amaechi, B., Higham, S., Edgar, W. and Milosevic, A., 1999c. Thickness of acquired salivary pellicle as a determinant of the sites of dental erosion. *Journal of Dental Research*, 78 (12): 1821-1828.
- Attin, T., Siegel, S., Buchalla, W., Lennon, A., Hannig, M. and Becker, K., 2004. Brushing abrasion of softened and remineralised dentin: an in situ study. *Caries Research*, 38: 62-66.
- Avery, J.K. (1992). *Essentials of Oral Histology and Embrology*. (Ed: Steele, P.F.) Mosby-Year Book Inc. St. Louis.
- Aw, T., Lepe, X., Johnson, G. and Mancl, L., 2002. Characteristics of noncarious cervical lesions. *Journal of the American Dental Association*, 133: 725-733.
- Azzopardi, A., Bartlett, D., Watson, T. and Sherrieff, M., 2001. The measurement and prevention of erosion and abrasion. *Journal of Dentistry*, 29 (6): 395-400.
- Azzopardi, A., Bartlett, D., Watson, T. and Sherrieff, M., 2004. The surface effects of erosion and abrasion on dentine with and without a protective layer. *British Dental Journal*, 196 (6): 351-354.

- Azzopardi, A., Bartlett, D., Watson, T. and Smith, B., 2000. A Literature Review of the Techniques to Measure Tooth Wear and Erosion. *European Journal of Prosthodontics and Restorative Dentistry*, 8 (3): 93-97.
- Bader, J., Levitch, L., Shugars, D., Heymann, H. and McClure, F., 1993. Dentist's classification and treatment of cervical lesions. *Journal of the American Dental Association*, 124 (5): 46-54.
- Bader, J., McClure, F., Scurria, M., Shugars, D. and Heymann, H., 1996. Case-control study of non-carious cervical lesions. *Community Dental Epidemiology*, 24: 286-291.
- Bartlett, D., 2003. Retrospective long term monitoring of tooth wear using study models. *British Dental Journal*, 194 (3): 211-213.
- Bartlett, D., Blunt, L. and Smith, B., 1997. Measurement of tooth wear in patients with palatal erosion. *British Dental Journal*, 182 (5): 179-184.
- Bartlett, D. and Coward, P., 2001. Comparison of the erosive potential of gastric juice and carbonated drink in vitro. *Journal of Oral Rehabilitation*, 28: 1045-1047.
- Bartlett, D., Coward, P., Nikkah, C. and Wilson, R., 1998. The prevalence of tooth wear in a cluster sample of adolescent schoolchildren and its relationship with potential explanatory factors. *British Dental Journal*, 184: 125-129.
- Bartlett, D., Palmer, I. and Shah, P., 2005. An audit of study casts used to monitor tooth wear in general practice. *British Dental Journal*, 199 (3): 143-145.
- Bartlett, D., and Shah, P., 2006. A critical review of non-carious cervical (wear) lesions and the role of abfraction, erosion, and abrasion. *Journal of Dental Research*, 85 (4): 306-312.
- Battagel, J. and Ryan, A., 1998. Treatment changes in Class I and mild Class II malocclusions using the *en masse* removable appliance. *European Journal of Orthodontics*, 20 (1): 5-15.

- Bell, C., 1990. Heinemann Dental Handbook. Heinemann Professional Publishing Inc., Oxford, UK.
- Bell, E.J., Kaidonis, J., Townsend, G.C. and Richards, L.C., 1998. Comparison of exposed dentinal surfaces resulting from abrasion and erosion. *Australian Dental Journal*, 43 (5): 362-366.
- Benzing, UR., Gall, H. and Weber, H., 1995. Biomechanical aspects of two different implant-prosthetic concepts for edentulous maxillae. *International Journal of Oral Maxillofacial Implants*, 10 (2): 188-98.
- Beuttell, J., 1998. Powdering for a perfect picture. *International Journal of Computerized Dentistry*, 1: 35-39.
- Bezzobs, T. and Sanson, G., 1997. The effects of plant and tooth structure on intake and digestibility in two small animals. *Physiol. Zoology* 70 (3): 338-351.
- Bhaskar, S., 1990. Orban's Oral histology and embryology, Mosby Year Book, Mosby-Year Book Inc, St. Louis.
- Borcic, J., Anic, I., Smojver, I., Catic, A., Miletic, I. and Ribaric, S., 2005. 3D finite element model and cervical lesion formation in normal occlusion and in malocclusion. *Journal of Oral Rehabilitation*, 32 (7): 504-510.
- Borcic, J., Anic, I., Urek, M. and Ferreri, S., 2004. The prevalence of non-carious cervical lesions in permanent dentition. *Journal of Oral Rehabilitation*, 31 (2): 117-123.
- Boyde, A., 1989. Enamel. In: Oksche, hcA. and Vollrath, L. (Eds.), *Teeth*, Springer-Verlag, Berlin, pp. 309-473.
- Braem, M., Lambrechts, P. and Vanherle, G., 1992. Sress-induced cervical lesions. *Journal of Prosthetic Dentistry*, 67: 18-22.
- Brosky, M., Pesun, I., Lowder, P., Delong, R. and Hodges, J., 2002. Laser digitization of casts to determine the effect of tray selection and cast formation technique on accuracy. *Journal of Prosthetic Dentistry*, 87 (2): 204-209.

- Chadwick, R., Mitchell, H., Cameron, I., Hunter, B. and Tulley, M., 1997. Development of a novel system for assessing tooth and restoration wear. *Journal of Dentistry*, 25 (1): 41-47.
- Chadwick, R., Mitchell, H., Manton, S., Ward, S., Ogston, S. and Brown, R., 2005. Maxillary incisor palatal erosion: no correlation with dietary variables? *Journal of Clinical Pediatric Dentistry*, 29 (2): 157-163.
- Chadwick, R., Mitchell, H. and Ward, S., 2002. Evaluation of the accuracy and reproducibility of a replication technique for the manufacture of electroconductive replicas for use in quantitative clinical dental wear studies. *Journal of Oral Rehabilitation*, 29: 540-545.
- Chaffee, N., Bailey, J. and Sherrard, D., 1997. Dimensional accuracy of improved dental stone and epoxy resin die materials. Part I: Single die. *Journal of Prosthetic Dentistry*, 77 (2): 131-135.
- Chandler, J., Lane, S. and Ashmore, P., 2000. Measuring river-bed and flume morphology and parameterising bed roughness with a Kodak DCS460 digital camera. *International Archives of Photogrammetry and Remote Sensing*, 23 (B7): 250-257.
- Charbeneau, G., Cartwright, B., Comstock, FW, Kahler, F., Snyder, D., Dennison, J. and Margeson, R., 1981. *Principles and Practice of Operative Dentistry*. 2nd Edition. Lea & Febiger, Philadelphia.
- Chu, S., Skultety, K., Suvinen, T., Clement, J. and Price, C., 1995. Computerized three-dimensional magnetic resonance imaging reconstructions of temporomandibular joints for both a model and patients with temporomandibular pain dysfunction. *Oral Surgery Oral Medicine Oral Pathology Oral Radiology Endodontics*, 80 (5): 604-611.
- Clancy, J., Scandrett, F. and Ettinger, R., 1983. Long-term dimensional stability of three current elastomers. *Journal of Oral Rehabilitation*, 10 (4): 325-333.

- Commer, P., Bourauel, C., Maier, K. and Jager, A., 2000. Construction and testing of a computer-based intraoral laser scanner for determining tooth positions. *Medical Engineering and Physics*, 22 (9): 625-635.
- Coward, T., Watson, R. and Scott, B., 1997. Laser scanning for the identification of repeatable landmarks of the ears and face. *British Journal of Plastic Surgery*, 50: 308-314.
- Curry, S., Baumrind, S. and Anderson, J., 1986. Calibration of an array camera. *Photogrammetric Engineering and Remote Sensing*, 52 (5): 627-636.
- D'Apuzza, N., 2002. Surface measurement and tracking of human body parts from multi-image video-sequences. *ISPRS Journal of Photogrammetry and Remote Sensing*, 56: 360-375.
- Dashner, R., Kangarlu, A., Clark, D., Abhik RayChaudhury, A. and Chakeres, D., 2004. Limits of 8-Tesla magnetic resonance imaging spatial resolution of the deoxygenated cerebral microvasculature. *Journal of Magnetic Resonance Imaging*, 19 (3): 303-307.
- Davis, W. and Winter, P., 1980. The effect of abrasion on enamel and dentine and exposure to dietary acid. *British Dental Journal*, 148 (11-12): 253-256.
- DeLong, R. and Douglas, W., 1983. A methodology for measurement of occlusal wear, using computer graphics. *Journal of Dental Research*, 62 (Abst. 456): 220.
- DeLong, R., Ko, C.-C., Anderson, G., Hodges, J. and Douglas, W., 2002. Comparing maximum intercuspal contacts of virtual dental patients and mounted dental casts. *Journal of Prosthetic Dentistry*, 88 (6): 622-630.
- DeLong, R., Pintado, M. and Douglas, W., 1985. Measurement of change in surface contour by computer graphics. *Dental Materials*, 1: 27-30.
- DeLong, R., Pintado, M., Ko, C., Hodges, J. and Douglas, W., 2001. Factors influencing optical 3D scanning of vinyl polysiloxane impression materials. *Journal of Prosthodontics*, 10 (2): 78-85.

- Evans, A., Harper, I. and Sanson, G., 2001. Confocal imaging, visualization and 3-D surface measurement of small mammalian teeth. *Journal of Microscopy*, 204 (2): 108-119.
- Fernandes, C. and Chevitarese, O., 1991. The orientation and direction of rods in dental enamel. *Journal of Prosthetic Dentistry*, 65 (6): 793-800.
- Frank, R. and Nalbandian, J., 1989. Structure and ultrastructure of dentine. In: Oksche, H. A. and Vollrath, L. (Eds.), *Teeth*, Springer-Verlag, Berlin, pp. 173-238.
- Fraser, C., 1998. Some Thoughts on the Emergence of Digital Close Range Photogrammetry. *Photogrammetric Record*, 16 (91): 37-50.
- Frazier, P., 1968. Adult human enamel: An electron microscope study of crystalline size and morphology. *Journal of Ultrastructure Research*, 22 (1): 1-11.
- Fricker, J., 1985. Projected grid facial photography. *Australian Dental Journal*, 30 (6): 414-417.
- Gale, M., Darvell, B., and Cheung, G., 1994. Three-dimensional reconstruction of microleakage pattern using a sequential grinding technique. *Journal of Dentistry*, 22 (6): 370-375.
- Garberoglio, R. and Brännström, M., 1976. Scanning electron microscopic investigation of human dentinal tubules. *Archives of Oral Biology*, 21 (6): 355-362.
- Gerrow, J. and Schneider, R., 1987. A comparison of the compatibility of elastomeric impression materials, type IV dental stones, and liquid media. *Journal of Prosthetic Dentistry*, 57: 292-298.
- Greener, E., Harcourt, J. and Lautenschlager, E., 1972. *Materials science in dentistry*. The Williams and Wilkins Company, Baltimore.
- Grippio, J. and Masi, J., 1991. Role of bi dental engineering factors (BEF) in the etiology of root caries. *Journal of Esthetic Dentistry*, 3 (2): 71-76.
- Gruner, H., Zulqar-Nain, J. and Zander, H., 1967. A short-range system for dental surgery. *Photogrammetric Engineering*, 33 (11): 1240-1245.

- Gwinnett, A., 1971. Histologic changes in human enamel following treatment with acidic adhesive conditioning agents. *Archives of Oral Biology*, 16 (7): 731-738.
- Gwinnett, A., 1992. Structure and composition of enamel. *Operative Dentistry Supplement*, 5: 10-17.
- Han, K., Lu, R., Ma, Y., Lu, P., Zhang, H. and Wang, W., 1998. Reconstruction of three-dimensional digital teeth. *Chinese Journal of Dental Research*, 1 (2): 22-25.
- Hannig, C., Hannig, M. and Attin, T., 2005. Enzymes in the acquired enamel pellicle. *European Journal of Oral Sciences*, 113 (1): 2-13.
- Hannig, M. and Balz, M., 2001. Protective properties of salivary pellicles from two different intraoral sites on enamel erosion. *Caries Research*, 35 (2): 142-148.
- Harris, C. and Gorgas, F., 1899. A dictionary of dental science. 6th Edition. P Blakiston's & Son, Philadelphia.
- Hollenback, G. and Smith, D., 1976. A further investigation of the physical properties of hard gypsum. *Journal of the Californian Dental Association*, 43: (221-227).
- Hooper, S., West, N., Pickles, M., Joiner, A., Newcombe, R. and Addy, M., 2003. Investigation of erosion and abrasion on enamel and dentine: a model in situ using toothpastes of different abrasivity. *Journal of Clinical Periodontology*, 30: 802-808.
- Hung, S., Purk, J., Tira, D. and Eick, J., 1992. Accuracy of one-step versus two-step putty wash addition silicone impression technique. *Journal of Prosthetic Dentistry*, 67 (5): 583-589.
- Jernvall, J. and Selanne, L., 1999. Laser confocal microscopy and geographic information systems in the study of dental morphology. *Palaeontologia Electronica*: 2 (1): 18 pages.
- Johnson, G., Benveniste, H., Black, R., Hedlund, L., Maronpot, L. and Smith, B., 1993. Histology by magnetic resonance microscopy. *Magnetic Resonance*, 9 (1): 1-30.

- Kaidonis, J., Gratiaen, J., Bhatia, N., Richards, L. and Townsend, G., 2003. Tooth wear prevention: a quantitative and qualitative *in vitro* study. Australian Dental Journal, 48 (1): 15-19.
- Khan, F., Young, W. and Daley, J., 1998. Dental erosion and bruxism. A tooth wear analysis from South Queensland. Australian Dental Journal, 43 (2): 117-127.
- Khan, F., Young, W., Shahabi, S. and Daley, T., 1999. Dental cervical lesions associated with occlusal erosion and attrition. Australian Dental Journal, 44 (3): 176-186.
- Korionth, T. and Hannan, A., 1994. Deformation of the human jaw during simulated jaw clenching. Journal of Dental Research, 73: 56-66.
- Kusnoto, B. and Evans, C., 2002. Reliability of a 3D surface laser scanner for orthodontic applications. American Journal of Orthodontics and Dentofacial Orthopedics, 122 (4): 342-348.
- Lamb, R., McGarrah, H., and Eick, J., 1987. Close-range photogrammetry with computer interface in dental research. Photogrammetric Engineering and Remote Sensing, 53 (12): 1685-1689.
- Lambrechts, P., Vanherle, G. and Davidson, C., 1981. An universal and accurate replica technique for scanning electron microscope study in clinical dentistry. Microscopica Acta, 85 (1): 45-48.
- Lambrechts, P., Vanherle, G., Vuylsteke, M. and Davidson, C., 1984. Quantitative evaluation of the wear resistance of posterior dental restorations: a new three-dimensional measuring technique. Journal of Dentistry, 12 (3): 252-267.
- Lear, A. and Earnshaw, R., 1985. Dimensional accuracy of ear impression materials. Australian Journal of Audiology, 9 (2): 55-95.
- Lee, I., DeLong, R., Pintado, M. and Malik, R., 1995. Evaluation of factors affecting the accuracy of impressions using quantitative surface analysis. Operative Dentistry, 20: 246-252.

- Lee, W. and Eakle, W., 1984. Possible role of tensile stress in the etiology of cervical erosive lesions of teeth. *Journal of Prosthetic Dentistry*, 52 (3): 374-380.
- Leinfelder, K., Isenberg, B. and Essig, M., 1989. A new method for generating ceramic restorations: a CAD-CAM system. *Journal of the American Dental Association*, 118 (6): 703-707.
- Lester, D., Lyon, R., McGregor, G., Engelhardt, R., Schmued, L., Johnson, G. and Johannessen, J., 1999. 3-Dimensional visualization of lesions in rat brain using magnetic resonance imaging microscopy. *Neuroreport*, 10 (4): 737-741.
- Levitch, L., Bader, J., Shugars, D. and Heymann, H., 1994. Non-carious cervical lesions. *Journal of Dentistry*, 22 (4): 195-207.
- Lin, C., Douglas, W., and Erlandsen, S., 1993. Scanning Electron Microscopy of Type I Collagen at the Dentin-Enamel Junction of Human Teeth. *The Journal of Histochemistry and Cytochemistry*, Vol. 41, (3): 381-388.
- Litonjua, L., Bush, P., Andreana, S., Tobias, T. and Cohen, R., 2004. Effects of occlusal load on cervical lesions. *Journal of Oral Rehabilitation*, 31 (3): 225-232.
- Lloyd, C., Scrimgeour, S., Chudeck, J., Chudek, G. and MacKay, R., 2000. Application of magnetic resonance microimaging to the study of dental caries. *Caries Research*, 34 (1): 53-58.
- Lu, P., Li, Z., Wang, Y., Chen, J. and Zhao, J., 2000. The research and development of noncontact 3-D laser dental model measuring and analyzing system. *Chinese Journal of Dental Research*, 3 (3): 4-14.
- Lussi, A. and Schaffner, M., 2000. Progression of and risk factors for dental erosion and wedge-shaped defects over a 6-year period. *Caries Research*, 34 (2): 182-187.
- Lussi, A., Schaffner, M., Hotz, P. and Suter, P., 1991. Dental erosion in a population of Swiss adults. *Community Dentistry and Oral Epidemiology*, 19 (5): 286-290.

- Luthardt, R., Kuhmstedt, P. and Walter, M., 2003. A new method for the computer-aided evaluation of three-dimensional changes in gypsum materials. *Dental Materials*, 19 (1): 19-24.
- Magne, P., 2007. Efficient 3D finite element analysis of dental restorative procedures using micro-CT data. *Dental Materials*, 23 (5): 539-548.
- Mason, F., 2001. Video measurement, *Quality in manufacturing*, Nelson Publishing Inc., 2 pages.
- Mayhew, R., Jesse, S. and Martin, R., 1998. Association of occlusal, periodontal, and dietary factors with the presence of non-carious cervical dental lesions. *American Journal of Dentistry*, 11 (1): 29-32.
- Mehl, A., Gloger, W., Kunzelmann, K.-H. and Hickel, R., 1997. A new optical 3D device for the detection of wear. *Journal of Dental Research*, 76 (11): 1799-1807.
- Mills, J., Schneider, D., Barber, D. and Byran, P., 2003. Geometric assessment of the Kodak DCS Pro Back. *Photogrammetric Record*, 18 (3): 193-208.
- Mitchell, H., Chadwick, R. and McCabe, J., 1989. Measurement at very close range using microscope photogrammetry. *The Australian Surveyor*, 34 (5): 463-471.
- Mitchell, H., Kniest, H. and Oh, W.-J., 1999. Digital photogrammetry and microscope photographs. *Photogrammetric Record*, 16 (94): 695-704.
- Mitchell, H. and Newton, I., 2002. Medical photogrammetric measurement: overview and prospects. *ISPRS Journal of Photogrammetry and Remote Sensing*, 56 (5-6): 286-294.
- Mou, S.-H., Chai, T., Wang, J.-S. and Shiau, Y.-Y., 2002. Influence of different convergence angles and tooth preparation heights on the internal adaptation of Cerec crowns. *Journal of Prosthetic Dentistry*, 87 (3): 248-255.
- Neilson, A. and Pitt, N., 1993. Development and application of a quantitative method of monitoring macroscopic cavitation in smooth surface carious lesions in vivo. *Caries Research*, 27 (2): 140-146.

- Nekrashevych, Y. and Stosser, L., 2003. Protective influence of experimentally formed salivary pellicle on enamel erosion. An in vitro study. *Caries Research*, 37 (3): 225-231.
- Owen, C., Wilding, R., and Adams, L., 1992. Dimensions of the temporal glenoid fossa and tooth wear in prehistoric human skeletons. *Archives of Oral Biology*, 37 (1): 63-67.
- Owman-Moll, P., Katsaros, C. and Friede, H., 1998. Development of the residual cleft in the hard palate after velar repair in a 2-stage palatal repair regimen. *Journal of Orofacial Orthopaedics*, 59 (5): 286-300.
- Palamara, D., Palamara, J., Tyas, M. and Messer, H., 2000. Strain patterns in cervical enamel of teeth subjected to occlusal loading. *Dental Materials*, 16 (6): 412-419.
- Palamara, D., Palamara, J., Tyas, M., Pintado and M., Messer, H., 2001. Effects of stress on acid dissolution of enamel. *Dental Materials*, 17 (2): 109-115.
- Palamara, J., Palamara, D., Messer, H. and Tyas, M., 2006. Tooth morphology and characteristics of non-carious cervical lesions. *Journal of Dentistry*, 34 (3): 185-194.
- Pegoraro, L., Scolaro, J., Conti, P., Telles, D. and Pegoraro, T., 2005. Noncarious cervical lesions in adults: prevalence and occlusal aspects. *Journal of the American Dental Association*, 136 (12): 1694-1700.
- Perry, R., Kugel, G., Kunzelmann, K.-H., Flessa, H.-P. and Estafan, D., 2000. Composite restoration wear analysis: conventional methods vs. three-dimensional laser digitizer. *Journal of the American Dental Association*, 131 (10): 1472-1477.
- Persson, A., Andersson, M., Oden, A. and Sandborgh-Englund, G., 2006. A three-dimensional evaluation of a laser scanner and a touch-probe scanner. *Journal of Prosthetic Dentistry*, 95 (3): 194-200.
- Persson, M., Andersson, M. and Bergman, B., 1995. The accuracy of a high-precision digitizer for CAD/CAM of crowns. *Journal of Prosthetic Dentistry*, 74 (3): 223-229.

- Peters, M., DeLong, R., Pintado, M., Pallesen, U., Qvist, V. and Douglas, W., 1999. Comparison of two measurement techniques for clinical wear. *Journal of Dentistry*, 27 (7): 479-485.
- Pfeiffer, J., 1999. Dental CAD/CAM technologies: The optical impression (II). *International Journal of Computerized Dentistry*, 2: 65-72.
- Phelan, J. and Rees, J., 2003. The erosive potential of some herbal teas. *Journal of Dentistry*, 31 (4): 241-246.
- Pintado, M., Anderson, G., DeLong, R. and Douglas, W., 1997. Variation in tooth wear in young adults over a two-year period. *Journal of Prosthetic Dentistry*, 77 (3): 313-320.
- Pintado, M., DeLong, R., Ko, C.-C., Sakaguchi, R. and Douglas, W., 2000. Correlation of noncarious cervical lesion size and occlusal wear in a single adult over a 14 year time span. *Journal of Prosthetic Dentistry*, 84 (4): 436 - 443.
- Piotrowski, B., Gillette, W. and Hancock, E., 2001. Examining the prevalence and characteristics of abfraction-like cervical lesions in a population of U.S. veterans. *Journal of the American Dental Association*, 132 (12): 1694-1701.
- Piwowarczyk, A., Ottl, P., Buchler, A., Lauer, H. and Hoffmann, A., 2002. In vitro study on the dimensional accuracy of selected materials for monophasic elastic impression making. *International Journal of Prosthodontics*, 15 (2): 168-174.
- Poynter, M. and Wright, P., 1990. Tooth wear and some factors influencing its severity. *Restorative Dentistry*, 6 (4): 8-11.
- Price, R., Gerrow, J., Sutow, E. and MacSween, R., 1991. The dimensional accuracy of 12 impression material and die stone combinations. *International Journal of Prosthodontics*, 4 (2): 169-174.
- Quick, D. and Holtan, J., 1991. Use of a scanning laser three-dimensional digitizer for analysis of dental materials. *Biomedical Instrumentation and Technology*, 25 (1): 60-67.

- Rees, J., 1998. The role of cuspal flexure in the development of abfraction lesions: a finite element study. *European Journal of Oral Sciences*, 106 (6): 1028-1032.
- Rees, J., 2000. A review of the biomechanics of abfraction. *European Journal of Prosthodontics and Restorative Dentistry*, 8 (4): 139-144.
- Roulet, J., Reich, T. and Lutz, F., 1983. High precision occlusal mapping: a new method for measuring wear of posterior composites. *Journal of Dental Research*, (Special Issue) 62: (Abstract Number 457) 220.
- Ryge, G. and Snyder, M., 1973. Evaluating the clinical quality of restorations. *Journal of the American Dental Association*, 87: 369-378.
- Scott, P., 1981. The reflex plotters: measurement without photographs. *Photogrammetric Record*, 10 (58): 435-446.
- Shearer, B., Gough, M. and Setchell, D., 1996. Influence of marginal configuration and porcelain addition on the fit of In-Ceram crowns. *Biomaterials*, 17 (19): 1891-1895.
- Shortis, M., Robson, S. and Beyer, H., 1998. Principal point behaviour and calibration parameter models for Kodak DCS cameras. *Photogrammetric Record*, 16 (92): 165-186.
- Smith, B. and Knight, J., 1984. A comparison of patterns of tooth wear with aetiological factors. *British Dental Journal*, 157 (1): 16-19.
- Smith, B. and Robb, N., 1996. The prevalence of tooth wear in 1007 dental patients. *Journal of Oral Rehabilitation*, 23: 232-239.
- Sognnaes, R., Wolcott, R. and Xhonga, F., 1972. Dental erosion. I. Erosion-like patterns occurring in association with other dental conditions. *Journal of the American Dental Association*, 84 (3): 571-576.
- Sohmura, T., Kojima, T., Wakabayashi, K. and Takahashi, J., 2000. Use of an ultra high-speed laser scanner for constructing three-dimensional shapes of dentition and occlusion. *Journal of Prosthetic Dentistry*, 84 (3): 345-352.

- Speculand, B., Butcher, G. and Stephens, C., 1988. Three-dimensional measurement: The accuracy and precision of the reflex microscope. *British Journal of Oral Maxillofacial Surgery*, 26: 276-283.
- Stinson, M. and Lawton, B., 1989. Specification of the geometry of the human ear canal for the prediction of sound-pressure level distribution. *Journal of the Acoustical Society of America*, 85 (6): 2492-2503.
- Thoma, K. and Robinson, H., 1955. *Oral and dental diagnosis*. WB Saunders Company, Philadelphia.
- Thomas, P., Newton, I. and Fanibunda, K., 1996. Evaluation of low cost digital photogrammetric system for medical applications. *International Archives of Photogrammetry and Remote Sensing*, 31 (PartB5): 405-410.
- Toreskog, S., Phillips, R. and Schnell, R., 1966. Properties of die materials: a comparative study. *Journal of Prosthetic Dentistry*, 16: 119-131.
- Ungar, P. and Williamson, M., 2000. Exploring the effects of toothwear on functional morphology: a preliminary study using dental topographic analysis. *Palaeontologia Electronica*: 3 (1): 18 pages
- van der Zel, J., Vlaar, S., de Ruiter, W. and Davidson, C., 2001. The CICERO system for CAD/CAM fabrication of full-ceramic crowns. *Journal of Prosthetic Dentistry*, 85 (3): 261-267.
- Vanuspong, W., Eisenburger, M. and Addy, M., 2002. Cervical tooth wear and sensitivity: erosion, softening and rehardening of dentine; effects of pH, time and ultrasonication. *Journal of Clinical Periodontology*, 29: 351-357.
- Verdonschot, N., Fennis, W., Kuijs, R., Stolk, J., Kreulen, C. and Cregers, N., 2001. Generation of 3-D finite element models of restored human teeth using micro-CT techniques. *International Journal of Prosthodontics*, 14 (4): 310-315.
- Vollmer, D., Meyer, U., Joos, U., Vègh, A. and Piffko, J., 2000. Experimental and finite element study of a human mandible. *Journal of Craniomaxillofacial Surgery*, 28 (2): 91-6.

- Watson, T., 1997. Fact and artefact in confocal microscopy. *Advances in Dental Research*, 11 (4): 433-441.
- White, I., McIntyre, J. and Logan, R., 2001. Studies on dental erosion: an in vitro model of root surface erosion. *Australian Dental Journal*, 46 (3): 203-207.
- Wilson, I., Snape, L., Fright, R. and Nixon, M., 1997. An investigation of laser scanning techniques for quantifying changes in facial soft-tissue volume. *New Zealand Dental Journal*, 93: 110-113.
- Xhonga, F. and Sognnaes, R., 1973. Dental erosion: progress of erosion measured clinically after various fluoride applications. *Journal of the American Dental Association*, 87 (6): 1223-1228.
- Xhonga, F. and Valdmanis, S., 1983. Geographic comparisons of the incidence of dental erosion: a two centre study. *Journal of Oral Rehabilitation*, 10 (3): 269-277.
- Xhonga, F., Wolcott, R. and Sognnaes, R., 1972. Dental Erosion II. Clinical measurements of dental erosion progress. *Journal of the American Dental Association*, 84 (3): 577-582.

Chapter 3

Aim and objectives

The aim of the research applied in this thesis is to develop and implement a method for photogrammetric mapping of non-carious cervical lesions (NCCLs) that is sufficiently accurate and efficient to enhance the study of their rate and distribution of change.

The objectives of the research are:

- 3.1 to demonstrate the photogrammetric modelling potential of an experimental casting material that incorporates optical texture, utilising a single film-based camera and digital photogrammetry software to generate 3D surface models of tooth replicas (Chapter 5),
- 3.2 to investigate convergent camera geometries and the effects of calibration errors using a high-resolution SLR digital camera and customised fixed focal length lens, and a test object fabricated from the casting material incorporating optical texture, together with photogrammetric simulation software (Chapter 6),
- 3.3 to assemble and test an experimental fixed base stereo digital camera and calibration artefact to be used for semi-automatic generation of 3D surface models of tooth replicas incorporating optical texture (Chapter 7),
- 3.4 to investigate alignment of a tooth surface model obtained with the fixed base stereo camera and photogrammetry software, including the effects of alignment variables, upon the repeatability and precision of mapping and alignment (together) and the alignment (alone) (Chapter 8), and
- 3.5 to investigate change detection of NCCLs over a one and two year period using two lesions, from two patients, that are of significantly differing appearance and occupy a significantly different proportion of the surface area of their respective tooth surfaces (Chapter 9).

Chapter 4

Preliminary investigations into the provision of optical texture on tooth replicas.

This chapter describes a series of preliminary trials of materials intended to achieve an optical texture suitable on teeth for photogrammetric image matching. These trials were not conducted in a systematic way and the details are presented in a narrative form. A detailed description of the calibration and photogrammetry methods used in this chapter appears in the later chapters.

The trials commenced with preparation of plaster casts poured from impressions of un-named dental casts, the application of particles to create optical texture and the use of clinical video cameras. They then progressed to the use of epoxy resin incorporating optical texture and film based photography. Prior to the commencement of this thesis, patients were recruited, by the author, for a long-term study to monitor the progression of NCCLs. This study was conducted through the School of Dental Science, University of Melbourne, with ethics approval given by the Ethics in Clinical Research Committee, Dental Health Services Victoria, approval No 161. Patients were free to participate or to withdraw from the project at any time without prejudice to any treatment. Impressions of dental arches of several patients were taken, diestone casts were poured and mapping procedures performed in accordance with the approval. Some impressions were re-poured with modified epoxy resin, also in accordance with the ethics approval. Some of the preliminary trials, and work reported later in this thesis, were conducted with impressions obtained from this patient group.

4.1 Trials with plaster replicas

In a series of preliminary trials, the author utilised plaster models and materials at hand in his private practice to achieve an optical texture on tooth replica surfaces. Various light curable dental resin polymers were applied to plaster cast surfaces with a small brush and 50 μm aluminium oxide powder applied into the moist polymer with an artist's airbrush. A large volume of resin was required to overcome the porous nature of the plaster. Application of aluminium oxide onto standard white or yellow dental plaster and/or dental stone did not result in a readily visible texture on the surface. To provide a plaster cast of contrasting colour, black water-based pigment was added to plaster during mixing and a new model poured. Despite the porous nature of the set plaster cast, multiple applications of resin and airbrushing with powder resulted in a suitable texture (Figure 4.1). The image shown in Figure 4.1 was taken with an intraoral video camera with a sensor size of 640 x 480 pixels (Cygnascope COS-235; Cygnus Instruments, Inc. Goleta, California).

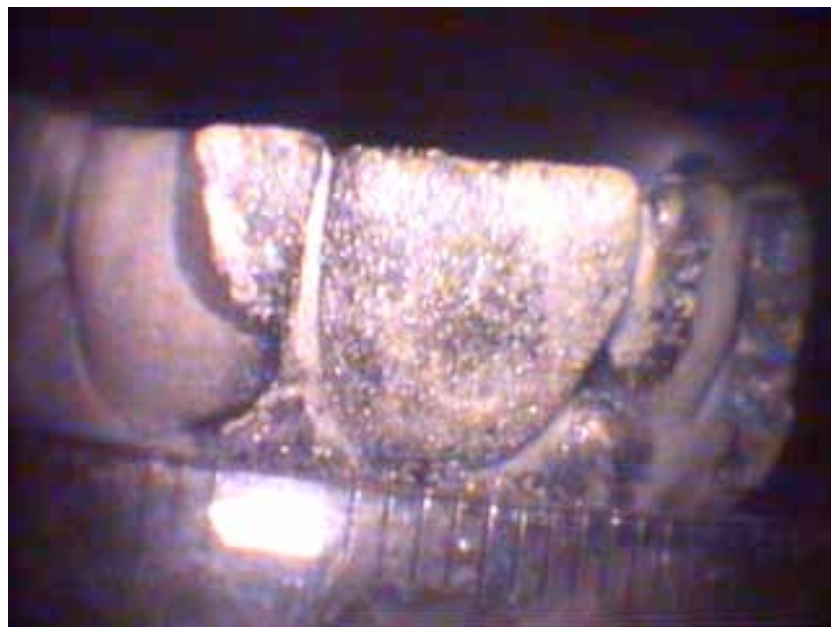


Figure 4.1. Plaster model, coloured with black pigment, enamel bonding resin, 50 μm aluminium oxide applied with air brush, imaged with intra oral video camera (Cygnascope COS-235; Cygnus Instruments, Inc.).

A calibration array was fabricated from a piece of 5 mm thick glass, coated with black paint, then scored with an 8 x 8 grid of lines. The grid lines were approximately 3.5 mm apart and were approximately 20 μ m wide (Figure 4.2). The coordinates of grid intersections on the array were measured using a stereocomparator (Stecometer; Carl Zeiss Jena, Oberkochen, Germany). The calibration array was transilluminated and imaged with the video camera. Camera calibration was performed using multiple convergent photography of the planar array and a MATLAB toolbox based on the method of Heikkilä and Silvén (1997). The computed focal length was 14.12 mm. Values of calibration parameters appear in Table 4.1. A description of the method of Heikkilä and Silvén (1997) and description of the parameters appears in Chapter 5, page 74.

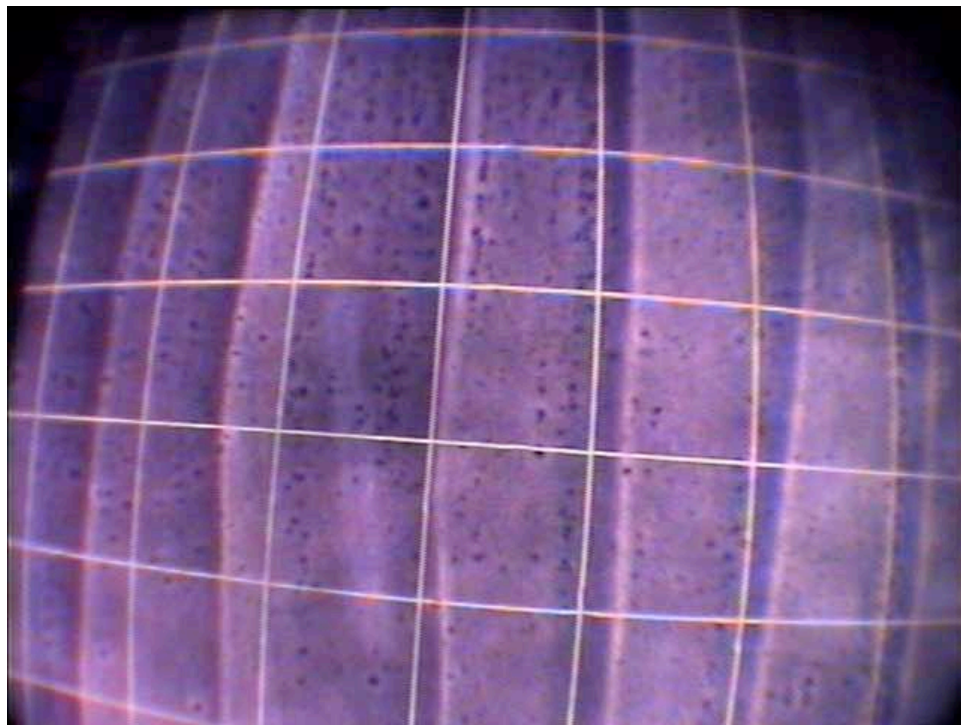


Figure 4.2. Calibration array used to calibrate the intraoral camera, grid line interval approximately 3.5 mm.

Parameter	Value	Error
Effective focal length (mm)	14.117	5.22×10^{-2}
Principal point offset: x (mm)	-0.2236	8.78×10^{-1}
y (mm)	1.1149	7.99×10^{-1}
Radial distortion, k_1 (mm)	-2.0343×10^{-3}	5.55×10^{-6}
Radial distortion, k_2 (mm)	3.4824×10^{-6}	3.22×10^{-8}
Tangential distortion, p_1 (mm)	3.5490×10^{-4}	2.16×10^{-5}
Tangential distortion, p_2	4.3618×10^{-5}	1.89×10^{-5}

Table 4.1. Camera calibration parameters of the intraoral video camera (Cygnascope COS-235; Cygnus Instruments, Inc.).

A control array was constructed from clear perspex with an opening cut into the centre to enable imaging of the tooth surface below, and control point marks scored at the four corners of the opening (Figure 4.3). Illumination was provided by the video camera and was not adjustable. Images were acquired with a translation of approximately 5 mm between left and right images and were captured with a video capture card in a desktop computer. A photogrammetric model was formed with photogrammetry software (VirtuoZo, version 3.3; Supersoft Inc., Wuhan, China) and, following relative and absolute orientation, a model was formed. It can be seen in Figure 4.3 that the majority of the texture that appears on the tooth surface in Figure 4.1 has been lost.



Figure 4.3. Image of tooth replica positioned under control grid with control points at corners of opening.

Coordinate data were imported into visualisation and analysis software (Surfer, version 6.04; Golden Software Inc., Golden, Colorado, USA) (Figure 4.4). The data generated from the photogrammetry software was clearly a tooth surface, however it was of insufficient quality for analysis, in large part due to the low resolution of the camera and the poor image quality.

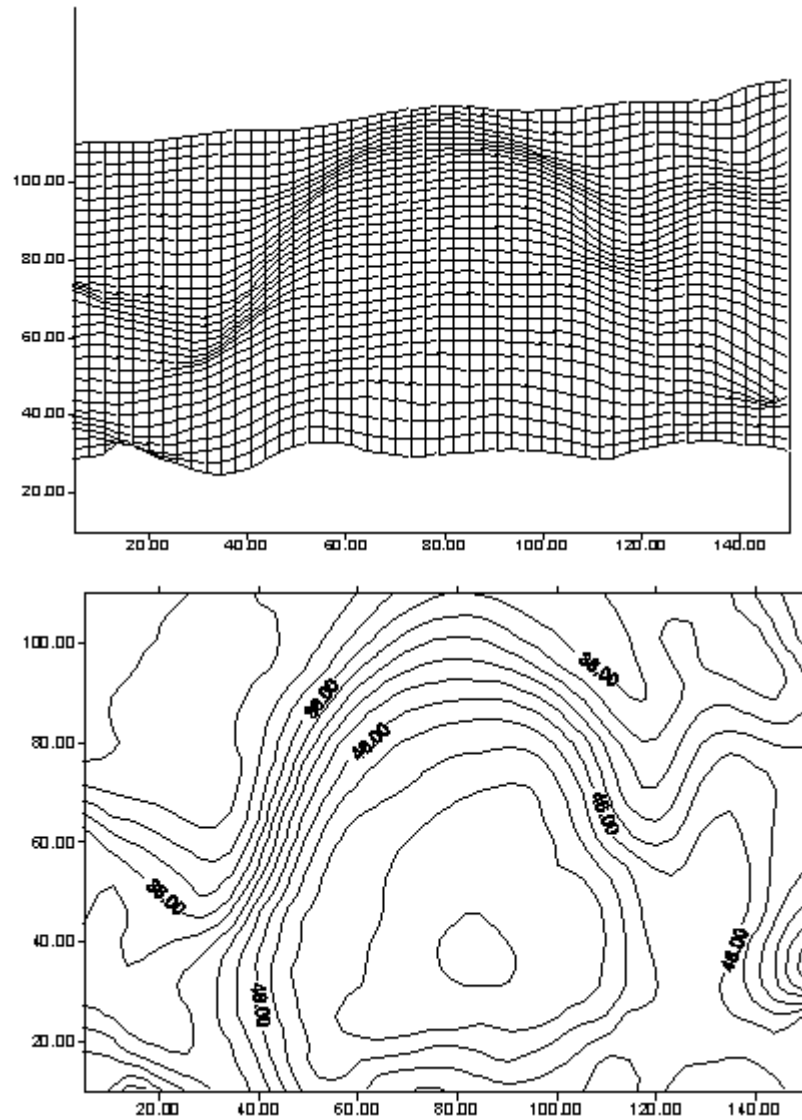


Figure 4.4. Wireframe and contour map of tooth surface.

The method of applying texture to casts was not durable, with loss of the aluminium oxide particles a constant impediment to repeat imaging and photogrammetric modelling of the same prepared replica. Figure 4.5 shows application of a resin polymer and aluminium oxide powder to another tooth surface of the same cast used in Figure 4.1. Clumping of the powder is evident and further work with this approach was abandoned.



Figure 4.5. Plaster model, coloured with black pigment, enamel bonding resin, 50 µm aluminium oxide applied with air brush. Imaged with video otoscope (MAICO-Vision MV10; MAICO Diagnostics GmbH, Rohrdamn, Germany).

In further trials, coloured particles of various sizes up to 2 mm in diameter were added to gypsum products used for creating dental casts, with the intention of achieving a surface optical texture suitable for automatic photogrammetric mapping. These were unsuccessful, with the particles not appearing on the surface of the casts.

4.2 Trials with epoxy resin

The addition of particles to epoxy resin casting material was also tested. Epoxy resin casting material is used for the fabrication of tooth replicas in the dental laboratory, although less frequently than gypsum products. Titanium oxide paint colourant obtained from a paint manufacturer (titanium dioxide mixed into a paint solvent) and coloured particles of various sizes up to 2 mm in diameter were added to an epoxy resin casting material (Daystar Australia P/L, Dandenong, Victoria, Australia). The titanium dioxide was

added for the purpose of providing contrast to the coloured particles and to render the material opaque. The resulting replicas were imaged with a 35 mm format semi-metric camera (Leica R5 Elcovision; Ernst Leitz Wetzlar GmbH, Wetzlar, Germany) fitted with a macro lens and 50 mm macro lens adapter (Macro-Elmar, $f = 100$ mm) (Leica R5 Elcovision; Ernst Leitz Wetzlar GmbH, Wetzlar, Germany), achieving its maximum photoscale reduction of $\times 2$ at an estimated object distance of 148 mm (Figure 4.6). The reseau marks in Figure 4.6 are on a glass plate in the focal plane of the camera and are incidental to the image. Their purpose as a part of photogrammetric method is referred to in Chapter 5, page 75. Illumination was provided by 12 volt halogen, fibre-optic 'swan lights' at a higher voltage leading to a 'whiter' image when photographed with 'daylight' film.



Figure 4.6. Epoxy resin replicas containing titanium oxide paint colourant and coloured particles. Image acquired with Lieca R5 Elcovision and macro lens, at a photoscale of $\times 2$ and swan halogen lighting.

The volume of paint solvent accompanying the titanium dioxide, when added to the epoxy resin, resulted in a dilution of the volume of coloured particles. While this replica could be used for photogrammetric image

matching, an increased density of coloured particles on the surface of replicas was likely to be achieved by eliminating the paint solvent from the casting mixture. Tooth replicas were poured with epoxy casting resin (Daystar Australia P/L, Dandenong, Victoria, Australia) and modified with the addition of titanium dioxide powder and coloured particles of various sizes up to 2 mm in diameter (Figure 4.7). The use of this 100 mm macro lens did not maximise the photoscale of imaging of one or two teeth with the 35 mm camera.



Figure 4.7. Epoxy resin replicas containing titanium oxide powder and coloured particles. Image taken with Lieca R5 Elcovision, 100mm macro lens, at a photoscale of x2 and swan halogen lighting.

A 100 mm macro prime lens was fitted to bellows at maximum extension and an additional 50 mm extension tube, and found to provide a photographic magnification of 1.6x, and a field of view of approximately 22 mm x 14 mm. This lens arrangement was used for further trials and was subsequently used in the work reported in Chapter 5. Images of the camera setup appear in the appendix to Chapter 5.

The first tooth surface replica from the long term study patient group appears in Figure 4.8. There is a NCCL present in the gingival one-third of the tooth, indicated with a black arrow. The NCCL is clearly visible in the image, however texture in the region of the NCCL may not be as dense as desired. Although the replica had a base colour of white, halogen lighting and daylight film has resulted in the yellow overall appearance.

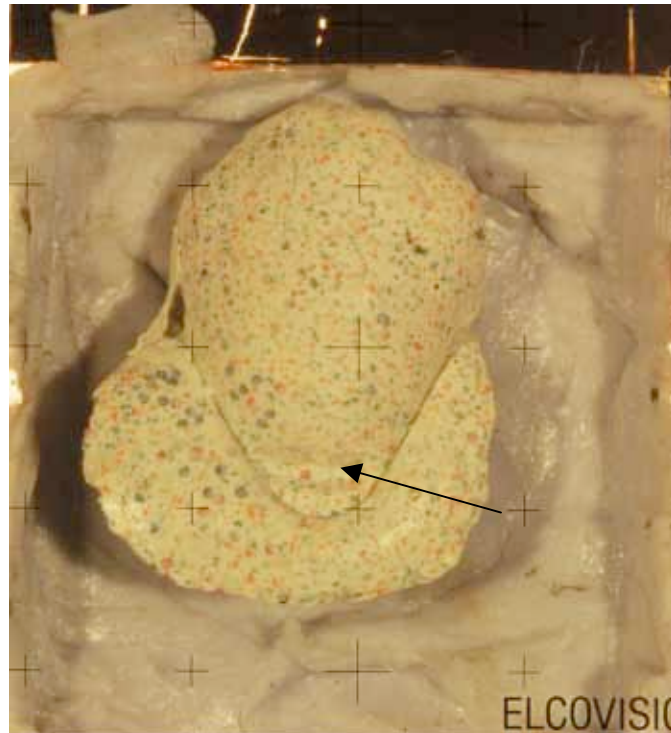


Figure 4.8 Lower premolar tooth with NCCL. Leica R5 Elcovision, 100mm lens on bellows, halogen lighting. Black arrow: NCCL.

A second tooth surface replica from this patient group appears in Figure 4.9. There is a NCCL present in the gingival one-third of the tooth. This replica was prepared with a brown tint to darken the overall colour of the replica and a single colour of finer particles has been used. The image below reveals a finer particle texture than the preceding images, however despite being 'opaque', it would be expected that the surface would contain some optical translucency to a depth of 5 to 10 μm . Tooth orientation is such that there is some shadowing at the base of the lesion (black arrow).



Figure 4.9. Lower left molar tooth replica, buccal surface with NCCL.

The occlusal surface of the same tooth appears in Figure 4.10. This tooth has a moderate amalgam filling on the occlusal surface, extending onto the mesial surface (left in image). The margins of the amalgam restoration are visible in the mesial area. Photogrammetric models of this surface were generated, however the extent to which this margin could be mapped was not explored.

A test object was also required to verify the accuracy of the tooth replica models. A test object was machined from a block of epoxy resin modified as described above. It was machined to contain three planes and three diameters. The approximate dimensions of this object were the same as another object fabricated from hardened steel and described in the Chapter 5. Close examination of images of this test object revealed gross surface defects where particulate material had been gouged from the surface, which limited its usefulness (Figure 4.11).



Figure 4.10. Lower left molar tooth replica, occlusal surface with restoration present.

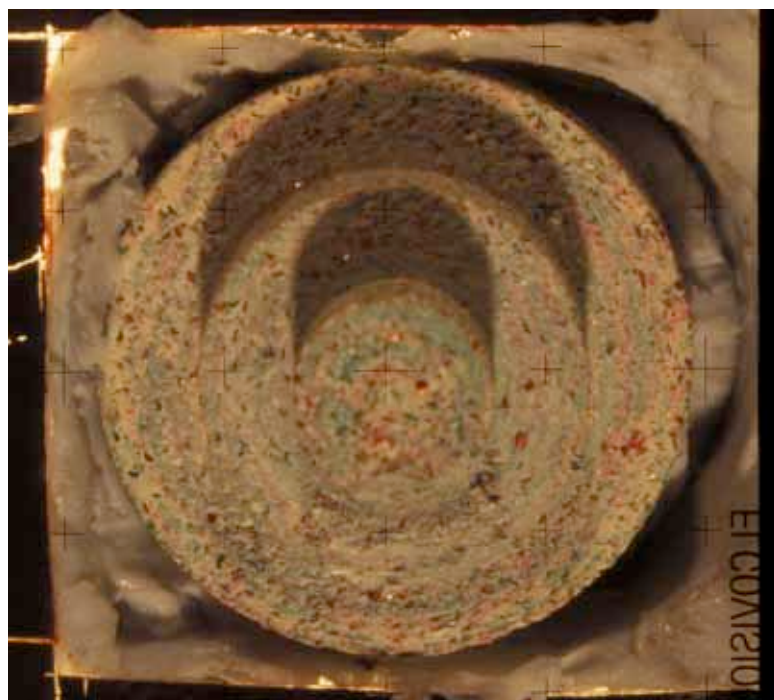


Figure 4.11. Machined test object fabricated from modified epoxy resin.

4.3 Camera systems

A number of camera/ lens combinations was trialled. As noted above, a 100 mm Macro Elmarit lens with macro lens adapter produced a maximum photoscale (reduction) of x2. A 50 mm Macro Elmarit lens was also trialled, however this lens resulted in a very short working distance from lens to object with insufficient distance for adequate illumination. Trial photos were taken with a camera used for dental clinical photography, an Elicar MS-10 film camera fitted with a V-HQ medical macro MC 90 mm lens and ringflash. At full extension, a magnification of 1x was achieved at a working distance of 180 mm. The lens assembly contained a helical lens mount for changing the photoscale and focussing. However, there was no mechanism to rigidly fix the amount of extension and the magnification could not be reliably maintained.

Digital cameras trialled included the Olympus C-2500 L. This camera included a 'super macro' setting and autofocus, neither of which operated efficiently. A Canon EOS D60 SLR digital camera with 100 mm macro lens and ringflash was trialled. This clinical camera captured 6.3 megapixel images at a maximum photoscale of 1x and a field view of 22 mm x 15 mm. Through-the-lens metering operated effectively. This camera had the same sensor as a later model camera described elsewhere in this thesis.

4.4 Conclusion

During a series of preliminary investigations, optical texture was successfully incorporated into epoxy resin tooth replicas. A semi-metric film camera fitted with a 100 mm macro prime lens on bellows and a further 50 mm extension was shown to provide suitable images for future work.

Chapter 5

Stereo-photogrammetric mapping of tooth replicas incorporating texture

A manuscript prepared for submission to the *Photogrammetric Record*

Published in *Photogrammetric Record*, 20(110): 147–161 (June 2005)

M. J. Grenness, The University of Tasmania,

J.E. Osborn, The University of Tasmania,

M. J. Tyas, The University of Melbourne,

Recipient of E. H. Thompson Award,

(Remote Sensing and Photogrammetry Society, UK, September 2007)

Abstract

Commercial digital photogrammetric software has been applied to convergent stereoscopic photography of human tooth replicas prepared to exhibit optical texture resulting in successful generation of 3D coordinate data. Tooth replicas were imaged using a semi-metric 35 mm camera and $f = 100$ mm macro lens on extension bellows. Model precision was within acceptable limits of 12 μm or better for manual target matching and 21 μm or better for automatic image matching. Further improvement in optical texture is required to achieve automatic image matching precision comparable to that of manual target matching. Small errors in interior orientation parameters attributed to instability in the bellows as well as small errors in the relative orientation resulted in some systematic errors. The use of a fixed camera lens system is expected to reduce these errors. When combined with commercially available, moderately priced, digital SLR cameras this brings 3D model generation closer to everyday clinical dental practice.

Keywords: dental mapping, digital photogrammetry, tooth surface mapping

5.1 Introduction

In dental research and clinical practice 2D representations or images are frequently required in order to aid diagnosis, analysis, communication with third parties, and for documentation and educational purposes (Haak and Schirra, 2000; Phelan, 2002). The acquisition of 3D models and data has, with some notable exceptions, been largely confined to the research arena. Generation of 2D images and 3D models for dentistry fall into three broad categories: facial, full dental arch and single tooth.

Imaging of single teeth is relevant to the documentation, monitoring and study of tooth surface loss (Xhonga et al., 1972), restoration performance and degradation (Roulet et al., 1983), 3D finite element analysis modelling (Palamara et al., 2000) and for the mapping of prepared teeth for computer-aided-design/computer assisted manufacture (CAD/CAM) restorative processes (Leinfelder et al., 1989). Laser scanning of tooth replicas has become commonplace since the mid-1990s (Azzopardi et al., 2001; Folwaczny et al., 2000; Mehl et al., 1997; Perry et al., 2000). Traditional photography has been used to aid in the diagnosis of tooth surface loss (erosion) on anterior teeth with limited success (Al-Malik et al., 2001), photography of light-induced fluorescence to detect dental caries has been trialled (Buchalla et al., 2002), and cross-polarised photography has been used to aid in the detection of enamel defects (Robertson and Toumba, 1999). Laser scanning of prepared teeth as a part of CAD/CAM procedures in the dental laboratory has become commonplace (van der Zel et al., 2001). A system (CEREC; Sirona Dental Systems GmbH, Bensheim, Germany) based on structured light and a charge-coupled device (CCD) camera has been developed for the capture and generation of 3D coordinate data from prepared teeth directly in the mouth as a part of a CAD/CAM system for the production of milled restorations. Accuracy of 25 μm is reported by the manufacturer (Leinfelder et al., 1989; Markowski, 1990; Mou et al., 2002; Parsell et al., 2000), although this may be reduced significantly due to the requirement for powdering the

tooth prior to imaging (Kurbad, 2000). Stereo- photogrammetric applications have been reviewed by (Chadwick, 1992) (for example, (Chadwick et al., 1991; Clarke et al., 1974; Lamb et al., 1987; Mitchell et al., 1989); however , the method has not found general utility or acceptance. Accuracies for all methods of 4 to 20 μm are reported (Chadwick et al., 2002; Mehl et al., 1997; Peters et al., 1999).

There is a need for high accuracy, in the order of 10 to 50 μm , in clinical mapping of teeth in order to monitor the development and progression of tooth wear and surface defects and lesions. This would enable better clinical decisions about the need and effectiveness of potential therapies, varying from the use of remineralisation preparations, surface coatings and varnishes through to restoration of the tooth surface with long-lasting restorative materials. There are presently no standards or criteria for accuracy and precision of clinical tooth mapping for monitoring purposes. A recent review of the techniques to measure tooth wear and erosion (Azzopardi et al., 2000) concluded that all current techniques were confined to the laboratory and that there was a need for a simple, reliable technique for clinical use. Digital photogrammetric techniques can produce accurate 3D models using traditional photography provided adequate surface optical texture is present on the surface of the object (Mitchell et al., 1999). Optical texture can be employed using structured light and a single camera (Leinfelder et al., 1989), unstructured light and two cameras (Dirksen et al., 2001), or targets applied in a thin film to the surface (Osborn and Wise, 1996). The incorporation of targets into the material used to produce tooth replicas has not been reported.

This paper describes the incorporation of optical texture incorporated into single tooth replicas, the use of digital stereo-photogrammetry to generate 3D surface models of the replicas, and presents the results of accuracy and precision testing.

5.2 Method

5.2.1 Preparation of Tooth Replicas and Photo Control

All teeth of a 45-year-old male patient were polished with polishing paste and a rubber cup. Upper and lower medium viscosity polyvinylsiloxane impressions (Reprosil; Dentsply International Inc., Milford, DE) were taken in custom made impressions trays and individual tooth replicas of teeth to be studied were poured with an epoxy casting resin (Daystar Australia P/L, Dandenong, Victoria, Australia) modified with the addition of TiO₂ powder and coloured particles of various sizes up to 2 mm in diameter. Tooth replicas were placed onto a recessed area of a planar control grid of black film (Lithfilm; Agfa-Gevaert, Belgium) with eight transparent control points of 40 µm diameter present at the right and left sides of the field of view (Figure 5.1). The control grid was produced by exposing a grid of black spots of 250 µm diameter¹ on a 25 mm grid onto film with a vector plotter (Protel P/L, Hobart, Tasmania, Australia). The resulting photoplot was photographed with a process camera at a photographic reduction of approximately 6x onto film, which after developing was fixed to a 5-mm glass slab with adhesive (Photo Mount; 3M Australia P/L, Sydney, NSW, Australia). The X and Y coordinates of the spots were measured with a stereocomparator (Stecometer; Carl Zeiss Jena, Oberkochen, Germany) at a measurement precision of 2.5 µm, and the Z coordinates were given an arbitrary constant value.

¹ The transparent control points were designed to be between 6 and 11 pixels of the scanned film images. This conforms to empirical data showing that target centroiding improves for targets between 6 and 11 pixel diameters (Beyer HA. Advances in characterisation and calibration of digital imaging systems. Paper presented at: International Archives of Photogrammetry and Remote Sensing XVII Congress, 1992; Washington DC.). Images taken with 35 mm film, at a magnification of 1.6x and scanned at a resolution of 10 mm have a pixel size 'on the ground' of (10/1.6) 6.25 mm. A target size of 40 mm equates to (40/6.25) 6.4 pixels, and falls within the optimum target size range.

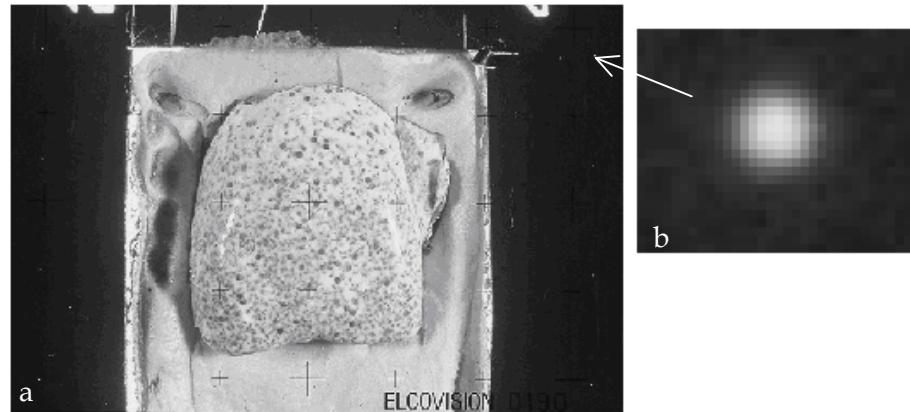


Figure 5.1. (a) Scanned image of tooth replica positioned on control grid with control points at right and left edges of image. (b) Enlargement of a control point.

5.2.2 Image Acquisition and Camera Calibration

The replicas and control grid were placed into a tilting light stage and were photographed with a 35 mm format semi-metric camera fitted with a macro lens ($f = 100$ mm) on extension bellows (Leica R5 Elcovision; Ernst Leitz Wetzlar GmbH, Wetzlar, Germany), achieving a magnification of 1.6x, and ASA400 slide film (Sensa 400; Fuji Photo Film Co. Ltd., Tokyo, Japan) at convergence angles of approximately 5, 10, 15, 20 and 25 degrees (Appendix Figure 5.6, pp.97). Processed film was scanned at a resolution of $10\text{ }\mu\text{m}$ using a film scanner (Super Coolscan 4000; Nikon Corp., Tokyo, Japan). Camera calibration was performed using multiple convergent photography of a planar array and a MATLAB toolbox based on the method of Heikkilä and Silvén, (1997). The toolbox used a direct linear transformation to compute initial values for all but the lens distortions, prior to an iterative least squares solution to a non-linear model that includes lens distortions. The method generated values for focal length, principal point of symmetry, radial (k_1, k_2) and decentring (p_1, p_2) lens distortions and a scaling factor. A planar array of 24 points of $40\text{ }\mu\text{m}$ diameter and spaced at approximately 4 mm intervals was exposed onto film using the method described earlier and the coordinates of points on the array were measured using the

stereocomparator as above. Two sets of multi-station photographs were taken with one view taken perpendicular to the calibration array and four quadrant views² taken at divergent angles of 7.5° for the first set and 10° for the second set. Between each view the lens aperture was opened to check placement of the calibration array.

5.2.3 Image matching³ and generation of 3D coordinate data

Digitised images of the tooth replicas were imported into the digital photogrammetric workstation software (VirtuoZo, version 3.3; Supersoft Inc., Wuhan, China), control point coordinates were entered in micrometres and camera calibration parameters including radial lens distortion data were also entered. Interior orientation was performed using reseau marks within the camera; exterior orientation was performed using up to eight control points and up to seven additional image-matched points from the tooth replica. Epipolar resampling, automatic image matching [Appendix Figure 5.7, pp.98], minor editing of matched points at the edges of the tooth stereomodel and automatic generation of 3D coordinate digital elevation model (DEM) on a 65 µm x 65 µm grid were performed. Coordinate data were imported into visualisation and analysis software (Surfer, version 6.04; Golden Software Inc., Golden, Colorado, USA).

5.2.4 Accuracy and precision testing

Accuracy was assessed using relative orientation y parallax error data from matched control and relative orientation points in image space coordinates, absolute orientation error data from matched control points in object space coordinates, and measurements from a test object. The object was machined from hardened steel on a lathe with three circular planes (Figure 5.2). The heights of the planes from the base of the object, and diameters, were

² Quadrant views: views from each side or corner of the calibration array.

³ Image matching techniques are described in Chapter 5, Appendix, pp. 98.

measured with a hand-held micrometer⁴. The test object was replicated as above, photographed at convergence angles of 5, 10, 15, 20 and 25 degrees [Appendix Figure 5.8, pp. 98] and, following photogrammetric processing, a DEM was generated in VirtuoZo [Appendix Figures 5.9, 5.10, pp. 99]. The mid-plane of the test object was assigned the value of the mean of the mid-plane values determined from the epoxy replica (calculated from stereomodels) and the top and lower plane values adjusted accordingly. Differences between the micrometer and calculated heights were also determined. The diameter of each plane was determined by extracting 10 points on the circumference of each plane manually in VirtuoZo-IGS *digitize* and using a least-squares circle fit algorithm to determine the diameter of the circle created by the points. The height of a point at the centre of each plane was computed from the least-squares solution of the equation of a plane of best fit using 3D coordinate data extracted from the DEM, with outliers exceeding $\pm 75 \mu\text{m}$ occurring at the rise between each plane excluded.

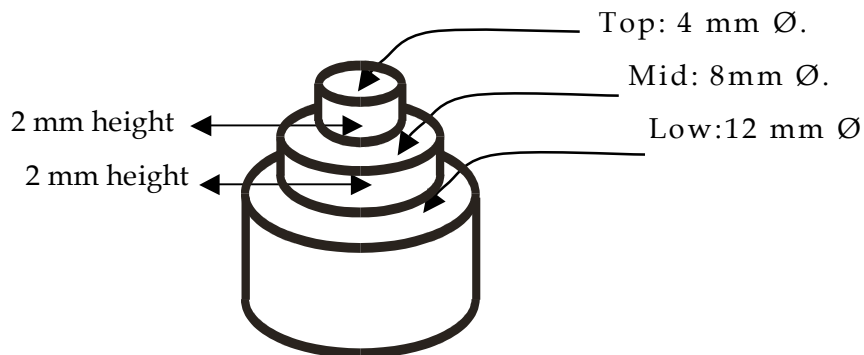


Figure 5.2. Test object with three circular planes and rises resulting in three heights and three diameters.

The precision of automatic image matching was assessed by extracting a small section (1.5 mm x 2 mm) of coordinate data from the top plane of each

⁴ Outside micrometer, 103-129, 0 – 25 mm; Mitutoyo, Japan.

Height and diameter measurement were taken 10x, and mean and standard deviations calculated.

DEM and determining the standard deviation of the z coordinate from the plane determined by the least squares plane fit algorithm. The location of the small section was selected to exclude the edge of the plane, shadows and reseau marks. No outliers were removed from these data sets. The effect of varying patch window size and match grid interval upon automatic image matching was examined for the convergence angle of 5° . DEMs were generated for each combination of patch size and grid interval and the same $1.5 \text{ mm} \times 2 \text{ mm}$ section was extracted from the data-sets and the standard deviation of the z coordinates fitted to a plane was calculated. The precision of manual image matching was also assessed by extracting 20 points from the top plane of each DEM manually in *VirtuoZo-IGS digitize* and determining the standard deviation of the z coordinate from the plane determined by the least squares plane fit algorithm. The precision the measurements was compared with expected precision formulae (Karara and Abdel-Aziz, 1974). Exterior orientation was performed multiple times upon a pair of images following re-measurement of control and image points to test the stability of the photogrammetric solution generated by the digital photogrammetric workstation software.

5.3 Results

5.3.1 Camera Calibration

The results of the calibration of the camera lens are presented in Table 5.1. Parameters k_1 and k_2 are coefficients of radial distortion to the second and fourth radial power. These coefficients resulted in maximum radial lens distortion of $-8.11 \text{ }\mu\text{m}$ at a radius of 22 mm (the corner of the image) from the centre of the image for the 7.5° divergent set. Maximum radial distortion for the 10° divergent set was $-8.29 \text{ }\mu\text{m}$. Focal length for the two series varied by almost 1 mm and the location of the principal point varied between approximately 0.3 and 0.4 mm. The focal length and principal point values from the 7.5° divergence series of calibration images were used for subsequent photogrammetric processing.

Parameter	7.5° divergence	10° divergence
Effective focal length (mm)	246.0	245.2
Principal point: x, y (mm)	-3.605, -3.876	-3.204, -4.1667
Radial distortion, k_1 (mm)	-1.671×10^{-6}	-1.821×10^{-6}
Radial distortion, k_2 (mm)	1.879×10^{-9}	2.155×10^{-9}
Maximum radial distortion (μm)	-8.11	-8.29

Table 5.1. Camera calibration parameters of the semi-metric camera and 100 mm macro lens on extension bellows at magnification of 1.6x.

5.3.2 Accuracy

Relative orientation parameters, y parallax error data and absolute orientation control point error data from VirtuoZo for the different convergence angles of the test object replica appear in Table 5.2. The y parallax error data (an assessment of image space accuracy) ranged from 3 to 8.5 μm . The control point error data (an assessment of object space accuracy) ranged from 3.3 to 12.3 μm .

The measured height differences of the steel test object and computed height differences of the modified epoxy replica calculated from the DEM generated by VirtuoZo, appear in Table 5.3. The trend of the height error (bottom line of Table 3) varied from -89 to +87 μm and typically reduced as convergence angle increased, although the height error at 5° convergence angle defied the trend. The range of height differences between the planes was between 27 and 46 μm when the 5° convergence data were excluded, giving an indication of overall stereomodel accuracy in the z direction.

<i>Relative orientation parameters</i>					
Nominal Convergence (degrees)	5	10	15	20	25
Calculated convergence (degrees)	5.48	10.32	15.20	20.39	24.40
No. of control and relative points	10	11	15	12	12
<i>y</i> -Parallax RMS error (μm)	5.7	4.8	2.9	2.6	8.5
<i>Absolute orientation parameters</i>					
No. of control points	7	6	8	7	7
<i>x</i> , <i>y</i> standard error (μm)	6.7	6.9	10.0	2.7	7.7
<i>z</i> standard error (μm)	3.3	2.5	7.0	1.8	8.3
<i>x</i> , <i>y</i> , <i>z</i> standard error (μm)	7.5	9.9	12.3	3.3	9.4

Table 5.2. Relative and absolute orientation data derived from test object replica at the different convergence angles.

The steel test object diameters and the modified epoxy replica diameters calculated from the stereomodel generated by *VirtuoZo-IGS digitize* appear in Table 5.4. The range of calculated diameter differences was 34 to 44 μm . The differences between the micrometer measurements and calculated diameters were negative for the top plane above the control point plane and positive for the bottom plane below the control point plane. The absolute mean of the diameter differences was 44 μm , giving an indication of overall stereomodel accuracy in the *x*, *y* plane.

Test object:	Machined steel	Modified epoxy replica					
	Micrometer measurement (mm) (s.d.)	VirtuoZo-DEM calculated height					
		Convergence angle (degrees)					
		5	10	15	20	25	Range
Top plane	4.943 (0.003)	4.906	4.869	4.888	4.866	4.911	0.045
Mid plane	2.970 (0.004)	2.954	2.970	2.977	2.970	2.981	0.027
Lower plane	0.976 (0.003)	0.852	0.991	0.959	0.949	0.945	0.139
Difference between top and lower plane	3.967	4.054	3.878	3.897	3.917	3.966	
Difference between micrometer and computed values		0.087	-0.089	-0.070	-0.050	-0.001	

Table 5.3. Height measurements of the test object and modified epoxy replica: heights and range, differences from the top to bottom plane, and difference in height between test object and the modified epoxy replica, calculated from VirtuoZo-DEM.

Test object:	Machined metal	Epoxy replica					
	Micrometer Measurement (mm) (s.d.)	VirtuoZo-IGS digitize calculated diameter					
		Convergence angle (degrees)					
		5	10	15	20	25	Range
Top plane	4.101 (0.0023)	4.051	4.045	4.040	4.079	4.043	0.039
Mid plane	8.141 (0.0037)	8.079	8.104	8.098	8.123	8.119	0.044
Lower plane	12.192 (0.0046)	12.229	12.234	12.234	12.253	12.242	0.034
Top plane	Difference	-0.050	-0.056	-0.061	-0.022	-0.058	
Mid plane	Difference	-0.062	-0.037	-0.043	-0.018	-0.022	
Lower plane	Difference	0.037	0.042	0.042	0.061	0.050	

Table 5.4. Diameters of the planes of the test object and modified epoxy replica calculated from VirtuoZo-IGS digitize.

The standard deviations of the z coordinates from the data-sets of each plane for the different convergence angles ranged from approximately 20 to 38 μm . To exclude coordinates representing the rise between each plane, outliers $\pm 75 \mu\text{m}$ were removed from the data-sets. This was typically less than 2% of each data-set.

The standard deviations of a small section (1.5 mm x 2 mm) of the top plane at different convergence angles ranged from approximately 11 to 22 μm (Table 5.5).

Test object:	Epoxy replica				
Convergence angle (degrees)	5	10	15	20	25
Top plane standard deviation (μm)	21.81	12.49	16.84	13.87	11.90
Number of points	731	749	740	705	747

Table 5.5. Automatic image matching precision: standard deviations of z coordinates of a section generated automatically from the top plane at different convergence angles.

The standard deviations of 20 x, y, z coordinates extracted manually from the top plane in *VirtuoZo-IGS digitize* at different convergence angles ranged from approximately 5 to 12 μm (Table 5.6).

Test object:	Epoxy replica				
Convergence angle (degrees)	5	10	15	20	25
Top plane standard deviation (μm)	11.44	5.47	7.38	4.99	5.45

Table 5.6. Manual target matching precision: standard deviations of z coordinates of 20 points recorded manually from the top plane at different convergence angles.

The results of varying patch window size and match grid interval upon image matching at a convergence angle of 5° appear in Table 5.7. Standard deviations of z coordinates from a 1.5 mm x 2 mm section of the top plane increased as the patch window size decreased and, as expected were insensitive to changes in patch grid interval.

Patch size (pixels)	15	15	15	25	25	25	35	35	35
Grid interval (pixels)	4	9	15	4	9	15	4	9	15
Top plane s.d. (μm)	66.19	74.33	78.46	31.09	32.11	32.76	25.30	24.98	26.12
No. of points	861	861	861	861	859	845	861	842	840

Table 5.7. The effect of variation of patch window size and grid interval on precision at a convergence angle of 5° .

5.3.3 Surface models

A surface relief of an automatically generated VirtuoZo-DEM (15 degrees convergence) of a central incisor (Figure 5.1) with contour overlay at $100\ \mu\text{m}$ intervals produced in Surfer appears in Figure 5.3. There was no editing of the tooth surface in the *VirtuoZo-Match edit* window prior to DEM generation.

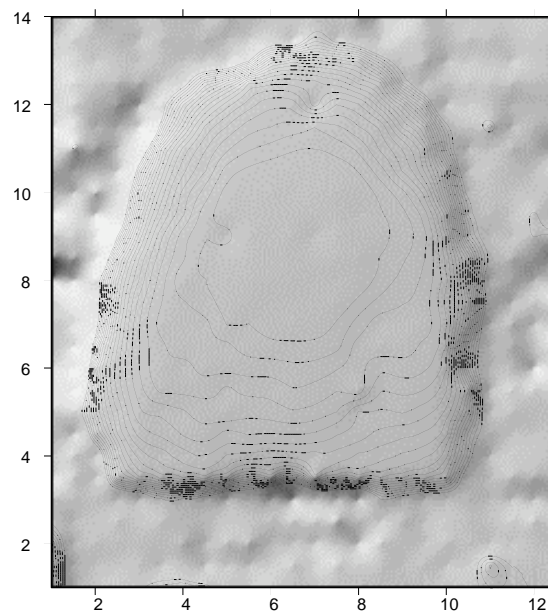


Figure 5.3. Surface relief of central incisor from Figure 5.1 with contour overlay at $100\ \mu\text{m}$ intervals; derived from 15° convergence stereo-photographs, processed with VirtuoZo, automatic image matching, no editing of tooth surface. Gross defects in contour lines co-incide with reseau marks in one of the stereopairs. (x, y scale in millimeters).

5.4 Discussion

Photogrammetric mapping of teeth has suffered from the limited number of recognisable targets on the tooth surface available for triangulation and determination of height values. Solutions to this problem have involved the use of structured light on powdered teeth or replicas, or laser stripe scanning of replicas. This paper has focused on providing optical texture to tooth replicas by modifying epoxy resin die material with coloured fillers and the use of moderately priced photographic equipment. The production of replicas of teeth is a familiar procedure in clinical and laboratory dentistry. Clinical photography is also a common procedure in clinical practice. The use of digital photogrammetric software is currently a relatively expensive and specialised task. However, once the software routines are learned, processing images is fast with the generation of digital terrain models (DTMs) and surface models completed within 10 minutes.

5.4.1 Tooth Replicas

The epoxy die material used in this study is not commonly used for tooth replication in clinical or laboratory practice. Type IV dental stone is the common material used for the replication of individual teeth and full dental arches, showing good dimensional accuracy and abrasion resistance. However Type IV dental stone and epoxy resin die systems provide a similar degree of dimensional stability in reproducing single teeth and full arches when used with polyvinylsiloxane impression materials (Chaffee et al., 1997). Epoxy resin die systems are reported to have a setting shrinkage of around 0.01%, i.e. 1 μm per 10 mm. Dimensional changes in the order of 20 μm when tooth dies were prepared from both Type IV dental stone and epoxy die systems when used with polyvinyl siloxane impression material have been reported (Chaffee et al., 1997; Lee et al., 1995). The filler added to the epoxy die material in this study would not be expected to result in reduced dimensional stability of the material and may reduce setting shrinkage further, however it may result in altered abrasion resistance and compressive

strength. Abrasion resistance is important where the replica is to be handled during laboratory-based technical procedures. In the conduct of a clinical study of tooth wear or the progression of surface defects, replicas could be discarded once imaging has been performed and their long-term durability would be of no concern.

5.4.2 Image acquisition and interior orientation

This study has used a semi-metric 35 mm format film camera resulting in time delays for film processing and scanning. Currently available high-resolution cameras (e.g. 6.3 megapixel, say) yield images of the same resolution as the film images scanned at 10 μm pixel size with the ability to accelerate and automate processing operations. The use of extension bellows in this paper also led to instability of interior orientation parameters as evidenced in Table 5.1 and resultant errors in the stereomodels as discussed later. The design and application of a fixed focal length stereometric camera system would negate this instability and reduce the requirement for interior and exterior orientation and lead directly to image matching, epipolar resampling and DEM generation, all of which could be performed as automatic operations.

5.4.3 Exterior orientation and model accuracy

Generation of exterior orientation is an automatic function in VirtuoZo following manual matching of control points and automatic matching of additional relative orientation points. Grossly erroneous orientation solutions were frequently generated, however as more than five control points were added and additional image points out of the control plane were added a 'correct solution' was attained. A correct solution was normally identified when the Y axis convergence for the two cameras was of the same order of magnitude but of opposite sign. Acceptance of different 'correct solutions' was found to have little effect on the precision of the resultant stereomodels.

The relative orientation y parallax rms error of approximately 3 to 8 μm in image space (Table 5.2) corresponds to 2 to 6 μm in object space and is consistent with the absolute orientation error data for x , y and z axes of 3 to 12 μm . This gives an indication of the accuracy of the positioning of the control points in VirtuoZo by the operator and the accuracy of measurement of the control grid points. The relatively flat lines for M_z , and M_{xyz} in Figure 5.4 indicate that the matching of control points was largely unaffected by convergence angle.

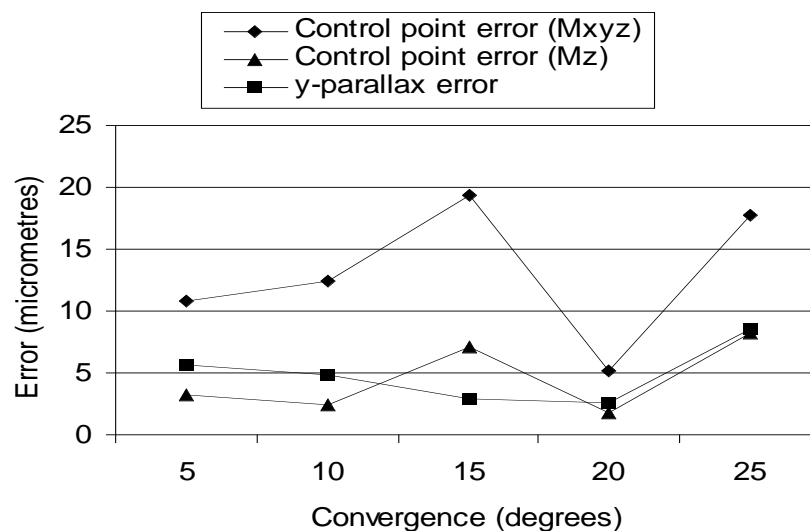


Figure 5.4. Orientation error data: absolute orientation control point error data M_{xyz} and M_z , and y parallax error data at different convergence angle.

A review of height data in Table 5.3 shows that for all models (except 5° convergence) model height has been contracted towards the control plane, with the height 1 mm below the control point plane being reduced by a mean of 15 μm (except for 5° convergence), and heights 3 mm above the control plane being reduced by a mean 57 μm . The horizontal (x , y diameters) data in Table 5.4 shows that model space has been expanded below the control plane and contracted above the control plane, with values at a height of approximately 1 mm below the control point plane increased by a mean of 46 μm , and with values approximately 3 mm above the control point plane

being reduced by a mean of 59 μm . The effect of errors in interior and exterior orientations for convergent photography has been considered in the analogue era (Hallert, 1954; Konecny, 1965). In the current case potential error in interior, relative and absolute orientation need to be considered because of the camera and stereo geometry employed. The large offsets for principal point values are not surprising given the use of bellows. Opening the aperture ring on the lens between exposures to ensure correct alignment of the object resulted in inevitable movement of the lens in relation to the camera body.

Given the instability in interior orientation, the potential effects of exterior orientation error have not been fully examined, however it is noted that of the exterior orientation elements, error in ϕ orientation (convergence angle) has the major effect upon model height error. The need for a vertical control point to improve the accuracy of the relative orientations in close-range photogrammetry has been described by (Adams, 1978). In traditional normal case photogrammetry, a base distance ratio of 1:4 is the usual minimum requirement for achieving an acceptable photogrammetric solution. This equates to a convergence angle of approximately 15° . Error in height appears to decrease with increasing convergence (Table 5.3, difference line), however this is unreliable given the instability in focal length. No account has been taken of residual errors as a result of scanning the film.

5.4.4 Image matching and precision

The standard deviations of the z coordinates from the data-sets of each plane for the different convergence angles ranged from approximately 20 to 38 μm . These give a measure of overall precision, being affected by camera geometry and image matching precision but also influenced by errors in interior and relative orientation. Shadows generated on the test object replica images during photography resulted in gross errors during automatic image matching. Manual matching of image points in *VirtuoZo-Prepare to Match*

largely eliminated these errors. Smaller matching errors occurred due to the presence of plane edges and reseau marks in the images. Natural tooth surfaces do not typically show abrupt right angles unless specifically prepared, such as in the case of cavity preparation prior to dental restoration. To negate the effect of the reseau, a 1 mm horizontal shift in addition to the object rotation was employed so that interior reseau marks did not appear in the same part of left and right images to confound auto-correlation in these areas. However, errors in the resultant DEMs due to the reseau marks were still present and were typically in the order of 50 μm . Optimum patch window size will vary with texture and surface topography. Matching precision increased with increasing patch size, because the spatial frequency of the targets (optical texture) in the image was relatively large. Optimum grid interval will vary with topography and to enable accurate interpolation of DEM points, the match grid interval should be about half the DTM interval. For the tooth replicas, the desired DEM output was a 50 μm x 50 μm grid. In this case, varying grid interval had little effect on the precision of surface points generated by automatic matching (Table 5.7), due to the planar nature of the test object.

In this study clear epoxy resin has been coloured to enhance its potential for photogrammetric autocorrelation. The precision data from autocorrelation (Table 5.5) are compared with predicted precisions computed using the formulae of Karara and Abdel-Aziz (1974) (Figure 5.5) and the general form of the autocorrelation precision data was consistent with predictions based upon an input image space coordinate accuracy of 4 μm , except for the convergence angle of 10°. The value of 4 μm , when related to the film scanning resolution of 10 μm indicates image space targetting of 0.4 pixels. This compares with target location on stereocomparators of approximately 3 μm and is typical of that expected from digital photogrammetric workstation systems and manual measurement.

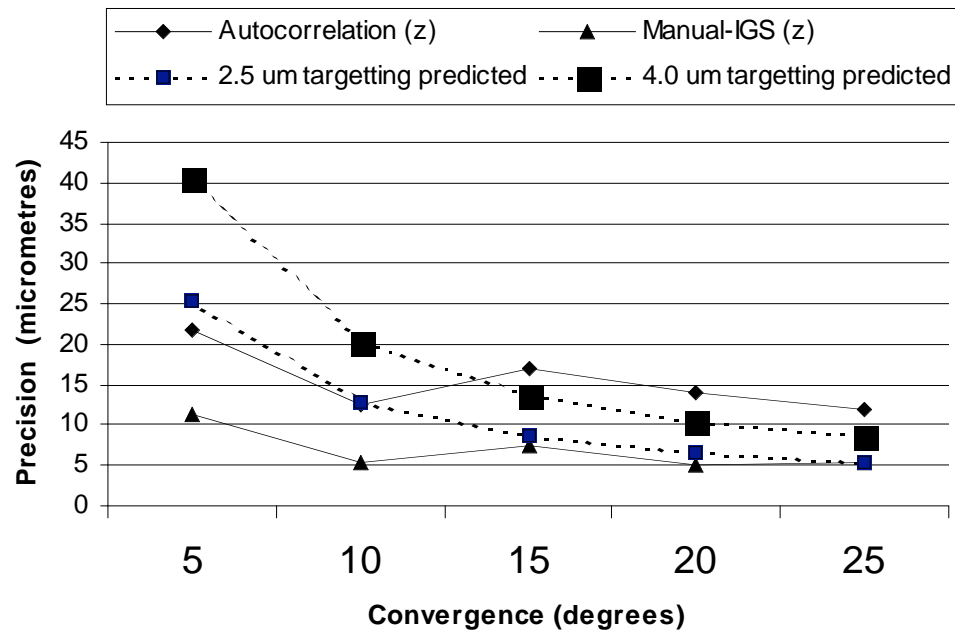


Figure 5.5. Actual and predicted object space precision at different convergence angles; actual data from autocorrelation and manual (IGS) target matching and predicted values applying 2.5 and 4 μm image space precision.

The manual measurement of surface targets in *VirtuoZo-IGS digitise* produced standard deviations on a least squares plane fit of Z values of 5 to 7.7 μm (Table 5.6), in the same range as the relative orientation y parallax rms error and also unaffected by convergence angle. This is consistent with object space pointing accuracy of approximately 2.5 μm or better (Figure 5.5). The manual recording of 12 points on the perimeter of each circle produced standard deviations on the x, y coordinates from the circle of best fit of between 4.1 and 11.2 μm , the same order as for the least squares plane fit above. The *VirtuoZo-IGS* coordinate data show the precision that can be achieved from the model and a future aim is to improve texture so that the same precision can be achieved with autocorrelation.

5.4.5 Surface models

VirtuoZo generated a point height file which consists of data points derived by autocorrelation on the grid interval specified in the *VirtuoZo-model setup*. VirtuoZo enables export of a DEM file which consists of data resampled on an ordered grid as specified in the *VirtuoZo-DEM spacing*. Coordinate data derived manually in *VirtuoZo-IGS digitize* can also be exported as a separate file to enable the identification and collection of points of specific features, such as the outline of wear facets, restoration and surface defects. These may be added to DEM file to enhance precision in those areas, or overlaid into the same coordinate system in a contrasting colour. The capture of feature edge data points can be beneficial in surface matching of featureless surfaces (Grenness et al., 2002).

There are many software packages for visualisation and analysis of 3D coordinate data. The surface relief presented in this paper is one example. The ease of interpretation and usefulness of different modes of presenting quantitative tooth wear data to clinicians has been studied, and combined surface difference plots found to be appropriate (Chadwick and Mitchell, 1999). In order to monitor wear and surface defects it is necessary to align sequential models from different time periods. This has been done using surface matching (Mitchell and Chadwick, 1998). Virtual Reality Modelling Language based software has been used to align dental segments with good results (DeLong et al., 2002). Mitchell and Chadwick (Mitchell and Chadwick, 1998) reported that more tests were needed of matching convergence ranges and the tolerance of surface matching algorithms to larger percentage surface changes.

Quantitative studies of the progression of surface loss are few in number and results vary widely, ranging from 10 to 300 $\mu\text{m year}^{-1}$. The variation in results is likely to be related to problems with the classification of lesions being recorded. The more sensitive, that is, precise, a mapping solution the shorter the interval that would be required for tooth surface change detection

and the identification of aetiological factors and the effects of clinical interventions. For patients being monitored on an annual basis in a clinical setting, detection of surface loss in the order of 30 to 50 μm could be a threshold for clinical decision-making. This range is not as precise as the limited number of contact stylus systems in use in research today (Roulet, Reich et al., 1983) but is certainly superior to the naked eye and memory. The accumulation of error from surface modelling and surface matching needs to be taken into account. Precision for manual measurement of 12 μm or better reported in this study is within this required accuracy range. However if this type of approach is to be successful, the density of optical texture will need to be increased so that precisions achieved with automatic image matching achieve the precisions gained from manual measurement.

This study has only considered the modelling of individual tooth surfaces. Multiple views of individual teeth are required to generate a complete surface model. Increasing convergence angle is typically associated with increased precision, but a decrease in the surface area modelled from each view. The results of accuracy testing in this study have not found a strong association between increasing convergence angle and increasing precision as predicted by the formulae of Karara and Abdel-Aziz (1974). Narrowing the convergence angle increases the amount of stereo overlap at the edges or limits of a tooth surface observed from any particular viewing angle. Where multiple views of a surface are taken this is of no significance. When only a single (stereo) view is taken, maximising the scene may be important. Further work is required to study the particular geometry of the different types of teeth found in the human dentition. The generation of complete tooth models is not an absolute requirement for the study of wear and development of surface defects such as non-carious cervical lesions (NCCLs). Non-carious cervical lesions occur in the gingival third of teeth and typically appear as angular defects. Studying NCCLs and tooth wear involves mapping the buccal and occlusal surfaces. There is no absolute requirement for the two surfaces to be connected spatially or to capture the surfaces on

the same image. The two surfaces operate in different functional environments, although there is evidence that wear on one surface may be related to the other (Pintado et al., 2000).

5.5 Conclusion

This paper has described the generation of 3D coordinate data from modified epoxy resin tooth replicas using camera equipment similar to commercially available, moderately priced digital cameras. This brings 3D model generation closer to everyday clinical practice. Model precision has been within acceptable limits of 12 μm or better for manual image matching, however systematic errors have resulted in unacceptably large model errors with the likely causes being the use of a semi-metric camera with unstable interior orientation and the reliability of the photogrammetric solutions formed by the photogrammetric workstation software. The use of a fixed camera lens and further improvement in optical texture is required to achieve these precision levels utilizing automatic image matching, a necessary requirement to enable automation of 3D model generation and the provision of a user-friendly application for clinical use.

5.6 References

- Adams, L., 1978. The use of a non-metric camera for very short range dental stereophotogrammetry. *Photogrammetric Record*, 9 (51): 405-414.
- Al-Malik, M., Holt, R. and Bedi, R., 2001. Clinical and photographic assessment of erosion in 2-5-year-old children in Saudi Arabia. *Community Dental Health*, 18 (4): 232-235.
- Azzopardi, A., Bartlett, D., Watson, T. and Sherriff, M., 2001. The measurement and prevention of erosion and abrasion. *Journal of Dentistry*, 29 (6): 395-400.
- Azzopardi, A., Bartlett, D., Watson, T. and Smith, B., 2000. A Literature Review of the Techniques to Measure Tooth Wear and Erosion.

- European Journal of Prosthodontics and Restorative Dentistry, 8 (3): 93-97.
- Buchalla, W., Lennon, A., van der Veen, M. and Stookey, G., 2002. Optimal camera and illumination angulations for detection of interproximal caries using quantitative light-induced fluorescence. *Caries Research*, 36 (5): 320-326.
- Chadwick, R., 1992. Close range photogrammetry--a clinical dental research tool. *Journal of Dentistry*, 20 (4): 235-239.
- Chadwick, R., McCabe, J., Walls, A., Mitchell, H. and Storer, R., 1991. Comparison of a novel photogrammetric technique and modified USPHS criteria to monitor the wear of restorations. *Journal of Dentistry*, 19 (1): 39-45.
- Chadwick, R. and Mitchell, H., 1999. Presentation of qualitative tooth wear data to clinicians. *Quintessence International*, 30 (6): 393-398.
- Chadwick, R., Mitchell, H. and Ward, S., 2002. Evaluation of the accuracy and reproducibility of a replication technique for the manufacture of electroconductive replicas for use in quantitative clinical dental wear studies. *Journal of Oral Rehabilitation*, 29: 540-545.
- Chaffee, N., Bailey, J. and Sherrard, D., 1997. Dimensional accuracy of improved dental stone and epoxy resin die materials. Part I: Single die. *Journal of Prosthetic Dentistry*, 77 (2): 131-135.
- Clarke, C., Flinn, R., Atkinson, K. and Wickens, E., 1974. The measurement and comparison of tooth shape using photogrammetry. *Photogrammetric Record*, 8 (44): 217-221.
- DeLong, R., Ko, C.-C., Anderson, G., Hodges, J. and Douglas, W., 2002. Comparing maximum intercuspal contacts of virtual dental patients and mounted dental casts. *Journal of Prosthetic Dentistry*, 88 (6): 622-630.
- Dirksen, D., Runte, C., Böröcz, Z., Thomas, C., von Bally, G. and Bollmann, F., 2001. Three-dimensional quantification of color-marked occlusal paths on anatomically oriented casts. *Journal of Prosthetic Dentistry*, 85 (2): 156-161.

- Folwaczny, M., Mehl, A., Kunzelmann, K.-H. and Hickel, R., 2000. Determination of changes on tooth-colored cervical restorations in vivo using a three-dimensional laser scanning device. *European Journal of Oral Sciences*, 108 (3): 233-238.
- Grenness, M., Osborn, J. and Weller, W., 2002. Mapping ear canal movement using area-based surface matching. *Journal of the Acoustical Society of America*, 111 (2): 960-971.
- Haak, R. and Schirra, C., 2000. Dental photography in support of patient documentation and communication. *Quintessence International*, 31 (9): 649-657.
- Hallert, B., 1954. Some remarks concerning the theory of errors for convergent aerial pictures in comparison with near vertical pictures. *Photogrammetric Engineering*, 20 (5): 749-757.
- Heikkilä, J. and Silvén, O., 1997. A four-step camera calibration procedure with implicit image correction, *Computer Vision and Pattern Recognition*, IEEE, Puerto Rico, pp. 1106-1112.
- Karara H.M. and Abdel-Aziz YI, 1974. Accuracy aspects of non-metric imageries. *Photogrammetric Engineering*, 40 (9): 1107-1117.
- Konecny, G., 1965. Interior orientation and convergent photography. *Photogrammetric Engineering*, 31 (4): 625-634.
- Kurbad, A., 2000. The optical conditioning of Cerec preparations with Scan Spray. *International Journal of Computerized Dentistry*, 3: 269-279.
- Lamb, R., McGarrah, H., and Eick, J., 1987. Close-range photogrammetry with computer interface in dental research. *Photogrammetric Engineering and Remote Sensing*, 53 (12): 1685-1689.
- Lee, I., DeLong, R., Pintado, M. and Malik, R., 1995. Evaluation of factors affecting the accuracy of impressions using quantitative surface analysis. *Operative Dentistry*, 20: 246-252.
- Leinfelder, K., Isenberg, B. and Essig, M., 1989. A new method for generating ceramic restorations: a CAD-CAM system. *Journal of the American Dental Association*, 118 (6): 703-707.

- Markowski, A., 1990. A CAD/CAM ceramic inlay technique. *Journal of Esthetic Dentistry* 2 (6): 170-176.
- Mehl, A., Gloger, W., Kunzelmann, K.-H. and Hickel, R., 1997. A new optical 3D device for the detection of wear. *Journal of Dental Research*, 76 (11): 1799-1807.
- Mitchell, H. and Chadwick, R., 1998. Mathematical shape matching as a tool in tooth wear assessment - development and conduct. *Journal of Oral Rehabilitation*, 25: 921-928.
- Mitchell, H., Chadwick, R. and McCabe, J., 1989. Stereo microscope photogrammetry for the measurement of small objects. *Photogrammetric Record*, 13 (74): 289-299.
- Mitchell, H., Kniest, H. and Oh, W.-J., 1999. Digital photogrammetry and microscope photographs. *Photogrammetric Record*, 16 (94): 695-704.
- Mou, S.-H., Chai, T., Wang, J.-S. and Shiau, Y.-Y., 2002. Influence of different convergence angles and tooth preparation heights on the internal adaptation of Cerec crowns. *Journal of Prosthetic Dentistry*, 87 (3): 248-255.
- Osborn, J. and Wise, G., 1996. Stereophotogrammetric mapping of the anterior surface of the human cornea. *International Archives of Photogrammetry and Remote Sensing*, 31 (B5): 443-449.
- Palamara, D., Palamara, J., Tyas, M. and Messer, H., 2000. Strain patterns in cervical enamel of teeth subjected to occlusal loading. *Dental Materials*, 16 (6): 412-419.
- Parsell, D., Anderson, B., Livingston, H., Rudd, J. and Tankersley, J., 2000. Effect of camera angulation on adaptation of CAD/CAM restorations. *Journal of Esthetic Dentistry*, 12 (2): 78-84.
- Perry, R., Kugel, G., Kunzelmann, K.-H., Flessa, H.-P. and Estafan, D., 2000. Composite restoration wear analysis: conventional methods vs. three-dimensional laser digitizer. *Journal of the American Dental Association*, 131 (10): 1472-1477.

- Peters, M., DeLong, R., Pintado, M., Pallesen, U., Qvist, V. and Douglas, W., 1999. Comparison of two measurement techniques for clinical wear. *Journal of Dentistry*, 27 (7): 479-485.
- Phelan, S., 2002. Use of photographs for communicating with the laboratory in indirect posterior restorations. *Journal of the Canadian Dental Association*, 68 (4): 239-242.
- Pintado, M., DeLong, R., Ko, C.-C., Sakaguchi, R. and Douglas, W., 2000. Correlation of noncarious cervical lesion size and occlusal wear in a single adult over a 14 year time span. *Journal of Prosthetic Dentistry*, 84 (4): 436 - 443.
- Robertson, A. and Toumba, K., 1999. Cross-polarized photography in the study of enamel defects in dental paediatrics. *Journal of Audiovisual Media in Medicine*, 22 (2): 63-70.
- Roulet, J., Reich, T. and Lutz, F., 1983. High precision occlusal mapping: a new method for measuring wear of posterior composites. *Journal of Dental Research*, (Special Issue) 62 (Abstract Number 457): 220.
- van der Zel, J., Vlaar, S., de Ruiter, W. and Davidson, C., 2001. The CICERO system for CAD/CAM fabrication of full-ceramic crowns. *Journal of Prosthetic Dentistry*, 85 (3): 261-267.
- Wolf, P.R. and Dewitt, B.A., 2000. *Elements of photogrammetry*. 3rd Edition. McGraw-Hill. Boston. p. 334.
- Xhonga, F., Wolcott, R. and Sognnaes, R., 1972. Dental Erosion II. Clinical measurements of dental erosion progress. *Journal of the American Dental Association*, 84 (3): 577-582.

5.7 Appendix

This appendix contains additional text and figures that do not appear in the Photogrammetric Record.

5.7.1 Film photographic setup



Figure 5.6. The photographic setup: Leica R5 'Elcovision' camera fitted with bellows at maximum extension with additional 50 mm extension tube and 100 mm macro lens, mounted on a Reprovit II copy stand. Side lighting provided by 50W-12V halogen bulbs. Object and control point plane mounted in tilting light box with 60W-240V incandescent bulb, and Abney level.

5.7.2 Image matching techniques

There are three approaches to image matching. These are feature-based techniques, which operate by finding “interesting” features in an image, area-based techniques, which operate by passing a search template (patch) across an image and calculating a correlation coefficient, and hybrid algorithms use a mix of feature-based and area-based techniques. For example, the software may identify features and then constrain the area-based matching to regions with those features.

Some other techniques used to improve the speed, reliability and accuracy of image matching include hierarchical matching, where resampling the images to a very low resolution and then applying the matching algorithms to increasingly high resolution versions, but over increasingly small regions, object space matching, where resampling the image pixels into object space (sometimes called ‘groundels’) and operating the correlation algorithm on the groundels, and radiometric modeling, which accounts for likely variations in illumination of the terrain due to different viewing angles (Wolf and Dewitt, 2000).

The *VirtuoZo* photogrammetry software used in this Chapter employs a hybrid algorithm and image matching parameter variables of patch height and width, patch sampling interval and terrain type (VirtuoZo, version 3.3, User Manual; VirtuoZo Systems International Pty. Ltd, South Brisbane, Australia).

Following image matching in *VirtuoZo*, the *VirtuoZo-match edit* window can be opened to display the correlation result. Coloured pegs identify patches (see above) that have been matched in the right and left images: green = excellent, yellow = very good, red = poor correlation. Figure 5.7 is of the example tooth surface reported earlier in this chapter. Poor correlation can be seen around reseau marks, areas of insufficient texture and the tooth mounting medium.

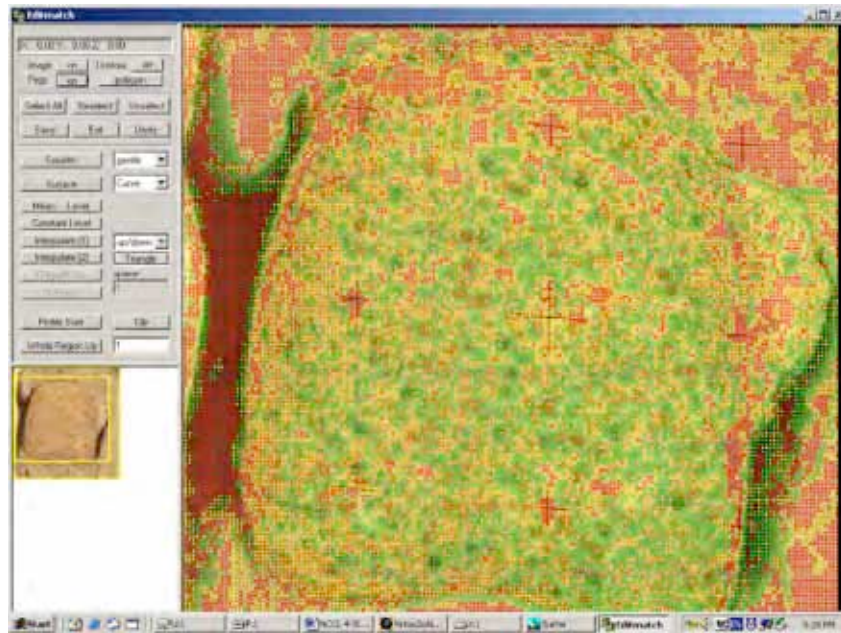


Figure 5.7. Tooth replica: VirtuoZo-match edit window displaying correlation pegs: green = excellent, yellow = very good, red = poor correlation; note poor correlation around reseau marks, areas of insufficient texture and the tooth mounting medium.



Figure 5.8. Test object: image of test object replica sitting in control array; note optical texture, reseau marks and shadowing.

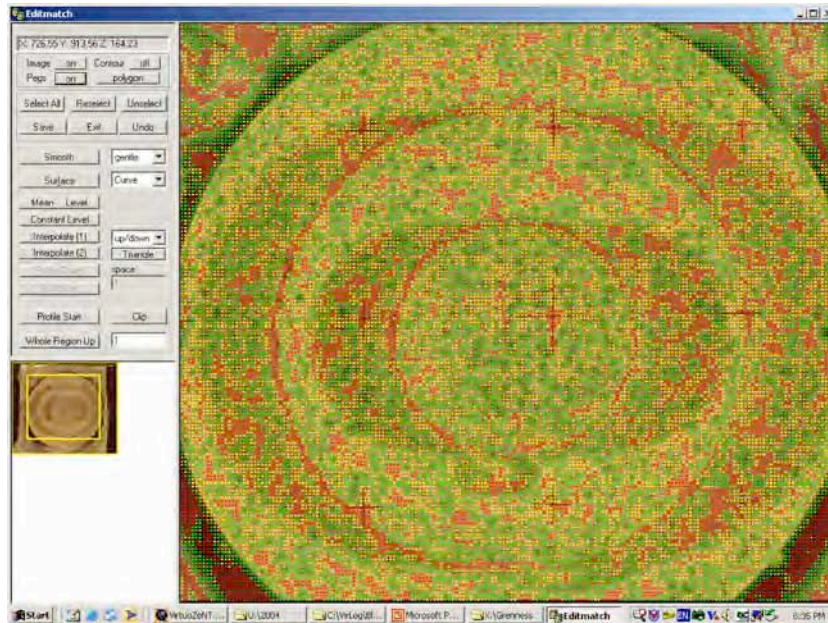


Figure 5.9. Test object: VirtuoZo-match edit window displaying correlation pegs; note poor correlation around reseau marks, shadowing has no effect on correlation.

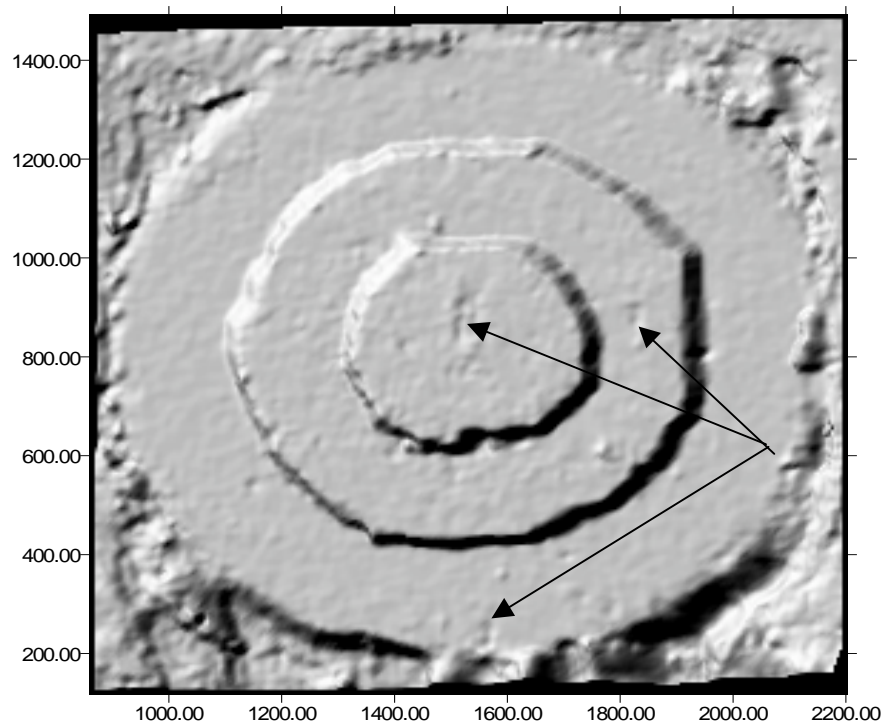


Figure 5.10. Test object: surface relief displayed using *Surfer* (15 degrees convergence); note surface defects associated with reseau marks (black arrows).

Chapter 6

Digital very close range photogrammetry of a test object incorporating optical texture

Presented at 7th Optical 3D Measurement Techniques Conference,
Oct 3-5, Vienna, Austria. (not refereed)

Malcolm Grenness Jon Osborn

Centre for Spatial Information Studies, University of Tasmania

Martin Tyas

School of Dental Science, University of Melbourne

Abstract

A digital camera and fixed lens has been used to obtain convergent stereopairs of a test object prepared from an experimental material containing optical texture. This is part of a project developing a stereo-photogrammetric technique for mapping individual human teeth. *VirtuoZo* (v3.3) photogrammetric workstation was used to process images with convergent geometries of 2 to 25 degrees and to generate DEMs. The precision of DEMs was typically around 10 μm for convergences of 4 to 25 degrees, decreasing to over 20 μm for convergence below 4 degrees. Relatively constant precision at the different convergence angles was attributed to improved image point measurement precision with decreasing convergence, with measurement precision estimated to be 0.6 μm (0.08 pixels) at 4 degrees and 2.8 μm (0.38 pixels) at 25 degrees. Photogrammetric solutions were not highly stable, with successive solutions at all convergence angles showing small variations in exterior orientation parameters. These variations in exterior orientation parameters were associated with systematic model height errors of up to

80 μm . It was concluded that the single camera and imaging geometry used was not reliably forming models of a tooth sized object given a need to achieve sub-30 μm accuracy, intended for the monitoring of tooth surface loss.

6.1 Introduction

Film-based stereo-photogrammetry for very close range (macro) applications has been described since the 1970s, with a variety of camera formats, lens systems, focal lengths and camera geometries reported. Teeth and dental subjects have been common application (Chadwick, 1992) and include mapping the surface of teeth dusted with graphite (Clarke et al., 1974), the dental palate (Adams, 1978), dental filling material degradation, root surface measurement, measurement of tooth movement under loading, and filling material wear (Lamb et al., 1987; Mitchell et al., 1989a). Layton and Cox (1982) used three different microscope camera systems to photograph a haemocytometer, steel washer, 1/64 inch diameter steel ball bearing and a sand particle. Subjects have also included small pebbles (Chiat, 1977), a steel specimen subjected to rolling-contact fatigue (Vozikis and Douzinas, 1984), frog ova (Li et al., 1986), and the human cornea (Osborn and Wise, 1996). In the digital era, Mitchell et al. (1999) used a microscope and tilting stage to produce convergent photography of several objects with a fractured concrete surface being successfully image-matched leading to a DEM. The recent report of Grenness et al. (2005) has described stereo- photogrammetric mapping of tooth replicas incorporating optical texture with successful image matching leading to a DEM.

Very close range photogrammetry typically requires the use of long focal length, narrow field angle lenses and convergent photography. Convergent stereo-photogrammetry was initially thought to significantly increase accuracy over normal case photographs (Radlinsky, 1952) with modelling (Hallert, 1954; Konecny, 1965) and empirical work (Faig and Moniwa, 1973)

supporting this view. However, Adams (1978) found that convergent geometry led to unacceptable inaccuracies, particularly in model height, and included a vertical control point to check the height accuracy of models and assist in refining the relative orientation. Lens systems have included single lenses (Adams, 1978; Chiat, 1977; Grenness et al., 2005), microscopes (Clarke et al., 1974; Mitchell et al., 1999), stereo microscopes (Layton and Cox, 1982; Li et al., 1986; Mitchell et al., 1989b; Vozikis and Douzinas, 1984), and stereometric cameras (Gruner et al., 1967; Lamb et al., 1987; Osborn and Wise, 1996). A summary of normal case or convergence angle, magnification or photoscale, sensor size, focal length and reported height error for the above authors (where data is reported) appears in Table 6.1.

These reports suggest that very close range photogrammetry reached a mature state of development in the analogue era around the late 1970s. The best results were achieved with greater magnifications, large format film and narrower convergence (e.g. Adams, 1978; Layton and Cox, 1982), or smaller film format, shorter focal length and a wider convergence angle (e.g. Chiat, 1977; Lamb et al., 1987). Over the last decade, multi-station convergent photogrammetry has been increasingly employed, firstly with relatively low-resolution digital cameras, or for very high accuracy applications using scanned or digitised film, and more recently with high-resolution digital cameras. Grenness et al (2005) utilised a 35-mm format film camera to achieve precision of better than 12 μm , but some systematic errors, particularly in height were present.

Author / Era	Date	Case	Scale	Sensor	Fl	Error	Error:
<i>Analogue</i>				(mm)	(mm)	(µm)	Object space
Clarke <i>et al</i>	1974	Normal	5.2x	90 x 120	750	90	1 : 256
Chiat	1977	20°	1x	35 x 24	120	10	1 : 3500
Adams	1978	Normal	1:40	130 x 100	150	250	1 : 20000
Layton <i>et al</i>	1977	10.8°	40x	35 x 24	200+	1.3	1 : 673
	1979	10.8°	10x	35 x 24	200+	2.0	1 : 1750
	1980	10.8°	23x	83 x 108	200+	0.94	1 : 4995
Vozikis <i>et al</i>	1984	Normal	10x	120 x 90	212	10	1 : 350
Lamb <i>et al</i>	1987	34°	1:2	35 x 24	55	21	1 : 3333
<i>Analytical</i>							
Li <i>et al</i>	1986	?	25x	35 x 24	200+	1	1 : 1400
Mitchell <i>et al</i>	1989	7.6°	6x	35 x 24	210	50	1 : 116
Obsorn <i>et al</i>	1996	15 - 25°	1.6x	35 x 24	250	20	1 : 1093
<i>Digital</i>							
Mitchell <i>et al</i>	1999	4°	1.8x	35 x 24	500	150	1 : 129
Grenness <i>et al</i>	2005	5 - 25°	1.6x	35 x 24	250	12	1 : 1822

Table 6.1. Very close range photogrammetry reports with camera convergence, photoscale, sensor size, focal length and reported accuracy/precision.

The use of a fixed camera lens system with stable interior orientation and the incorporation of vertical control is expected to provide more robust photogrammetric solutions, with a goal to increase accuracy to $\pm 10 - 30 \mu\text{m}$, intended for the monitoring of tooth surface loss. The use of a digital camera when combined with automatic image matching may lead to the prospect of a fully automatic measurement system.

The aim of the work reported in this paper is to determine the accuracy and precision of 3D surface models derived from convergent digital stereo-photogrammetry of a tooth sized test object using a fixed focal length lens and digital camera, convergent geometries of 2 to 25 degrees, coplanar and vertical control, and a test object incorporating optical texture.

6.2 Method

A vinyl siloxane impression (Reposil; Dentsply International Inc., Milford, DE) was taken of a hardened steel test object with three circular planes of 4, 8 and 12 mm diameter with risers of 2 mm between the planes (Grenness et al., 2005). This was poured with an experimental die material that consisted of epoxy resin modified with the addition of coloured fillers, to produce a replica of the test object but incorporating optical texture (Figure 6.1). The test object was placed into a planar control grid of black film (Lithfilm; Agfa-Gevaert, Belgium) with 29 transparent targets of $40 \mu\text{m}$ diameter present around the field of view at intervals of approximately 2mm. The X and Y coordinates of the targets were measured with a stereocomparator (Stecometer; Carl Zeiss Jena, Oberkochen, Germany) at a measurement precision of $2.5 \mu\text{m}$, and the Z coordinates were taken as being planar and given an arbitrary constant value. The coordinates of a readily identifiable target on the top plane of the test object was determined from stereomodels at 15, 20 and 25 degrees convergence, judged to be reliable (model height within $10 \mu\text{m}$).

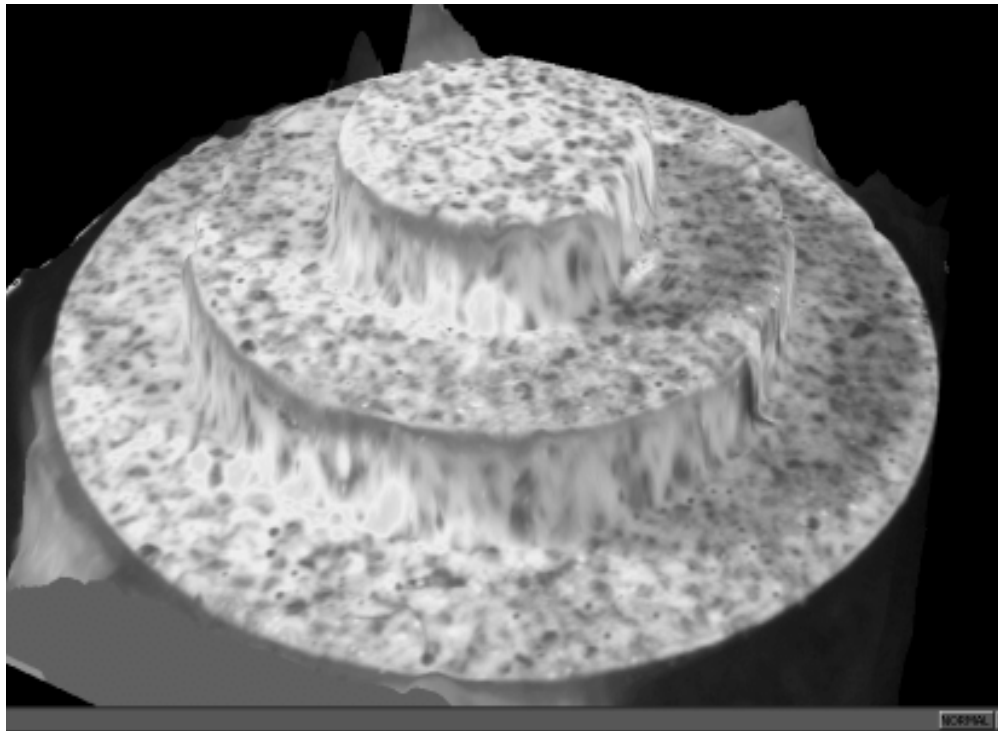


Figure 6.1. Test object incorporating optical texture: digital orthoimage draped on DEM. Diameter of the outside circle is 12 mm.

The replica was imaged with a 22.7-mm format digital camera (Canon 300D; Canon Inc, Japan) and a 80-mm enlarger lens (Componon; Schneider-Kreuznach, Germany) fitted to an aluminium extension tube, achieving a magnification of 1x, at convergence angles of approximately 2, 3, 4, 5, 6, 8, 10, 15, 20 and 25 degrees on a tilting light box. Camera calibration was performed using convergent images of a planar calibration array with one view taken perpendicular to the calibration array and four quadrant views taken at divergent angles of 5 degrees and a MATLAB toolbox based on the method of Heikkilä and Silvén (Heikkilä and Silvén, 1996). The toolbox used a direct linear transformation to compute initial values for all but the lens distortions, prior to an iterative least squares solution to a non-linear model that includes lens distortions. The method generated values for focal length, principal point of symmetry, radial (k_1 , k_2) and decentring (p_1 , p_2) lens distortions and a scaling factor. The planar calibration array comprised 63 points of 40- μ m diameter and spaced at approximately 2-mm intervals

exposed onto film and with the coordinates of points on the array measured using the stereocomparator.

Digital images of the test object replicas were imported into the digital photogrammetric workstation station (VirtuoZo, version 3.3; Supersoft Inc., Wuhan, Hubei, China) and camera calibration parameters including radial lens distortion data were entered. Interior orientation was performed using the corners of the digital images. Exterior orientation was performed using up to eight control points, including the vertical control point identified on the test object and up to seven additional image-matched points from the tooth replica with further refinement aided by use of the *VirtuoZo-control point adjustment* function. Epipolar resampling, automatic image matching with a 15 x 15 pixel patch window on a 9 x 9 pixel grid interval, and automatic generation of 3D coordinate digital elevation model (DEM) on a 65 μm x 65 μm grid was performed. Coordinate data were imported into visualisation and analysis software (Surfer, version 6.04; Golden Software Inc., Golden, Colorado, USA) and a surface relief generated.

Accuracy was assessed using relative orientation y-parallax error in image space coordinates, absolute orientation error data in object space coordinates, height measurements calculated from the DEMs, and hand-held micrometer measurements from the test object. Differences between the micrometer and calculated heights for each convergence angle were determined. The height of a point at the centre of each plane was computed from a least squares solution of the equation of a plane of best fit using 3D coordinate data extracted from the DEM, with outliers exceeding $\pm 75 \mu\text{m}$ occurring at the rise between each plane excluded. Precision of automatic image matching was assessed on a 1 x 2 mm section of coordinate data from the top plane of each DEM by determining the standard deviation of the z coordinate from the plane determined by the least-squares plane fit algorithm. No outliers were removed from these data sets. The measurement precisions were compared

with expected precisions, generated using the formulae of Karara and Abdel-Aziz (1974).

Convergent geometries of 5, 10 and 15 degrees were also investigated using network simulation software (Vision Measurement System (VMS), v7.6 ; Geometric Software, Melbourne, Australia), a photogrammetric network adjustment program with simultaneous camera calibration. Simulations were run according to the same basic empirical setup used above, namely sensor dimensions of 22.7 x 15.1 mm, focal length 150 mm, a photoscale of 1:1. Additional image points of unknown object space coordinates were added to the synthetic images and image point measurement error (s.d.) was varied from $x, y = 0.5, 0.1, 1.4$, and $2.0 \mu\text{m}$. Simulations were run to test the effect on orientation precision of the presence of six von Gruber points and the addition of a vertical control point; to test the effect on model height error of adding an image point with unknown object space coordinate at a height of 4 mm above the control plane; to test the effect of varying image point measurement precision; and to test the effect on model height error of introducing ϕ (camera convergence angle) orientation errors. VMS reported orientation precisions as least squares estimates of the precision (error) of the output orientation parameters and are a product of the bundle adjustment. These camera calibration precision estimates were one standard deviation.

6.3 Results

Camera calibration results appear in Table 6.2. Parameters k_1 and k_2 , coefficients of radial distortion (r^3 and r^5), resulted in a maximum radial lens distortion value of $-5.5 \mu\text{m}$, less than 1 pixel in image space units. Parameters p_1 and p_2 are coefficients of decentring distortion and resulted in a maximum magnitude of $4.1 \mu\text{m}$.

Parameter	Value
Effective focal length	156.442
Principal point: x, y (mm)	-0.052, -0.894
Radial distortion, k_1, k_2	-9.254×10^{-6} , 4.268×10^{-8}
Decentring distortion, p_1, p_2	-6.943×10^{-6} , 3.684×10^{-6}
Max dist: radial, decent. (μm)	-5.5, 4.1

Table 6.2. Calibration parameters of the digital camera and lens system.

Repeated observation of relative and absolute orientation points resulted in numerous photogrammetric solutions, with small variations in the computed exterior orientation produced at all convergence angles. In some cases the best accuracy and precision data was achieved at the first orientation solution, in other cases between ten and twenty solutions were generated and tested. Relative orientation parameter, y parallax error data and absolute orientation control point error data for the different convergence angles appear in Table 6.3. The y parallax error data (an assessment of image space accuracy) ranged between 1.1 and 3.2 μm . The control point error data (an assessment of object space accuracy) ranged between 1.51 and 16.42 μm .

The standard deviations of z coordinates from a small section of the top plane at different convergence angles ranged from approximately 8 to 26 μm (Table 6.4)⁵. The height differences from the top to bottom plane of the steel die measured with a micrometer, and of the modified epoxy replica calculated from the DEMs generated by VirtuoZo, appear in Table 6.4. The height differences varied from -36 to +76 μm (excluding one outlier result of 191 μm).

⁵ The effect of surface opacity on image matching has not been investigated. Best precision values around 8 μm suggest that surface translucency is well below this value.

Nominal convergence (deg.)	2	3	4	5	6	8	10	15	20	25
Computed convergence (deg.)	2.23	3.15	4.20	5.06	6.20	7.78	10.12	15.00	20.01	24.87
<i>Relative orientation parameters</i>										
y Parallax RMS error (μm)	2.2	3.0	1.2	2.1	1.5	1.1	2.1	2.9	2.9	3.2
<i>Absolute orientation parameters</i>										
x, y, z standard error (μm)	10.13	10.97	9.52	1.51	2.48	9.01	7.06	6.94	16.42	13.02

Table 6.3. Relative and absolute orientation error data derived from modified epoxy replica at the different convergence angles.

Object:	Machined steel	Modified epoxy replica									
	Micrometer (μm)	VirtuoZo-DTM → plane extraction→height calculation (μm)									
		Convergence angle (deg.)									
		2	3	4	5	6	8	10	15	20	25
Height	3967	3943	3931	4158	3968	3956	4043	3993	3980	3965	3973
Difference		-24	-36	191	1	-11	76	26	13	-2	6
Top plane st.dev. (μm)		26.3	19.4	8.95	15.1	15.5	8.18	11.19	11.20	9.91	9.81

Table 6.4. Height measurements and differences of the steel die and modified epoxy replica, standard deviations of z coordinates of a 2 x 1 mm section of the top plane.

Surface relief plots of the DEMs for several convergent angles, produced with Surfer, appear in Figure 6.4. The surface 'roughness' of the top (central) plane correlates to the precision value for that convergence angle. For example, Figure 6.4-8° is smoother than Figure 6.4-10°. For Figures 6.4-15° to Figure 6.4-20° the surface is consistently smooth, in line with the improved precision values in Table 6.4. However loss of data at the risers between each plane increases with increasing convergence angle (reducing stereo overlap).

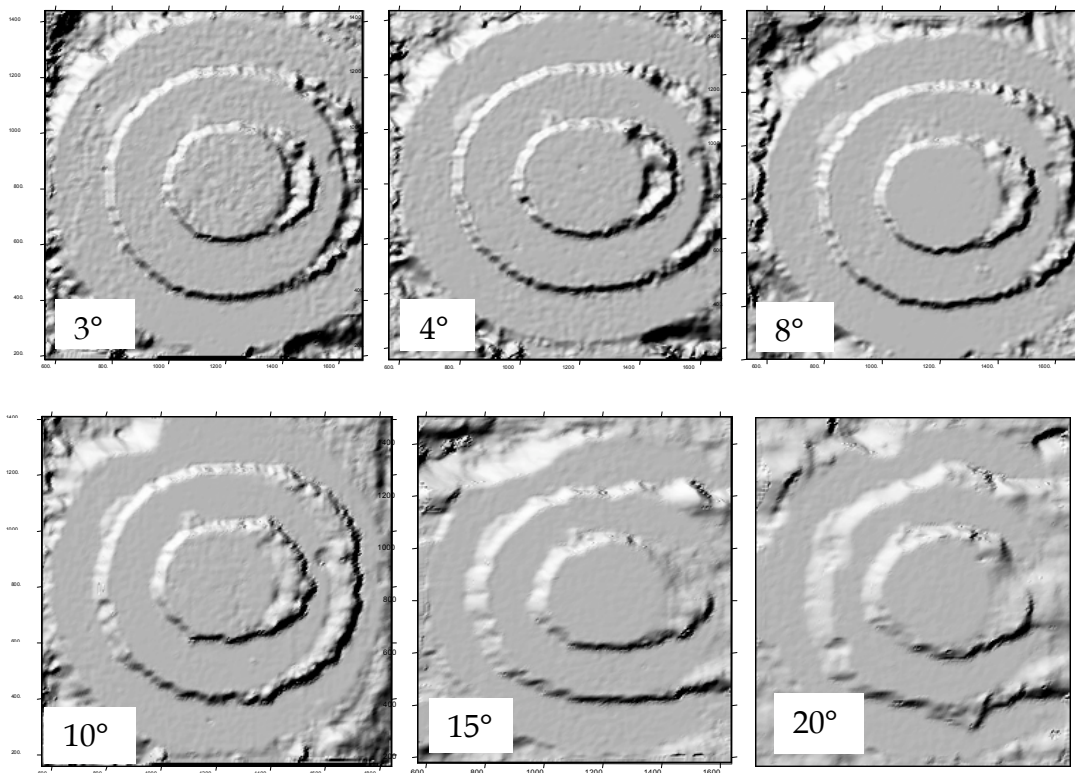


Figure 6.4. Surface reliefs of test object replica DEM at convergence angles of 3, 4, 8, 10, 15 and 20 degrees. Note loss of data at the rise between each plane with increasing convergence angle (reducing stereo overlap)⁶; more reliable and improved precision with increasing convergence.

Exterior orientation was repeated multiple times for the 15 ° convergence pair of images to test the reliability of the photogrammetric solution

⁶ Gross model defects concentrated to the right of each image in Figure 6.4 are due to matching errors associated with shadowing in the images. Illumination was concentrated to the left of the test object to assist image clarity.

generated. Similar relative and absolute orientation error data and top plane precision data to that appearing in Table 6.3 was achieved for all solutions, however model height error varied between -42 and $+115\text{ }\mu\text{m}$. There was a clear trend between computed *phi* orientation and model height error with model error minimized to an acceptable range of $10\text{ }\mu\text{m}$ when convergence was between 14.962 and 15.003 degrees (range 0.041).

Only key results and summaries of the network geometry simulations are presented here. The simulations showed that the inclusion of a central vertical control point reduced orientation error by approximately one half (0.526) for all parameters except *kappa* (*sK*) where orientation error was already very low. The optimal position for the vertical control point was in the centre of the image. There was a 4% reduction in orientation precision when the point was moved to the centre top of the field of view and a reduction of 10% when the point was moved to the top-left and centre-left of the field of view. Also, as convergence decreased, orientation error increased for all parameters. For example, for a focal length of 150mm and convergence angles of 15 , 10 and 5 degrees, the standard deviation of the precision estimate of *phi* orientation (*sP*) is 284 , 305 and 431 seconds of arc respectively when no vertical control point was present. This is compared with the values of 108 , 126 and 140 respectively when a central vertical control point was present (Table 6.5). When an image point of unknown coordinate was included at a height of 4 mm above the control plane in addition to the six planar control points and one centrally placed vertical control point, the 15 degrees height error (*sZ*) for that point was below $10\text{ }\mu\text{m}$, whereas at 10 and 5 degrees height errors were 15.4 and $27.3\text{ }\mu\text{m}$ respectively.

	Orientation precision						Height error		
	sX	sY	sZ	sO	sP	sK	sx	sy	sz
Conv.	(μm)			(seconds of arc)			(μm)		
5	101.9	108.15	20.4	149	140	25	2.9	2.9	27.3
10	91.75	96.25	22.85	132	126	25	2.7	2.6	15.4
15	77.6	80.65	25.9	111	108	26	2.4	2.3	9.7

Table 6.5. The effect of convergence angle on orientation precision (sX, sY, sZ, sO, sP, sK) and model height error (sx, sy, sz) at the top of the model; focal length of 150 mm, target measurement precision of 1.4 μm.

Simulations to test the effect of varying image point measurement precision showed that increased targeting precision resulted in a marked improvement in orientation precision and height error (sZ) (Table 6.6).

The camera geometry (focal length, object distance, convergence) appeared to result in particularly weak solutions for *phi* leading to systematic distortions in height. VMS was used to test this effect by adding *phi* orientation errors of 0.0002, 0.0004, 0.0010 and 0.0020 to the photo orientation file, then intersecting the synthetic images to calculate new coordinates for the target points. Updated coordinates were saved and compared with the original targets. The resultant model height errors (sZ) were 5.9, 11.7, 28.9 and 57.3 μm respectively. Running the above simulations with omega orientation error added yielded model height errors of around 0.2 μm for all introduced errors.

Targeting	Orientation error						Height error		
Precision	sX	sY	sZ	sO	sP	sK	sx	sy	sz
(μm)	(μm)		(second of arc)				(μm)		
2.0	95.9	99.6	30.2	137	133	28	2.9	2.8	13.9
1.4	77.6	80.65	25.9	111	108	26	2.4	2.3	9.7
1.0	61.9	64	22.7	88	86	24	2	2	7
0.5	35.8	37.15	18.6	51	49	23	1.5	1.5	3.6

Table 6.6. Orientation height errors – varying targeting precision; focal length of 150mm, convergence 15°.

6.4 Discussion

Photography with the digital SLR camera and lens assembly was straightforward, with the camera set to manual exposure mode, the aperture of the lens stopped down, and the exposure level indicator used to manually set the shutter speed. Enlarger lenses are designed to produce a very flat field with minimal distortion. This is reflected in the very low lens distortion values reported in Table 6.2. Fraser (1997) noted it is unwise to recover decentring distortion parameters if the digital photogrammetric workstation (such as VirtuoZo v3.3) does not accommodate such an image corrections. The data camera calibration data in Table 6.2 shows that the decentring distortion was the same order of magnitude radial distortion. Decentring lens distortion and principal point coordinates are highly correlated, so that it would be preferable to exclude decentring distortion from the calibration and let the principal point coordinates compensate. Photogrammetric network design considerations include the need for highly convergent imaging configuration and an object point field that is well distributed in three dimensions. The narrow depth of field of the camera has limited the convergence of imaging available for calibration images and the planar test field was not ideal for recovering the calibration parameters (Mills et al.,

2003). As will be seen below, the presence of vertical control points greatly assists in the location of an image (and camera station) in 3D space.

The relative orientation y parallax RMS error of approximately 1.1 to 2.3 μm in image space and the absolute orientation error data for the coplanar control points of 1.1- 13.0 μm (Table 6.3) did not correspond to model height accuracy determined from DEMs, with height errors varying from -36 to +76 μm . Despite the use of a rigid camera lens system, height errors in the models noted in Grenness et al (2005) are still present and of similar magnitude. The inclusion of the vertical control point had no effect on the accuracy of exterior orientation, although it did allow for model height error to be detected in the absolute orientation residuals. The determination of the coordinates for the vertical control point has relied on the method it was designed to test, however this has not contributed to the variability in orientations recorded. There appeared to be no facility in VirtuoZo to directly manipulate the orientation parameters to reduce model height error. Following generation of an exterior orientation, further refinement of the parameters is possible using the *adjust control dialog* box. However, this was of no reliable assistance in refining the solution with apparently random alterations to the orientation. As noted in the results, model height error was minimized to the desired range of 10 μm when convergence was between 14.9617 and 15.0027 degrees, (range 0.041degrees, or 148 seconds of arc, 0.0007 radians).

Table 6.7 and Figures 6.6 and 6.7 show the computed convergence (used as input for the predicted precision formulae of Karara and Abdel-Aziz (1974), predicted object space precision (assuming 1 μm targeting precision), actual precision results from Table 6.4, and calculated targeting precision required to achieve the actual precision results. The data shows actual object space precision relatively constant, with a fall in precision only evident below 4 degrees.

Computed convergence (Table 6.3) (degrees)	Predicted precision at 1 μ m target precision (μ m)	Actual precision (Table 6.4) (μ m)	Calculated targeting precision (μ m)
2.23	27.0	26.3	1.0
3.15	20.7	19.4	0.9
4.20	16.3	8.95	0.6
5.06	13.8	15.1	1.1
6.20	11.6	15.5	1.3
7.78	9.5	8.18	0.9
10.12	7.5	11.19	1.5
15.00	5.3	11.2	2.1
20.01	4.1	9.91	2.4
24.57	3.5	9.81	2.8

Table 6.7. Computed convergence, predicted precision assuming 1 μ m targeting precision, actual precision results from Table 6.4, and calculated targeting precision required to achieve the actual precision results.

The line showing predicted object space precision in Figure 6.6 is based upon a constant targeting precision of 1 μ m and shows precision improving with increasing convergence angle. However the actual precision line departs from this line at higher convergence angles, suggesting that targeting precision varies with convergence angle particularly as convergence exceeds 15 degrees. This is analogous to manual target matching in the pre-digital era with stereo observation being unsatisfactory when the convergence angle is greater than 15 degrees (Wang Z, 1990).

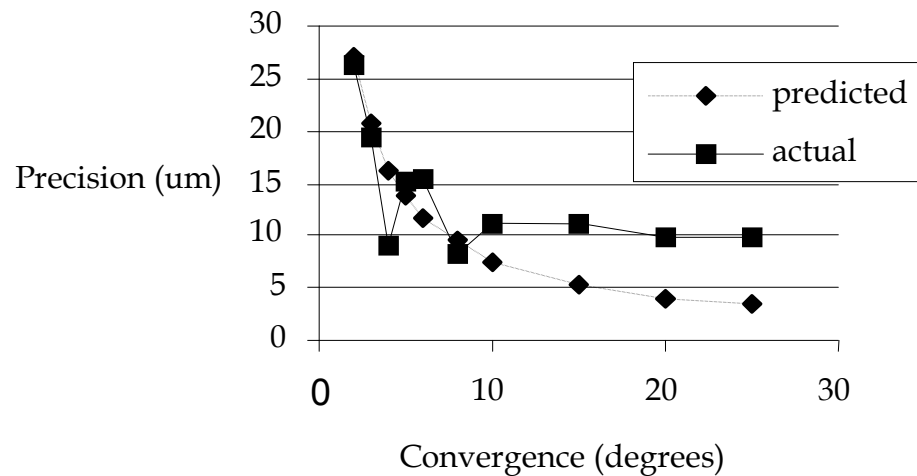


Figure 6.6. Object space precision compared with predicted precision for a targeting precision of $1\mu\text{m}$.

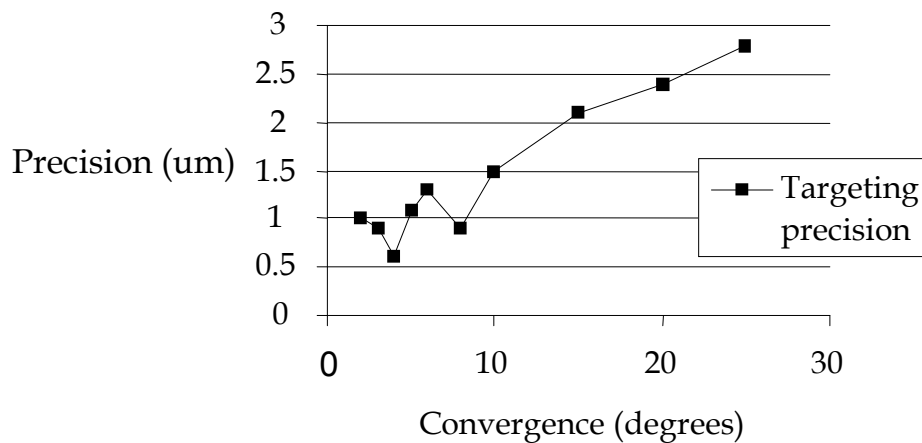


Figure 6.7. Targeting precision values and convergence.

The improved value of $8.95\mu\text{m}$ at convergence of 4 degrees over that at 5 and 6 degrees would suggest that with optimal solutions similar values should be attainable for these convergences as well. Despite extended efforts at these convergences, similar precision values were not achieved. Data from Table 6.7 also shows that targeting precision improves as convergence angle narrows. This is graphically displayed in Figure 6.7 with targeting precision of $0.6\mu\text{m}$ (0.08 pixels) at 4 degrees but reducing to $2.8\mu\text{m}$ (0.38 pixels) at 25 degrees convergence. The improvement in automatic image matching that occurs at narrower convergence angle suggests that image matching

algorithms that take into account the convergence angle of photography could result in improvements in target matching at wider convergence angles.

The simulations confirmed the need for vertical control in convergent photogrammetry with the centre of the image as the optimum location. In very close range applications this is unlikely to be practical and the next best location is on the upper (or lower) centre of the image. Orientation precision requirements become more stringent as the convergence angle decreases with *phi* orientation having a significant impact on model height error. The simulations showed that at 15 degrees convergence and a targeting precision of 1.4 μm , in order to reduce model height error below 10 μm , *phi* error must be in the order of 100 seconds of arc (~ 0.0005 radians) or below. This is in general agreement with the empirical finding with models created by VirtuoZo, that model height error would be within this desired range when the *phi* orientation was within a 0.0007 radian range of the true value.

Manual point measurement in VirtuoZo is available to 0.2 pixels precision which, for the current empirical, work translates to 1.4 μm . However achieving this precision requires optimal target imaging and location. Note that the precision of automatic image matching at 15 degrees was 2.1 μm (Table 6.7) and if manual target matching was to fall to this value then height error would be outside the desired range, at over 14.5 μm (Table 6.7). In order to achieve the desired height error from models at 15 degrees convergence at a photoscale of 1:1, optimum target imaging and location is required. The alternative is to construct a fixed base stereo camera, as was done by several authors in the pre-digital era noted in the introduction and use a self-calibrating bundle adjustment to optimise the camera calibration and orientations. While it would be desirable to narrow the convergence angle for tooth mapping work in order to maximise the area of stereo overlap in regions of steep relief, a 15 degrees convergence angle should be adequate for the mapping of non carious cervical lesions which are the specific subject

of this work. This method is currently being directed to various tooth forms and surfaces to aid in the monitoring of tooth surface loss. This approach may be suitable for a clinically based method of mapping and monitoring surface defects on teeth. It is important for the photogrammetric method to be robust and require low level operator intervention to ensure reliable results.

6.5 Conclusion

The generation of 3D coordinate data from a modified epoxy resin replica using a moderately priced digital camera and lens assembly has resulted in precision of 10 μm for convergences from 4 to 25 degrees. A stereopair from a single camera has not proved sufficiently reliable at forming models of a tooth sized test object with model height error below a desired 10 μm . It was found that automatic image point measurement precision improved with decreasing convergence. Below 10 degrees convergence measurement precision was 1 μm . The improvement in automatic target matching that occurs at narrower convergence angle suggests that image matching algorithms that take into account the convergence angle of photography could result in improvements in target matching at wider convergence angles.

6.6 References

- Abdel-Aziz, Y., 1974. Expected accuracy of convergent photos. *Photogrammetric Engineering*, 40: 1341-1346.
- Adams, L., 1978. The use of a non-metric camera for very short range dental stereophotogrammetry. *Photogrammetric Record*, 9 (51): 405-414.
- Chadwick, R., 1992. Close range photogrammetry - a clinical dental research tool. *Journal of Dentistry*, 20 (4): 235-239.
- Chiat, B., 1977. The shapes of small pebbles. *Photogrammetric Record*, 9 (49): 77-82.

- Clarke, C., Flinn, R., Atkinson, K. and Wickens, E., 1974. The measurement and comparison of tooth shape using photogrammetry. *Photogrammetric Record*, 8 (44): 217-221.
- Faig, W. and Moniwa, H., 1973. Convergent photos for close range. *Photogrammetric Engineering*, 39 (6): 605-610.
- Fraser, C., 1997. Digital camera self-calibration. *ISPRS Journal of Photogrammetry and Remote Sensing*, 52 (4): 149-159.
- Grenness, M., Osborn, J. and Tyas, M., 2005. Stereo-photogrammetric mapping of tooth replicas incorporating texture. *Photogrammetric Record*, 20 (110): 147-161.
- Gruner, H., Zulqar-Nain, J. and Zander, H., 1967. A short-range system for dental surgery. *Photogrammetric Engineering*, 33 (11): 1240-1245.
- Hallert, B., 1954. Some remarks concerning the theory of errors for convergent aerial pictures in comparison with near vertical pictures. *Photogrammetric Engineering*, 20 (5): 749-757.
- Heikkilä, J. and Silvén, O., 1996. Calibration procedure for short focal length off-the-shelf CCD-cameras, *International Conference on Pattern Recognition*, IEEE Inc, Vienna, Austria, pp. 166-170.
- Karara, H. and Abdel-Aziz, Y., 1974. Accuracy aspects of non-metric imageries. *Photogrammetric Engineering*, 40 (9): 1107-1117.
- Konecny, G., 1965. Interior orientation and convergent photography. *Photogrammetric Engineering*, 31 (4): 625-634.
- Lamb, R., McGarrah, H. and Eick, J., 1987. Close-range photogrammetry with computer interface in dental research. *Photogrammetric Engineering and Remote Sensing*, 53 (12): 1685-1689.
- Layton, E. and Cox, P., 1982. The application of photogrammetry to quantitative microscopy. *Photogrammetria*, 37 (6): 203-218.
- Li, G., Li, W. and Yang, S., 1986. Research on micro-stereophotogrammetry. *International Archives of Photogrammetry and Remote Sensing*, 26 (A5): 303-309.
- Mills, J., Schneider, D., Barber, D. and Byran, P., 2003. Geometric assessment of the Kodak DCS Pro Back. *Photogrammetric Record*, 18 (3): 193-208.

- Mitchell, H., Chadwick, R. and McCabe, J., 1989a. Measurement at very close range using microscope photogrammetry. *The Australian Surveyor*, 34 (5): 463-471.
- Mitchell, H. and Chadwick, R., McCabe, J., 1989b. Stereo microscope photogrammetry for the measurement of small objects. *Photogrammetric Record*, 13 (74): 289-299.
- Mitchell, H., Kniest, H. and Oh, W.-J., 1999. Digital photogrammetry and microscope photographs. *Photogrammetric Record*, 16 (94): 695-704.
- Osborn, J. and Wise, G., 1996. Stereophotogrammetric mapping of the anterior surface of the human cornea. *International Archives of Photogrammetry and Remote Sensing*, 31 (B5): 443-449.
- Radlinsky, W., 1952. Convergent low oblique photography and its application to the Twinplex. *Photogrammetric Engineering*, 18 (3): 591-597.
- Vozikis, E. and Douzinas, N., 1984. Results of an attempt to carry out photogrammetric restitution of photomacrographs. *International Archives of Photogrammetry and Remote Sensing*, 25 (A5), 716-731.
- Wang Z, 1990. Principles of photogrammetry (with remote sensing). Publishing house of surveying and mapping, Beijing.

Chapter 7

Calibration of a fixed-base stereo camera for tooth replicas

7.1 Introduction

In medical photogrammetric measurement, two common difficulties are encountered when applied to the measurement and mapping of teeth (Mitchell and Newton 2002). These are the lack of texture on the subjects and the difficulty of determining reliably the camera orientation parameters. These difficulties apply to the subject of this work, which is the mapping of non-carious cervical lesions on human teeth. These lesions occur in most adults, enlarge in size over time and often require restoration. They vary from shallow grooves, to broad dished-out lesions, to large wedge-shaped defects. The floor of the lesions may range in shape from flat, to rounded, to sharply angled (Fig. 7.1).



Figure 7.1. Intra-oral image of posterior teeth with non-carious cervical lesions adjacent to the gum margin (arrows).

In previous chapters, photogrammetric mapping of tooth replicas that incorporated texture was reported, firstly using a film camera (Chapter 5) and secondly using a digital camera (Chapter 6). In both cases, the precision achieved was acceptable but accuracy was degraded by systematic errors attributed to the non-metric behaviour of the film camera and then to small errors in the recovery of the exterior orientation parameters.

Close range applications, by their compact nature, are well suited to fixed base stereo camera equipment. If the stereo camera is sufficiently rigid then, once fully calibrated, object space control is not required. Designs for fixed base stereo systems may include various combinations of single or twin lenses, beamsplitter, plane or semi-silvered mirrors, and single or twin sensors (Ray 1992). For a twin camera/lens system built using commercially available digital SLR cameras, the size of the cameras and lenses places a physical limitation on the proximity of the cameras and hence the base distance. Including a mirror between the object and lens allows the optical paths for the two cameras and therefore the cameras themselves to be separated, and the base distance and convergence angle to be chosen depending on the demands of the particular measurement task.

Methods for laboratory and field calibration of single cameras have been well described (Fraser, 1997; Fryer, 1992). However reports on the calibration of fixed base stereo cameras are more sparse, particularly in the case of very close range applications. Examples are line of sight calibration for a dental application (Gruner et al., 1967) and algorithmic calibration of a stereo light microscope (Danuser, 1999). The relative orientation of a fixed base stereo camera may be held as model invariant in the solution (King, 1995), or model variant and the mean computed from multiple stereopairs (Shortis and Harvey, 1998). A strong network and depth in the target array are required to minimise correlations between interior and exterior parameters (Shortis and Hall, 1989). Calibration arrays used for very close range applications have included a planar array (Chapter 5), a planar array translated to

provide a three-dimensional test field (Curry et al., 1981; Curry et al., 1986; Danuser 1996), a three-dimensional object constructed from steps of known height fixed to a plane (Vozikis and Douzinas 1984), and a glass sphere with trans-illuminated targets on a thin, dark surface coating (Osborn and Wise 1996).

This paper describes the construction and measurement of a composite calibration artefact and the calibration of an experimental fixed base stereo digital camera for very close range photogrammetry applications, principally the mapping of individual tooth replicas. Models of the central part of the artifact were created with photogrammetric software using the pre-calibrated camera parameters and additional stereopairs not used for the calibration. Models were then tested for accuracy and precision.

7.2 Method

A fixed base stereo camera was assembled using two 22.7 × 15.1 mm format digital cameras (Canon EOS 300D; Canon Inc., Tokyo, Japan) fitted with 80 mm lenses (Componon; Schneider-Kreuznach, Germany), extension tubes and T-2 adapters, achieving a photoscale of 1:1. The camera and lens assemblies were mounted facing a front-silvered 90° mirror achieving a convergence angle of approximately 15°. A ring flash (Macro Ring Lite MR-14Ex; Canon Inc., Tokyo, Japan) was fitted below the mirror (Figure 7.2). A remote switch was used to simultaneously trigger both cameras and flash.

A composite calibration artifact was constructed from a tiered object incorporating optical texture, fixed to black film with a planar array consisting of 100 transilluminated targets of 40 µm diameter, spaced at approximately 2 mm (Figure 7.3).

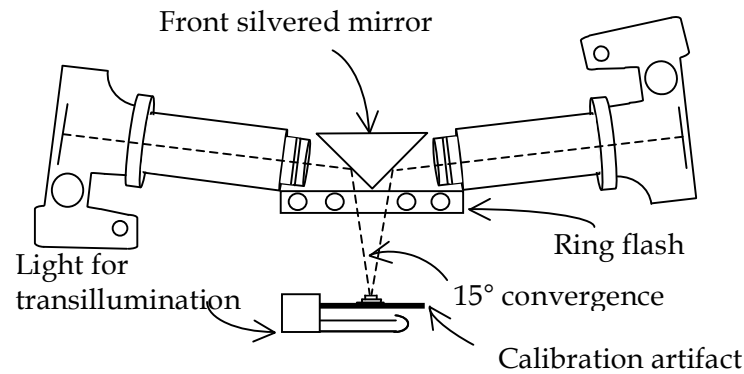


Figure 7.2. Schematic of fixed base stereo camera, lens and mirror assembly with ring flash. (also refer to Figure 9.3, pp. 182)

The method of construction of the planar array and tiered object have been separately described in Chapter 5. The tiered object was fixed to the planar array with cyanoacrylate and 39 readily identifiable near-circular natural targets were identified on the three planes of the object. All targets were measured with a non-contact coordinate measurement machine (CMM) (Starlite 250/300; Optical Gauging Products Inc. Rochester, NY, USA) to a reported precision of $2.6\ \mu\text{m}$ (X , Y , planimetric) over the measuring length and $7\ \mu\text{m}$ (Z , vertical) over the measuring height. The height values of the transilluminated planar targets were adjusted by half the thickness of the film ($0.05\ \text{mm}$).

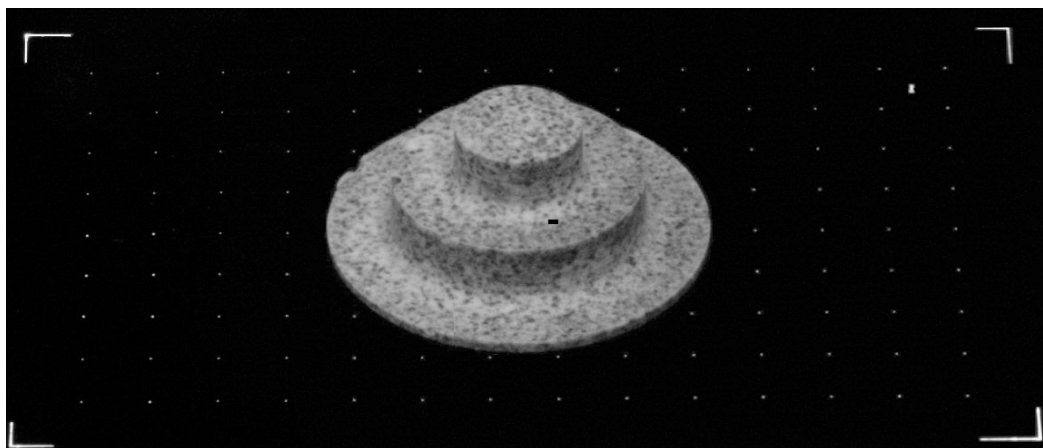


Figure 7.3. Composite artifact: tiered object incorporating optical texture fixed to the planar array of transilluminated targets.

The composite artifact was seated on a light box and both were tilted to achieve stereoimages from five positions (0° and four 5° quadrant views, from Right, Left, Top, Bottom) with the divergence normal to the artifact being limited by the depth of field (DOF). The artefact was rotated at each camera position to achieve roll angles of 0° , $\pm 90^\circ$ and 180° , resulting in a total of 20 stereopairs. The lens aperture was approximately 4 mm and the shutter speed was 1/15 second. The acquired images were transformed with a 'mirror' function using MS Paint to account for their capture via the mirror.

Bundle adjustment calibration software (3DM Calib Cam v2.2a; ADAM Technology P/L, Perth, Australia) was used for manual measurement of image points and, following resection and bundle adjustment, for the calculation of interior and exterior camera orientation parameters in a single adjustment, updated target coordinates, and various error statistics. The bundle adjustment employed was model invariant with a single set of relative orientation parameters solved for all stereopairs.

7.2.1 Model generation and accuracy testing

Six stereopairs were combined with camera calibration data and separately processed to produce stereomodels (3DM Analyst v2.2a; ADAM Technology P/L, Perth, Australia). No further orientation procedures were required. For each model, the 39 natural targets on the tiered object were manually measured with a floating mark in 3DM Analyst-*stereo view* (object space) and exported. A digital terrain model (DTM) of the test object was automatically generated using image matching of the optically textured surface and the DTM was then exported.

Accuracy of models was evaluated in object space:

- i) Manual floating mark measurements of the 39 targets were compared with the CMM measurements and with updated target coordinates from the camera calibration using a least-squares rigid motion.

- ii) Automatic DTM data from the top and low tiers were used to compute a plane of best fit and height distance normal to the top and low plane of the tiered object. Height distances were compared with CMM and updated target height distances computed by the same method.

Precision of models was evaluated in object space:

- i) Manual floating mark measurements of the 39 targets on the tiers of a single model were used to compute the standard deviation from the mean for X, Y and Z coordinates for each tier and the tiers combined.
- ii) Automatic DTM data were cropped to 1 mm × 1 mm sections from various locations on the DTM and used to compute the standard deviation of the Z coordinate from the plane determined by the least-squares plane fit algorithm.

Precision of image space and object space errors was evaluated by performing various bundle adjustments with the relative orientation held as model variant (not constrained) with:

- i) Manual measurement of the transilluminated planar targets alone.
- ii) Manual measurement of the natural targets alone.
- iii) Manual measurement of both types of targets together.
- iv) Automatic measurement of the transilluminated planar targets alone.

7.2.2 Tooth surface modeling

The teeth shown in Figure 7.1 were replicated with the experimental die material described in (Chapter 5) to produce a replica incorporating optical texture. This replica was imaged using the digital stereo camera, and the images and camera orientation data were loaded into the photogrammetric software. Following image matching, the *spike removal* utility was used to remove gross matching errors, a surface DTM was derived and an image draped over the DTM to review the fidelity of the resulting model.

7.3 Results

Targets from 13 stereopairs were measured and included in the bundle adjustment calibration. It was found that a sudden change in relative *kappa* orientation between the two cameras occurred between stereopairs 4 and 5. The first four stereopairs were excluded from further processing. The remaining nine stereopairs were included in a bundle adjustment calibration. The calibration parameter values and errors for the left camera appear in Table 7.1. Calibration accuracy statistics appear in Table 7.2.

Interior orientation parameters			Relative orientation parameters		
Parameter	Value	σ Value	Parameter	Value	σ Value
c (mm)	156.7141	3.54×10^{-1}	Base X (mm)	42.0515	0.0000
x_p (mm)	8.30×10^{-1}	3.77×10^{-1}	Y (mm)	-0.4099	0.0000
y_p (mm)	1.95×10^{-1}	2.53×10^{-1}	Z (mm)	-8.4009	0.0000
k_1	6.35×10^{-6}	1.09×10^{-5}	<i>Omega</i> (deg.)	0.5558	0.0001
k_2	-2.75×10^{-8}	2.09×10^{-7}	<i>Phi</i> (deg.)	-14.8138	0.0000
k_3	4.30×10^{-10}	1.61×10^{-9}	<i>Kappa</i> (deg.)	0.1462	0.0000
k_4	-1.34×10^{-12}	4.24×10^{-12}			
p_1	-3.53×10^{-5}	6.28×10^{-6}			
p_2	-4.07×10^{-6}	4.33×10^{-6}			
b_1	-4.95×10^{-4}	4.19×10^{-5}			
b_2	2.15×10^{-4}	4.10×10^{-5}			

Table 7.1. Interior and exterior calibration parameters and errors
(c: principal distance; x_p , y_p : principal points; k_1 , k_2 , k_3 , k_4 : 1st, 3rd, 5th, 7th polynomial radial distortion; p_1 , p_2 : decentring distortion; b_1 , b_2 : pixel affinity and orthogonality).

Object rms errors (μm)			Image rms errors (μm)		Image rms errors (pixels)	
X	Y	Z	x	y	x	y
3.67	3.69	8.53	2.64	3.39	0.36	0.46

Table 7.2. Calibration accuracy statistics: object and image space residual errors.

7.3.1 Model accuracy

Stereomodels were formed from six stereopairs with photogrammetric software using the calibration data. Object space measurements were repeated three times except for one model which were repeated seven times to facilitate estimation of precision. The mean of measured object space coordinates was fitted to the CMM coordinates and updated target coordinates using a rigid motion best fit. The means and standard deviations of the residuals (σX , σY , σZ) appear in Table 7.3. Residual data were used to create residual vectors (σXYZ). The means (\pm s.d.) of the residual vectors of coordinates fitted to the CMM coordinates were 15.74 (± 10.49) μm , and for coordinates fitted to the updated coordinates were 12.10 (± 7.23) μm .

Object space coordinates fitted to CMM coordinates				
Models 1-6	σX	σY	σZ	σXYZ
Mean(μm)	0.00	0.00	0.00	15.74
s.d. (μm)	5.50	5.07	17.45	10.49
Object space coordinates fitted to updated target coordinates				
Models 1-6	σX	σY	σZ	σXYZ
Mean(μm)	0.00	0.00	0.00	12.10
s.d. (μm)	3.87	3.46	13.27	7.23

Table 7.3. Object space accuracy/ manual measurement: object space coordinates fitted to CMM and updated target coordinates (residual errors: σX , σY , σZ ; residual vector errors: σXYZ ; mean and s.d.).

Following model formation and automatic DTM generation, the number of points generated in the low and top planes of the tiered object was typically about 16,000 and 4,600 respectively, an average point spacing of 0.055 mm. The mean height (normal distance) between the low and top planes, the standard deviation of the height, and the range of the three height measurements are given in Table 7.4. The mean (\pm s.d.) distance from the low to top plane for the six models was 4.000 (± 0.002) mm. The range of heights from the three in-plane locations varied from 0.003 to 0.008 mm. This is

indicative of slight non-orthogonality of the planes. CMM and updated target coordinates were also used to calculate planes of best fit for the top and low tiers of the tiered object. Mean height computed from the CMM coordinates was computed to be 3.997 (± 0.006) mm and for the updated coordinates was 3.998 (± 0.004) mm

Model	Station	Roll angle	Mean height (mm)	s.d. (mm)	Range of 3 measurements (mm)	Position of top plane in DOF (mm)
1	5°R	0°	3.999	0.00047	0.006	+0.6
2	5°R	270°	3.999	0.00038	0.008	+0.9
3	5°T	270°	4.000	0.00033	0.005	+1.3
4	5°B	90°	4.004	0.00040	0.007	+0.3
5	5°B	180°	4.001	0.00028	0.003	+2.0
6	5°B	270°	3.999	0.00033	0.006	+4.3
Mean			4.000			
s.d.			0.002			
CMM height (mm)			3.997	0.00596	0.006	
Updated target height (mm)			3.998	0.00381	0.003	

Table 7.4. Object space accuracy/ automatic measurement: object space DTM height, CMM height, updated target height (mean, s.d., range of 3 measurements, position within DOF). Camera stations: Right, Top, Bottom.

Movement of the object to enable acquisition of multi-station stereoimages resulted in different positions of the artifact within the depth of field of the cameras. For the models tested, this ranged from 0.3 to 4.0 mm for the top plane, indicating that model accuracy was not influenced by vertical positioning of the artifact within the centre of the depth of field.

7.3.2 Model precision

The precision of manual measurement from a stereomodel was assessed by calculating the standard deviation from the mean of X, Y and Z coordinates of seven repeat measurements of 39 targets on the tiered object. The standard

deviations appear in Table 7.5 together with the location of the tier within the depth of field. Overall, precision in X, Y and Z was 3.2, 2.8 and 15.3 μm respectively.

Plane/coordinate	X s.d. (μm)	Y s.d. (μm)	Z s.d. (μm)	Position of model in DOF (mm)
top	3.0	1.9	9.8	0.8
mid	2.7	2.7	14.8	-1.3
low	3.7	3.3	18.6	-3.4
all	3.2	2.8	15.3	

Table 7.5. Object space precision/ manual measurement: object space coordinate repeat measurement (s.d. of X, Y, Z measurements, position within depth of field).

The precision of automatic DTM generation from one model was assessed by determining the standard error of the Z coordinate from the plane determined by the least squares plane fit algorithm of 1 x 1-mm sections (Figure 7.4). The standard deviations appear in Table 7.6 together with the location of the tier within the depth of field. Standard deviations varied between 12.9 and 21.8 μm . These results are typical of many models.

Section	s.d. (μm)	No. of points	Mean Z (μm)
A	14.6	455	2.42
B	14.7	299	2.3
C	16.6	151	0.69
D	13.5	165	0.68
E	16.8	219	0.24
F	12.9	213	0.1
G	18.4	298	-1.19
H	15.8	369	-1.27
I	21.8	400	-1.94
J	19.6	280	-2.16

Table 7.6. Object space precision/ automatic measurement: DTM fitted to plane of best fit (s.d., no of points, location within depth of field).

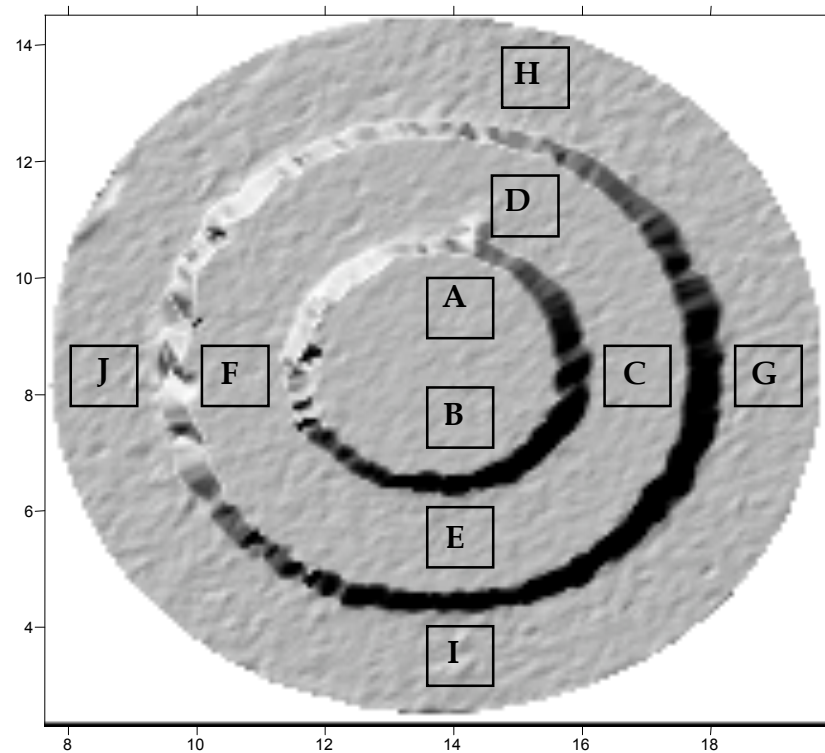


Figure 7.4. Model 5 surface relief showing location of 1×1 mm sections used for precision calculation (s.d.). Scale units: mm.

7.3.2 Image and object space errors

Image and object space errors from the various model variant (not constrained) bundle adjustments appear in Table 7.7. Image rms errors are similar regardless of the type of target or method of measurement (approximately $3 \mu\text{m}$), with a slight improvement with automatic measurement. The use of 'planar transilluminated points only' resulted in a reduction in object space rms errors, particularly in Z. An examination of the full calibration results associated with each adjustment showed that there were greater errors associated with the relative orientation between the two cameras, which was known to be rigidly fixed.

	Object rms errors			Image rms errors		Image rms errors (pixels)	
	X	Y	Z	x	y	x	y
<i>Manual measurement</i>							
Planar transilluminated points only	2.90	2.55	4.57	2.81	3.02	0.38	0.41
Natural points only	2.60	3.76	10.20	2.81	2.95	0.38	0.40
Planar transilluminated and natural points	3.85	3.76	8.10	2.88	3.02	0.39	0.41
<i>Automatic measurement</i>							
Planar transilluminated points only	2.3	2.2	5.1	2.66	2.36	0.36	0.32

Table 7.7. Calibration accuracy statistics for the different target type and measurement method: object and image space residual errors.

7.3.3 Tooth surface modelling

Figure 7.5 shows an orthoimage of the epoxy replica of the teeth (Figure 7.1) overlaid with a 0.1 x 0.1 mm grid derived from the DTM. The non carious cervical lesions are indicated by an arrow. These lesions are clearly evident in both the surface image and the wireframe.

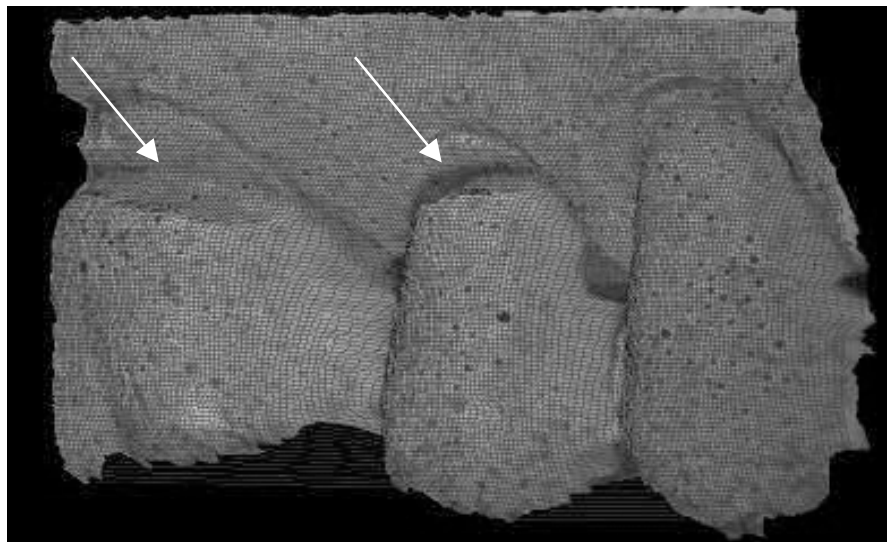


Figure 7.5. Tooth replica with non-carious cervical lesions (arrow): digital orthoimage draped over DEM with 0.1 mm x 0.1 mm grid.

7.4 Discussion

Investigations employing self-calibration have dominated the literature in recent years. These have typically employed target arrays consisting of multiple elements, with targets distributed in three dimensions throughout the full measurement volume, together with a highly convergent network (Fraser 1997). For this very close range calibration, the narrow depth of field severely restricted the network so that a measured camera calibration array was still required.

7.4.1 Target measurement

Automatic measurement of circular, evenly illuminated targets in close range applications can achieve precisions of 0.02 pixels or better (Fraser 1997), while manual measurement of targets achieving precisions of about 0.2 pixels are more typical (e.g. Chandler et al., 2005). In this current work, the measurement error for manually measured image points was about 0.4 pixel, for both directly and trans-illuminated targets. Automatic target measurement performed more poorly. Target quality was not optimal: the transillumination of targets resulted in uneven light scatter at the edges of targets, while direct illumination of natural targets on the tiered object was not consistent, resulting in a different appearance between right and left images and between subsequent stereopairs. This different appearance was attributed to the placement of the ring flash closer to the object than would normally be the case with macro photography. The precision of manually measured targets proved adequate for the geometry of the camera setup and accuracy requirements of the calibration. While the internal precision data in Table 7.7 suggests improved precision of automatic point measurement over manual point measurement, the precision of automatically measured targets was inadequate, with subsequent models containing excessive systematic height errors.

7.4.2 Parameter set

The full parameter set available in the software was utilised. Some of the estimates of parameter precisions, particularly radial distortion reported in Table 7.1, were of greater magnitude than th

e associated parameter values. Danuser (1999) noted that the narrow depth of field associated with very close range photography leads to a weaker convergent network, which can in turn lead to parameter precisions that are significantly larger than the parameter values.

7.4.3 Object space accuracy and precision

Manual object space measurements of the tiered object compared with updated target coordinates (Table 7.3) showed very similar model errors to the rms errors on object coordinates from the calibration (Table 7.2). When manual measurements were compared with CMM measurements, the errors were greater. Limited access to the CMM resulted in measurements being taken only once and the accuracy and precision of these measurements were not tested.

There was considerable difference in errors between object space measurements in Z measured manually and measurements derived from mass DTM points fitted to planes (Table 7.4). Given the increased uncertainty surrounding manual point image measurement associated with variations in illumination and image clarity, the result from mass DTM points is more likely to give a true indication of object space accuracy derived from the calibration, with the conclusion that accuracy was well within desired limits of approximately 3 μm . There is no suggestion of systematic bias in the distribution of mass DTM points with residuals on points fitted to a plane being normally distributed around a mean of zero.

Small 1 x 1 mm sections were used to minimize the effects of plane edge data and shadows, and model distortions which have a primary effect on accuracy, but will also impact on precision. Object space precision varied

according to image and target clarity. Object space precision in Z from mass DTM points varied from 13 to 22 μm dependent on image clarity and location within the depth of field. Best precision of 9.8 μm was obtained from a stereopair excluded from the calibration. Precision around 10 μm has previously been reported (Chapter 6), where the use of a single camera allowed optimal focussing to be achieved on both images of a stereopair. The use of a stereo camera and positioning of the object within the field of view is likely to have resulted in less than optimal image clarity in both images of a stereopair.

In terrestrial photogrammetry, depth of field issues do not generally limit the measurement volume. In this work, the tiered object had targets over a height of 4 mm, and the variation in position of the object within the depth of field of models tested (Table 7.4) was 3.7 mm. The variations in precision within the zone were not significant, suggesting that the useful depth of field within the centre of the image may have been a total of 7.7 mm. While the limits of the useful depth of field were not tested, this value probably was close to the limit, with the smallest aperture setting on the lenses being used.

The area of best focus of images was typically centred around the middle tier. Optimum precision could be expected to occur where image clarity was greatest at the centre of the depth of field. This was not fully reflected in the precision data of Table 7.6, where better precision results were obtained from two of the four areas of the mid tier. A precision result of 20 μm from areas of the low tier was a common finding. This was not due to difference in the texture of the low plane compared with other planes. Potential causes were greater machining marks in the low plane, diminished image clarity, altered appearance of the surface texture due to slight differences in illumination between left right images, or residual errors in interior and exterior orientation.

The sudden change in *kappa* orientation between images 4 and 5 revealed that the bayonet mount and T-2 adapters were not rigid enough for the

current project without further modification of the attachment mechanism or rigidity of the overall setup. This is unsurprising for consumer level products where insufficient CCD fixation within the camera, body flex and instability in the lens mounting system have all been described (Shortis and Harvey, 1998).

7.5 Conclusion

A composite calibration artifact and manual image point measurement were used in combination with bundle adjustment calibration software to calibrate a fixed base stereo camera for very close range photogrammetry. The commercial software allowed for a straightforward calibration and model generation. Variations in illumination and image clarity across the entire measurement volume restricted the use of automatic control point measurement. However manual point measurement proved satisfactory with precision in object space for individual point measurement of approximately 15 μm , and accuracy of surfaces derived from automatic measurement of surface texture of approximately 3 μm .

Further improvement in precision reported here could be expected by varying the use of outlier detection and data smoothing. The grid geometry and point density required to represent the surface of a tooth will vary with the accuracy requirement of a particular application, such as change detection, or reverse engineering. The results reported in this paper are confined to system calibration and accuracy assessment.

7.5 References

Chandler, J.H., Fryer, J.G. and Jack A., 2005. Metric Capabilities of low-cost digital cameras for close range surface measurement. Photogrammetric Record, 20 (109): 12-26.

- Curry, S., Anderson, J.M. and Moffitt, F.H., 1981. Calibration of extreme close-range stereometric cameras. *American Society of Photogrammetry*, pp. 311-324.
- Curry, S., Baumrind, S. and Anderson, J.M., 1986. Calibration of an array camera. *Photogrammetric Engineering and Remote Sensing*, 52 (5): 627-636.
- Danuser, G., 1996. Stereo light microscope calibration for 3D submicron vision. *International Archives of Photogrammetry and Remote Sensing*, 31 (Part B5): 101-108.
- Danuser, G., 1999. Photogrammetric calibration of a stereo light microscope. *Journal of Microscopy*, 193 (1): 62-63.
- Fraser, C.S., 1997. Digital camera self-calibration. *ISPRS Journal of Photogrammetry and Remote Sensing*, 52 (4): 149-159.
- Fraser, C. and Shortis M., 1995. Metric exploitation of still video imagery. *Photogrammetric Record*, 15(85): 107-122.
- Fryer, J.G., 1992. Recent developments in camera calibration for close-range applications. *International Archives of Photogrammetry and Remote Sensing*, 29: (594-599).
- Gruner, H., Zulqar-Nain, J. and Zander, H.A., 1967. A short-range system for dental surgery. *Photogrammetric Engineering*, 33 (11): 1240-1245.
- King, B., 1995. Bundle adjustment of constrained stereopairs- mathematical models. *Geomatics Research Australasia*, 63 (December):67-92.
- Mitchell, H.L. and Newton, I., 2002. Medical photogrammetric measurement: overview and prospects. *ISPRS Journal of Photogrammetry and Remote Sensing*, 56 (5-6): 286-294.
- Osborn, J.E. and Wise, G.M., 1996., Stereophotogrammetric mapping of the anterior surface of the human cornea. *International Archives of Photogrammetry and Remote Sensing*, 31 (B5): 443-449.
- Ray, S.F., 1992. *The photographic lens*. 2nd edition: Focal Press, Oxford. 355 pages.

Shortis, M.R. and Hall, C.J., 1989. Network design methods for close-range photogrammetry. *Australian Journal of Geodesy, Photogrammetry and Surveying*, 50 (June): 51-72.

Shortis, M.R. and Harvey, E.S., 1998. Design and calibration of an underwater stereo-video system for the monitoring of marine fauna populations. *International Archives of Photogrammetry and Remote Sensing*, 32 (5): 792-799.

Vozikis, E. and Douzinas, N., 1984. Results of an attempt to carry out photogrammetric restitution of photomacrographs. *International Archives of Photogrammetry and Remote Sensing*, 25 (A5): 716-731.

Chapter 8

Tooth surface alignment using two methods

8.1 Introduction

In the previous chapter, the construction and calibration of an experimental stereo camera for very close range photogrammetry was described. This camera system and photogrammetry software generated 3D surface models of tooth replicas incorporating optical texture without the need for photogrammetric control points. In operational terms, the tooth replica was placed into the measurement zone of the camera system, stereoimagery was captured and after a short processing time and editing if required, a high density, random or unorganized point cloud was generated. The point cloud was exported as a raw digital terrain model (DTM) or sampled into a digital elevation model (DEM), at regular grid intervals in X and Y. The format of the surface data can be changed for different applications. Data can be manipulated by outlier detection to remove any gross measurement errors, sampled to reduce the density of the surface data as an ordered array, or interpolated to generate likely surfaces in any small areas of missing data.

The clinical model under study in this thesis is change detection of non carious cervical lesions on teeth (Figure 8.1, left). Change detection requires alignment of surface models obtained at different times, and analysis of differences between the surfaces. Prior to alignment of surface models, the format and density of the data needs to be considered. Change detection *per se* is considered in the next chapter.

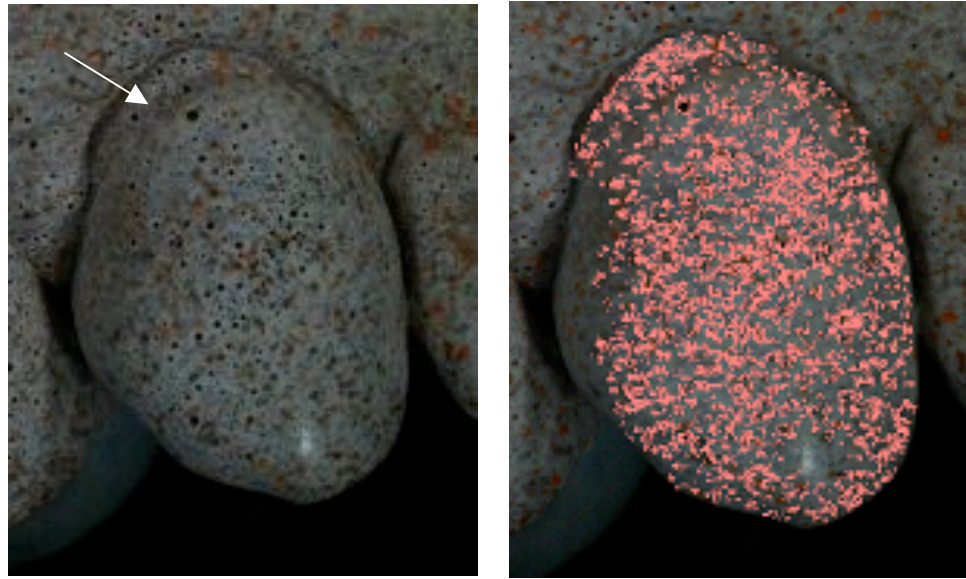


Figure 8.1. Tooth replica with arrow indicating a non carious cervical lesion (left); tooth replica image with point cloud overlay generated by 3DM Analyst (right). Note region of light reflection that inhibited mapping and resulted in missing surface data in the point cloud.

Measurement systems for mapping tooth surfaces were summarized in Chapter 5. A small number of automated, high accuracy measurement systems for teeth have been applied to surface alignment and change detection, initially for the measurement of restoration wear (DeLong et al., 1985; Roulet, 1985), more latterly for the measurement of erosion (Azzopardi et al., 2001; Bartlett et al., 1997; Chadwick et al., 1997) and non carious cervical lesions (Pintado et al., 2000) (Table 8.1). Some of these systems have been refined over several years with altered specifications referred to in the literature. Systems have reported accuracy of $<10\ \mu\text{m}$ and precision $<3\ \mu\text{m}$.

These measurement systems have utilised a variety of grid intervals, with the contact stylus systems employing X and Y intervals between 100 and 150 μm and the number of points measured in the order of 2000+, and the newer non contact systems utilising intervals between 20 and 50 μm and up to 76,000 points measured for a tooth surface.

Author	Type	Date	Grid interval	Accuracy (precision)	Matching precision	Manufacturer
Roulet	Contact stylus	1985	100 x 100 µm	<10 µm	-	-
DeLong et al.	Contact stylus	1985	125 x 100 µm	<10 µm	22µm	-
Lee et al.	Contact stylus	1995	100 x 50 µm	4.4 µm	21 – 24 µm	See DeLong et al., 1985
Persson et al.	Contact stylus	1995	50-100x200 µm	10 µm		M50; Nobel Biocare AB, Sweden
Bartlett et al.	Contact laser	1997	30 µm	10 nm	25 µm	Rank Taylor Hobson, England
Mehl et al.	Laser stripe	1997	27 x 25 µm	6 (±3) µm	10 µm	-
Chadwick et al.	Contact stylus	1997	150 x 150 µm	4.4 (2.8) µm	20 µm (2001)	-
Peters et al.	Contact stylus	1999	125 x 100 µm	±7 µm		See DeLong et al., 1985
Azzopardi et al.	Laser stripe	2001	45x20 µm	1.4 µm		UBMMesstechnik, Germany
Van der Zel et al.	Laser stripe	2001	200 µm	10 µm	-	CICERO Dental Systems, Neth.
Persson et al.	Laser stripe	2006	150 x 150 µm?	10 µm	-	3Dshape A/S, Denmark

Table 8.1. Automated tooth surface measurement reports

Commercial systems have also been developed for CAD/CAM purposes with Leinfelder et al. (1989) reporting on an intra-oral structured-light system (CEREC; Sirona Dental Systems GmbH, Bensheim, Germany), Persson et al. (1995) reporting on a contact stylus system (M50; Nobel Biocare AB) and Persson et al. (2006) reporting on a experimental laser stripe scanner (3Dshape A/S, Copenhagen, Denmark), all of which operate at a lower resolution than the majority of systems described for diagnosis utilizing change detection.

There are few reports investigating tooth surface alignment using surface alignment algorithms. DeLong and Douglas (1990) found that the minimum number of points required for alignment, which did not alter the final rms/point significantly, was 500 points. Lee et al. (1995) used the contact stylus system of DeLong and Douglas (1985) and the tooth surface alignment system of DeLong and Douglas (1990) to perform 10 repeat mappings of a master model, separated by mapping of replicas of the master model. The overall accuracy of the mapping and alignment system was determined by sequential alignment of the master model data-sets and found to have a rms error of $3.6 \pm 0.5 \mu\text{m}$ with a further $1.3 \mu\text{m}$ attributed to stylus wear.

Sequential alignment of 10 repeat mapping of replicas with the master model resulted in rms errors between $21 \mu\text{m}$ and $24 \mu\text{m}$ for various impression technique variables tested. Occasionally, replicas of the same tooth failed to align; no explanation was found for this occurrence.

The newer higher resolution non contact systems have a reported combined measurement and alignment precision of around $10 \mu\text{m}$ (Mehl et al., 1997). Mehl et al., (1997) reported alignment accuracy alone of less than $1 \mu\text{m}$ where the same surface was transformed and then realigned to the original. When an independent replica of the same surface was aligned, the alignment error was reported to be up to $20 \mu\text{m}$, suggesting that impression and replication techniques and non-coincident grid geometries introduce significant errors. In the case of non contact systems which measure a very large number of

points in less than a minute, there may not be a significant overall measurement advantage in alignment accuracy when compared with systems that measure fewer points.

The report of Price et al. (1991), which examined replication errors, concluded that replication technique may be a source of dimensional variations and non-reproducible errors of up to 9 μm . This figure has been often cited (Azzopardi et al., 2000; Mehl et al., 1997), however, in the Price et al. (1991) study, when replicas were compared with the master model, a mean increase of 10 μm in two dimensions and 27 μm in the third dimension was reported. The significance of dimensional changes in impression and casting materials in the clinical setting is that shrinkage of the impression materials leads to a mould space, and therefore a replica, which is slightly oversized. In the case of metal and/or ceramic tooth-forms (crown) that fit over a prepared tooth surface and are cemented into place, the slight over-sizing of the tooth-form replica leads to an increased space between the crown and the prepared tooth, to be filled in with the cement, and there is no difficulty fitting the oversized crown to the prepared tooth. In the case of metal and/or ceramic inlays that fit within a prepared cavity in a tooth and are cemented into place, the slight over-sizing of the tooth-form replica may lead to an over-sized inlay, creating difficulty in fitting the inlay into the prepared tooth cavity. A tooth-restoration (crown or inlay) gap of 50 – 100 μm is generally recommended (Leinfelder et al., 1989).

Four different types of three dimensional matching are prominent in the spatial sciences literature (Pilgrim, 1996): (i) 3D object identification using relational matching; (ii) least squares surface matching of 3D data sets; (iii) feature based matching; and (iv) contour matching. In dental research, feature based matching has been used by grinding small depressions into teeth (Lambrechts et al., 1981), cementing metal disks covering 5-10% of the tooth surface (Bartlett et al., 1997), and using natural morphologic features of gorilla molar teeth (Ungar and Williamson, 2000). However, least squares

surface matching is now well established in the dental literature as a method for aligning tooth surface models in the dental literature (DeLong and Douglas, 1990; Mehl et al., 1997; Mitchell and Chadwick, 1998) and more recently least squares minimisation of tooth solid models (Persson et al., 2006). All the above authors have reported alignment algorithms that involve interpolation to resample one surface to the same grid geometry of the other surface and least squares minimization by iteration. Methods of resampling are quadrilateral interpolation (DeLong and Douglas, 1990; Mehl et al., 1997), bilinear interpolation and triangulation and linear interpolation (Mitchell and Chadwick, 1998).

More recently, visualisation techniques using Virtual Reality Modelling Language (VRML) have been used to represent objects in three dimensions, allowing the observer to view teeth and dental arches from any orientation and distance (Evans et al., 2001). This approach has been reported for calculating occlusal contacts using virtual casts aligned with virtual interocclusal records (DeLong et al., 2001), and to perform best-fit registration of surface models of tooth replicas prepared for full crowns (Luthardt et al., 2003). Full validation is yet to be reported in the dental literature.

A significant factor when performing an alignment is the choice of a threshold value for the exclusion of points from the alignment. An alignment would otherwise be corrupted by points that contained measurement, sampling or interpolation errors, or that represented areas of change. For their non-contact laser stripe system, Mehl et al. (1997) considered matching to be successful when matched areas showed errors similar to the accuracy of the primary measurement system. Generally, difference values of more than three times the sensor accuracy were considered outliers.

There are presently few standards or criteria for assessing and describing the accuracy and precision of clinical tooth mapping for monitoring purposes. Mehl et al. (1997) proposed that the entire tooth surface should be mapped

with a large number of points, the measurement and analysis time should be short, and the method should be accurate enough to detect minimal tooth loss. There does not appear to be clear specifications for tooth mapping in the dental literature, in terms of what constitutes appropriate grid intervals, point accuracy and precision.

This chapter reports on an investigation of surface alignment of a tooth surface replica incorporating texture obtained using the fixed base stereo camera and photogrammetry software. The aim of the investigation was to examine the effects of:

- i) outlier exclusion threshold,
- ii) interpolation of missing data, and
- iii) grid interval

upon the repeatability and precision of mapping and alignment (together) and alignment (alone) using two alignment software programs.

8.2 Method

8.2.1 Data Acquisition and sampling

The experimental camera system was reassembled with modification to the backing frame to render the assembly sufficiently rigid to prevent small movements of the camera-lens attachment mechanism, and replacement of the macro ring flash used for the previous work with an array of multiple-element LED lighting. The stereo camera was re-calibrated using the method described in the previous chapter and used to acquire ten repeat stereoimages of a tooth replica, poured with epoxy resin incorporating optical texture (Figure 8.1, left), with each stereopair captured from different locations. The tooth surface chosen, an upper canine, has a small NCCL present at the gum margin and is typical of the type of tooth surface that might be monitored for clinical or research purposes. Surface models, consisting of a random point cloud (Figure 8.1 right) of data points (DTM) were generated with photogrammetry software (3DM Analyst v2.2a; ADAM

Technology P/L, Perth, Australia) and pre-calibration data. The ten DTM datasets (Figure 8.2 left), while representing the same surface, contained different coordinate measurements and different boundaries with the greatest variation occurring at the right and left margins of the models. The ten repeat DTM datasets were exported as point clouds (DTMs), and also sampled to create digital elevation model (DEM) grids at regular intervals in X and Y, with nominated starting values in X and Y used to offset the grid nodes in different datasets (Figure 8.2 right). The spacing of DTM point cloud data was examined using geographic information system software (ArcGIS v.9.2; ERSI Inc., Redlands, California).

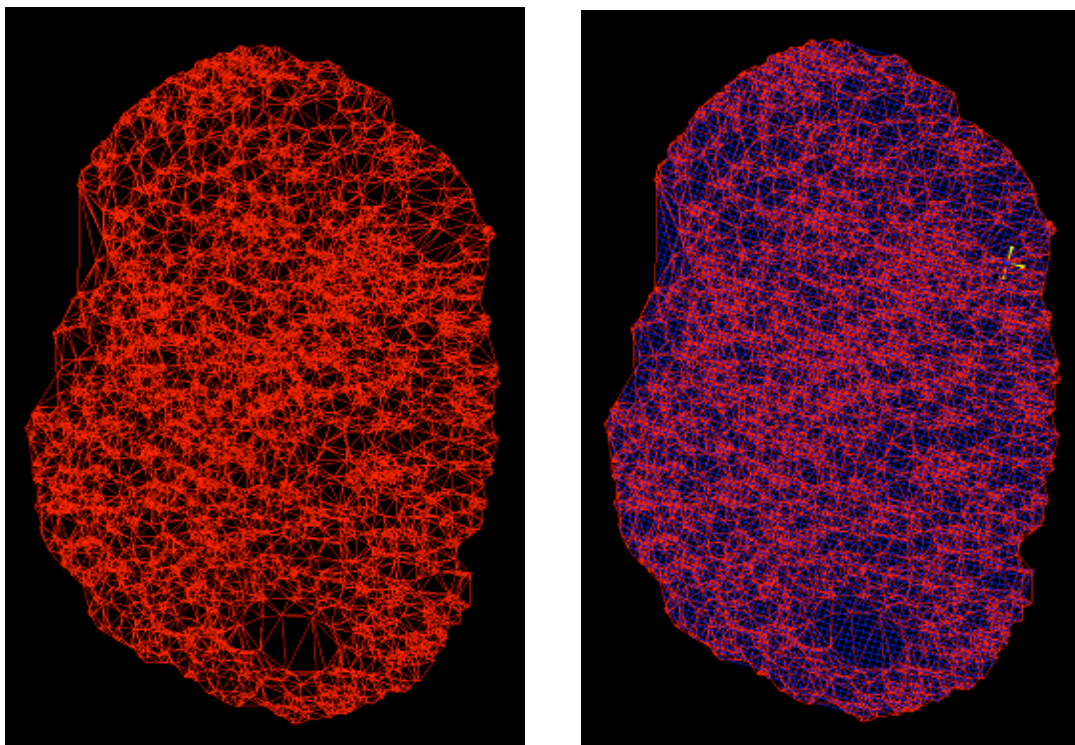


Figure 8.2. Tooth DTM (triangulated) generated by 3DM Analyst (left); tooth DEM draped over DTM, 0.1 x 0.1 mm grid interval, exported from 3DM Analyst (right).

8.2.2 Data alignment

The ten datasets were processed and aligned with proprietary software (DSMatch v9, H Mitchell, 2005) and with commercial software (Polyworks v 9.1.7, Innovmetric Software Inc, Canada).

DSMatch triangulates and interpolates the data points on one surface to enable the z-axis values of one surface to be subtracted from the other to produce difference or residual data, and uses an iteration process to shift the two surfaces. The iteration process converges to a solution by a least squares minimization of the differences between the z-values of the two surfaces. The version of software used accepts convergence when the most recent corrections to all unknowns, i.e. rotation and translation parameters, is less than ± 0.001 (units). When convergence occurs, the mean of the differences (residuals) between the two surfaces can be calculated. The root mean square (rms) of the residuals gives a measure of the coincidence of the two surfaces (Personal communication, Mitchell, 2007).

Polyworks also uses a least-squares iterative algorithm to align datasets. It averages alignment parameters of each data point and distributes the alignment error over all dataset transformation matrices. The discrepancy or residual difference of a data point is computed as the maximum 3D distance along the surface normal direction between this point and an overlapping dataset. The standard deviation of these discrepancies is reported (*Polyworks v 9.1.7 -Help menu*).

The two software packages have different data handling capabilities and the datasets were processed in different ways with the aim of gaining the most direct comparison between solutions. Data processed with DSMatch was graphically displayed with visualisation and analysis software (Surfer, version 6.04; Golden Software Inc., Golden, Colorado, USA). Data processed with *Polyworks* was graphically displayed using the *Polyworks* software.

8.2.3 Mapping and alignment precision

Alignment of DTMs, of the same surface generated from separate stereopairs, is influenced by mapping errors and alignment variables. Three procedures were used to assess the repeatability and precision of mapping and alignment precision (combined). The first procedure was the sequential alignment of the ten datasets, the second was the alignment of two datasets of varying grid interval and various exclusion thresholds, and the third was the alignment of two datasets using varying exclusion threshold.

8.2.3.1 DSMatch - Sequential alignment

Mapping and alignment precision (rms residuals) was tested by sampling the ten DEM datasets of the replica, using *3DM Analyst*, at an interval of 0.1 mm x 0.1 mm and aligning the datasets sequentially (1 compared with 2, 2 with 3, etc) with *DSMatch* using exclusion thresholds of 2.0, 0.07 and 0.05 mm. The grid interval of 0.1 mm x 0.1 mm was chosen following examination of point cloud spacing data (section 8.3.1) and the exclusion thresholds were chosen initially as default values and values that excluded only gross outliers.

8.2.3.2 DSMatch - Varying grid interval and exclusion threshold

The effect of varying grid interval and exclusion threshold upon mapping and alignment precision (rms residuals) was tested by sampling datasets 1 and 2 at varying grid intervals from 0.07 to 0.4 mm and aligning the datasets with exclusion thresholds of 0.07 to 0.03 mm.

8.2.3.3 DSMatch - Varying exclusion threshold

The effect of varying the exclusion threshold upon mapping and alignment precision (rms residuals) and the quality of the alignment (the percentage of points included in the alignment solution and the standard deviations of the transformation parameters) was tested by sampling datasets 1 and 2 at a grid interval of 0.1 x 0.1 mm and aligning the datasets with exclusion thresholds of 0.07 to 0.015 mm. The residual difference data following alignment, with

exclusion thresholds of 0.07, 0.05, 0.04 and 0.03 mm, was graphically displayed using *Surfer*.

8.2.3.4 Polyworks - Sequential alignment

Mapping and alignment precision (s.d. residuals) was tested by sampling the ten DTM datasets, using *Polyworks*, at an interval of 0.1 x 0.1 mm and maximum (triangle) edge length of 1000 (default value, Figure 8.3 left) and 0.75 mm (Figure 8.3 right), and aligning the datasets sequentially with *Polyworks - IMAlign* using exclusion thresholds of 2.0, 0.07 and 0.05 mm. The *maximum edge length* option limits the interpolation of data points to within triangles of a nominated length. The effect on precision (s.d. residuals) of sampling the ten datasets to DEMs using *3DM Analyst* prior to sampling with *Polyworks* was also tested. There was also a facility to lock one dataset and align the remaining datasets to the locked dataset. Precision (sd residuals) was tested using this method with datasets nos.1 and 10 locked.

8.2.3.5 Polyworks - Varying grid interval and exclusion threshold

The effect of varying grid interval and exclusion threshold upon mapping and alignment precision (s.d. residuals) was tested by sampling datasets 1 and 2 at varying grid intervals from 0.07 to 0.4 mm and aligning the datasets with exclusion thresholds of 0.07 to 0.03 mm.

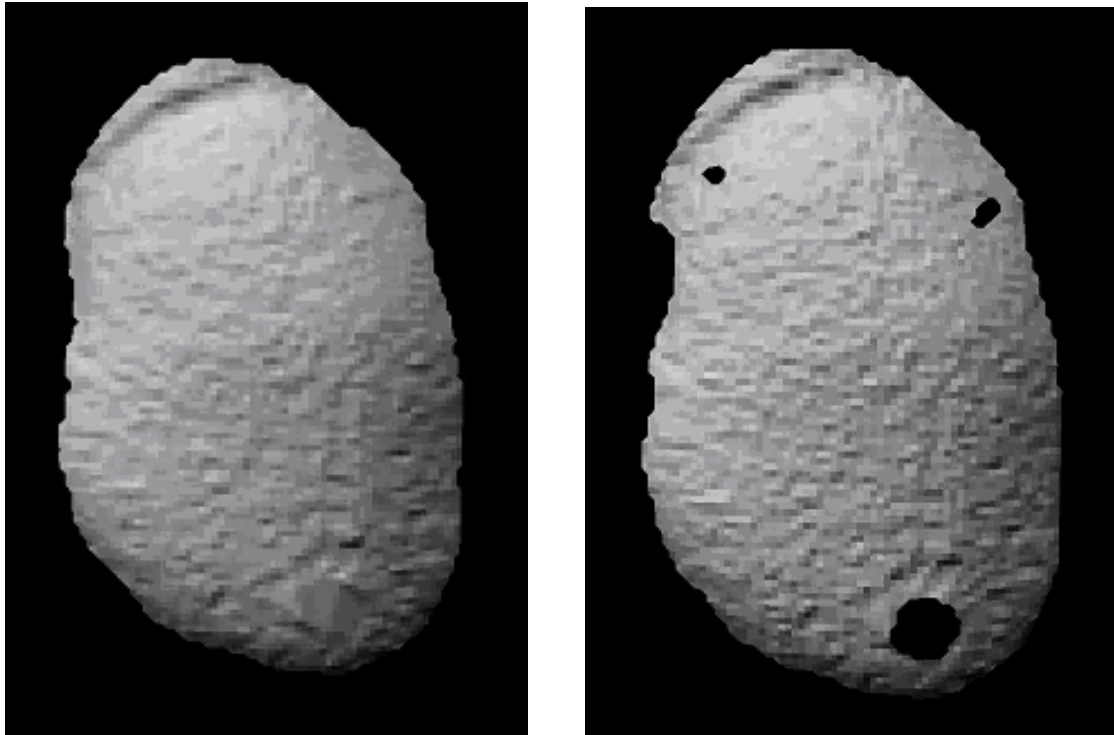


Figure 8.3. Tooth DTM imported into *Polyworks*, 0.1 x 0.1 mm grid interval, maximum edge length for triangulation of 1000 mm (left); tooth DTM imported into *Polyworks* on 0.1 x 0.1 mm grid interval, maximum edge length for triangulation of 0.75 mm (right).

8.2.3.6 Polyworks - Varying exclusion threshold

The effect of varying the exclusion threshold upon mapping and alignment precision (s.d. residuals) and the quality of the alignment (number of points included in the alignment solution and the standard deviation on the transformation parameters) was tested by sampling datasets 1 and 2 at a grid interval of 0.1 x 0.1 mm and aligning the datasets with exclusion thresholds of 0.07 to 0.015 mm. The residual difference data following alignment, with exclusion thresholds of 0.07, 0.05, 0.04 and 0.03 mm, was graphically displayed using *Polyworks*.

8.2.4 Alignment precision

Alignment precision (alone) was tested by alignment of a single dataset sampled at different grid intervals with grid node offsets. The inclusion of grid node offsets generated a new dataset of coordinates, at the same grid interval as the original dataset, while maintaining the surface noise of the original dataset, thereby excluding the effect of mapping precision on the alignment precision.

8.2.4.1 DSMatch and Polyworks

Alignment error, excluding mapping errors, was examined by aligning various DEM and DTM datasets sampled from dataset 1, with *DSMatch* and *Polyworks*. DEM datasets were created using the photogrammetry software with grid intervals from 0.07 to 0.14 mm and grid offsets from 0.01 to 0.08 mm. Grid node offsets could not be provided in *Polyworks* and so DTM datasets were imported into *Polyworks* with grid intervals of 0.10 x 0.10 mm for the first dataset and grid intervals of 0.11 x 0.11 mm for the second dataset. An exclusion threshold on 0.07 mm was used for all alignments.

8.3 Results

8.3.1 Data acquisition and sampling

Calibration results appear in greater detail in the next chapter, however the precision of the mapping system was found to be 13.0 μm . To make an assessment of the mean and distribution of point spacing, a raw point cloud was converted to a triangulated irregular network (TIN) and the triangle lengths determined using *ArcGIS*. The triangle lengths, the number of points, and their percentage of the total number below various thresholds appear in Table 8.2.

The mean (s.d.) of the DTM point cloud spacing was 67.4 (73.3) μm . Where triangle edge lengths in excess of 0.75 mm were excluded the mean (s.d.) of the point distribution was 66.0 (57.3) μm . There was a tendency for points to

be clustered around areas of well-defined texture on the replica, and to not be evenly distributed over the entire surface.

Length (mm)	No. points below length	% points below length
0.065	29006	68.8
0.070	30123	71.4
0.075	31130	73.8
0.080	31875	75.6
0.085	32718	77.6
0.090	33540	79.6
0.095	34234	81.2
0.100	34655	82.2
0.105	35341	83.8
0.110	35772	84.8
0.115	36143	85.7
0.120	36635	86.9
0.150	38645	91.7
0.200	40488	96.0
0.300	41781	99.1
0.400	42015	99.7
0.500	42074	99.8
0.750	42110	99.9
total	42160	100.0

Table 8.2. Point cloud point spacing length distribution for a TIN representation of one dataset.

The number of DTM points varied from 10,852 (dataset no. 8) to 16,605 (dataset no. 3) with a mean of 14,196 points. The number of DEM points on the tooth surfaces varied according to the grid geometry (Table 8.3). *DSMatch* has a limit on the maximum number of points per dataset of 13,000 points. Therefore a grid interval of 0.07 x 0.07 mm was the smallest grid interval tested using both software packages; intervals below this were not tested.

Grid interval (mm)	No. of points
0.05 x 0.05	21,659
0.06 x 0.06	15,042
0.07 x 0.07	11,039
0.08 x 0.08	8,463
0.1 x 0.1	5,036
0.12 x 0.12	3,762
0.14 x 0.14	2,758
0.2 x 0.2	1,370
0.3 x 0.3	605
0.4 x 0.4	339

Table 8.3. The number of points in DEMs of varying grid intervals.

8.3.2 Mapping and alignment precision

8.3.2.1 DSMatch – sequential alignment

DEMs of the same replica, mapped ten times, were generated on a 0.1 x 0.1 mm interval and aligned sequentially using *DSMatch* with a threshold for exclusion of 2.0, 0.07 and 0.05 mm. The rms of residual data from the alignments and the percentage of points below the threshold and therefore included in the alignment solution are shown in Table 8.4. For the threshold of 0.07 mm, the mean rms was 21.8 μm with 98.9% of points being included in the alignment solution; for a threshold of 0.05 mm the rms was 19.7 μm with 96.5% of points included in the solution. The rms represents the overall precision of the mapping and alignment method. Reducing the threshold and excluding further points resulted in an improvement in the precision value. Increasing the exclusion threshold above 0.07 mm did not significantly alter the precision of the alignments.

Exclusion threshold		0.07 (mm)		0.05 (mm)	
		rms (μm)	% < threshold	rms (μm)	% < threshold
Dataset nos.	2-1	20.6	98.8	18.9	96.5
	3-2	20.9	99.1	18.8	96.2
	4-3	21.2	98.6	19.4	96
	5-4	22.3	98.9	20.2	96
	6-5	22.2	98.7	20.2	95.9
	7-6	20.9	99.6	19.1	97
	8-7	23.8	98.6	21.1	94.4
	9-8	22.4	98.5	20.1	95
	10-9	22.2	99	19.8	95.6
	Mean	21.8	98.9	19.7	96.8
s.d.		1.0	0.3	0.7	0.8

Table 8.4. rms of residual data (μm) and percentage of points below threshold following sequential alignment of ten DEMs with *DSMatch*, exclusion thresholds 0.07 and 0.05 mm.

8.3.2.2 *DSMatch* – alignment of unsampled data

The maximum number of points in a dataset that could be handled by *DSMatch* was 13,000. DTM dataset numbers 4 and 5 had fewer points than this limit and so these DTM datasets were aligned using *DSMatch*. For exclusion thresholds of 0.07 and 0.05 mm, the alignment errors were 20.5 and 18.8 μm (compared to alignment of DEM datasets sampled from the same underlying DTM of 22.3 and 20.2 μm (Table 8.4)). This suggests that DEM sampling in 3DM Analyst resulted in additional alignment error of approximately 1.5 μm , possible caused by interpolation of points in areas of missing data during DEM sampling. This issue was not investigated further.

8.3.2.3 *DSMatch* – varying grid interval and exclusion threshold

DEM numbers 1 and 2 above, sampled at intervals from 0.07 to 0.4 mm, were aligned with *DSMatch* with exclusion thresholds from 0.07 to 0.03 mm. The rms of residual data were recorded (Table 8.5). Alignment solutions achieved

the convergence criteria of the software up to the 0.2 mm interval but did not converge at intervals of 0.3 and 0.4 mm. The alignment solutions for the 0.3 and 0.4 mm intervals were close to the convergence criteria and the error data were accepted. Alignment was not affected by grid interval however, as would be expected, as more 'noise' is removed from the datasets by the exclusion threshold, the alignment rms residual data values decreased.

Threshold (mm)	0.07	0.05	0.04	0.03
Grid interval (mm)	rms (μm)	rms (μm)	rms (μm)	rms (μm)
0.07 x 0.07	21.0	19.1	17.2	14.5
0.1 x 0.1	20.6	18.9	17.2	14.5
0.14, 0.14	20.2	18.6	17.1	14.5
0.2, 0.2	20.6	18.5	17.0	14.6
0.3 x 0.3	20.9*	19.5*	17.2*	14.3*
0.4 x 0.4	21.2*	19.2*	17.7*	15.3*

Table 8.5. Residual data (μm) following alignment of two DEMs with *DSMatch*: varying grid interval and exclusion threshold.

* denotes convergence criteria not met.

8.3.2.4 DSMatch- varying exclusion threshold

DEMs numbers 1 and 2, sampled on a 0.1 x 0.1 mm grid interval, were also aligned at exclusion thresholds of 0.015 to 0.07 mm with *DSMatch*.

Alignment statistics appear in Table 8.6. As the threshold decreased and more points were excluded from the solution the rms value decreased, standard deviations on the alignment translation parameters remained constant, and alignment rotation errors decreased.

Threshold (mm)	rms (μ m)	%< threshold	s.d. on parameters: translations (mm), rotations (deg.)					
			X	Y	Z	Kappa	Omega	Phi
0.070	20.6	98.8	0.001	0.001	0.000	0.016	0.010	0.023
0.050	18.9	96.5	0.001	0.001	0.000	0.015	0.009	0.021
0.045	18.1	94.9	0.001	0.001	0.000	0.014	0.009	0.021
0.040	17.2	92.9	0.001	0.001	0.000	0.014	0.008	0.020
0.030	14.5	84.9	0.001	0.001	0.000	0.012	0.008	0.018
0.020	10.5	68.0	0.001	0.001	0.000	0.010	0.006	0.014
0.015	8.2	55.4	0.001	0.001	0.000	0.009	0.005	0.013

Table 8.6. Alignment statistics for DEM nos. 1 and 2, sampled on a 0.1 mm x 0.1 mm grid interval, with *DSMatch* ; varying threshold: rms error, % points below the threshold, s.d. on alignment orientations.

Residual difference data for thresholds 0.03 to 0.07 mm were presented as contour maps using *Surfer* (Figure 8.4). Examination of the contour difference maps shows that reducing the exclusion threshold from 0.07 to 0.03 mm has not affected the difference data and therefore the actual alignment result.

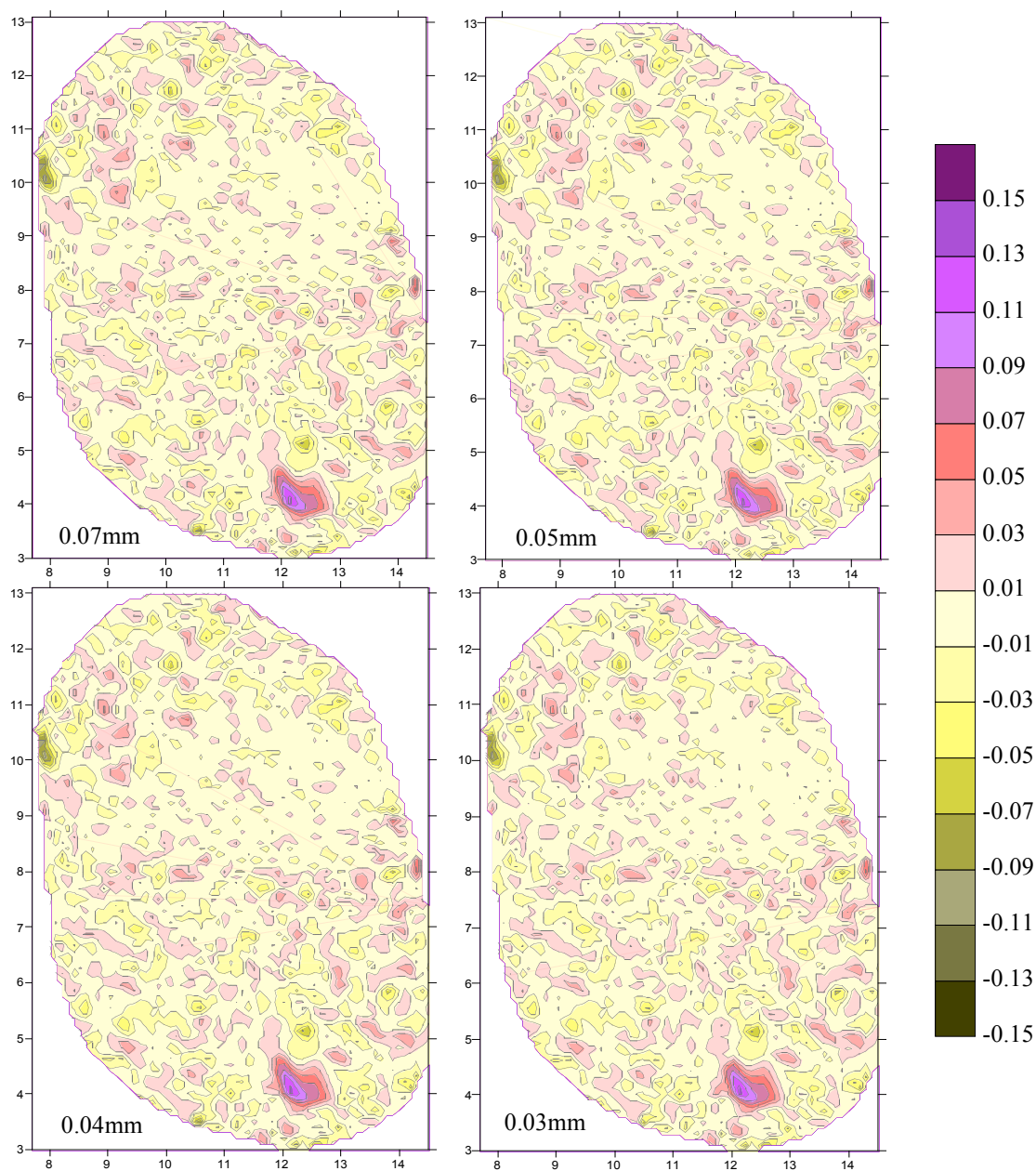


Figure 8.4. *DSMatch* residual difference data, DEM datasets 1 and 2, threshold for exclusion 0.07, 0.05, 0.04 and 0.03 mm. Scale units: mm.

8.3.2.5 Polyworks – sequential alignment

DTMs of the same replica, mapped ten times, were imported into *Polyworks* on a 0.1 × 0.1 mm grid interval and the (default) maximum edge length of 1000 mm. This edge length resulted in interpolation of missing data (Figure 8.3, right) and provided a comparable dataset to the DEM exported from *3DM Analyst* and aligned with *DSMatch*. The DTMs were sequentially aligned using *Polyworks*. When the DTM datasets were aligned with exclusion thresholds of 2.0, 0.07 and 0.05 mm, the mean standard deviations on the residual data were 19.4, 18.9 and 17.7 µm (Table 8.7). *Polyworks* provides an option of aligning all datasets to a single locked dataset in a single operation. The standard deviations of residual data following alignment of nine datasets to single dataset numbers 1 and 10 were 19.2 and 19.0 µm, respectively. This capability of *Polyworks* gave a similar result to sequential alignment and was considerably faster.

Exclusion threshold:		2.0 (mm)	0.07 (mm)	0.05 (mm)	Locked dataset:	0.07 (mm)	0.07 (mm)
		s.d. (µm)	s.d. (µm)	s.d. (µm)		Lock 1 s.d. (µm)	Lock 10 s.d. (µm)
Dataset nos.	2-1	18.4	17.6	16.9		18.5	18.6
	3-2	19.4	18.0	16.7		18.8	18.4
	4-3	19.6	18.8	17.4		19.2	18.8
	5-4	19.5	19.2	17.9		19.4	19.2
	6-5	19.6	19.4	18.2		19.0	19.4
	7-6	17.6	17.6	16.7		18.4	19.0
	8-7	20.6	20.5	18.8		20.7	18.4
	9-8	19.8	19.4	18.3		18.8	20.7
	10-9	20.0	19.8	17.8		20.1	18.8
Mean		19.4	18.9	17.7		19.2	19.0
s.d.		0.9	1.0	0.8		0.8	0.7

Table 8.7. Sequential alignment of ten DTMs with *Polyworks*: standard deviations of residual data (µm), exclusion thresholds: 2.0, 0.07 and 0.05 mm. Alignment of nine datasets to a single (locked) dataset. Grid interval: 0.1 × 0.1 mm, maximum edge length of 1000 mm.

Polyworks was used interactively to vary the maximum edge length of DTM datasets from 0.2 to 1.0 mm. The *maximum edge length* option limits the interpolation of data points to within triangles of a nominated length. As the nominated value was reduced, fewer data points were interpolated and more gaps in the surface appeared. The value of 0.75 mm was chosen as a length that prevented interpolation into areas of gross data deficiency. DTMs were imported into *Polyworks* on a 0.1 x 0.1 mm grid interval and a maximum edge length of 0.75 mm (Figure 8.2 right). The precisions of the alignments are shown in Table 8.8. The difference in results, using a threshold for exclusion of 2.0 mm, was small and is not reported here. The precision of alignment (mean s.d.) using thresholds of 0.07 and 0.05 mm was 18.7 and 17.6 μm .

Exclusion threshold:		0.07 (mm)	0.05 (mm)	Locked dataset:	0.07 (mm) Lock 1	0.07 (mm) Lock 10
		s.d. (μm)	s.d. (μm)		s.d. (μm)	s.d. (μm)
Dataset nos.	2-1	17.0	16.6		18.3	18.4
	3-2	17.1	16.4		18.3	18.3
	4-3	18.2	17.2		19.1	18.2
	5-4	19.1	17.9		19.3	19.1
	6-5	19.2	18.2		19.0	19.3
	7-6	17.5	16.6		18.2	18.4
	8-7	20.5	18.8		20.9	18.2
	9-8	19.4	18.4		18.9	20.9
	10-9	19.9	17.9		20.4	18.9
Mean		18.7	17.6		19.2	18.9
s.d.		1.3	0.9		0.9	0.9

Table 8.8. Precision of sequential alignment and alignment to a single dataset of DTMs with *Polyworks*. DTMs imported on 0.1 x 0.1 mm grid interval and maximum edge length of 0.75 mm.

The DEMs (ten repeat mappings), aligned with *DSMatch* (Table 8.4 above), were imported into *Polyworks* on a 0.1 x 0.1 mm grid as above and maximum edge length of 0.75 mm and aligned using *Polyworks*. When the imported DEM datasets were sequentially aligned using a threshold of 0.07 and 0.05

mm, the means of the standard deviations were 16.6 and 15.8 μm (Table 8.9). When the datasets were aligned to single datasets 1 and 10 the means of the standard deviations were 16.82 and 16.96 μm .

Exclusion threshold:		0.07 (mm)	0.05 (mm)	Locked dataset:	0.07 (mm)	0.07 (mm)
		s.d. (μm)	s.d. (μm)		Lock 1 s.d. (μm)	Lock 10 s.d. (μm)
Dataset nos.	2-1	14.9	14.5		16.2	16.1
	3-2	15.4	14.6		16.2	16.5
	4-3	16.6	15.6		16.6	17.0
	5-4	14.2	16.1		17.0	17.7
	6-5	17.1	16.8		17.7	16.6
	7-6	15.4	14.9		16.6	16.1
	8-7	18.1	17.2		16.1	18.3
	9-8	17.4	16.4		18.4	16.6
	10-9	16.8	16.1		16.7	17.5
Mean		16.6	15.8		16.8	17.0
s.d.		1.1	1.0		0.8	0.8

Table 8.9. Precision of sequential alignment and alignment to a single dataset of DEMs with *Polyworks*. DEMs imported on 0.1 x 0.1 mm grid interval and maximum edge length of 0.75 mm.

8.3.2.6 Polyworks - varying grid interval and exclusion threshold

DTM numbers 1 and 2, imported into *Polyworks* at intervals from 0.07 to 0.4 mm, were aligned with *Polyworks* with exclusion thresholds from 0.07 to 0.03 mm. The standard deviations of the residual data were recorded (Table 8.10). Alignment failed at the grid interval of 0.4 (threshold 0.03 mm). There was some improvement in the rms residuals from the 0.07 to the 0.1 mm grids. Alignment was slightly affected by grid interval and, as was the case with *DSMatch*, as more 'noise' was removed from the datasets by the decreasing exclusion threshold, the alignment residual data rms values decreased.

Threshold (mm):	0.07	0.05	0.04	0.03
Grid interval (mm)	s.d. (µm)	s.d. (µm)	s.d. (µm)	s.d. (µm)
0.07 x .07	17.7	16.9	15.7	13.6
0.1 x 0.1	17.3	16.7	15.7	13.5
0.14, 0.14	17.4	16.7	15.9	13.8
0.2, 0.2	17.1	16.8	15.6	13.4
0.3 x 0.3	17.9	17.1	16.4	13.6
0.4 x .04	18.2	16.9	15.6	x

Table 8.10. Alignment of DTM numbers 1 and 2 with *Polyworks*, maximum edge length of 0.75 mm; varying grid interval: exclusion thresholds 0.07 to 0.03 mm, s. d. of residual data (µm), x denotes alignment failure.

8.3.2.7 Polyworks - varying exclusion threshold

DTM numbers 1 and 2, imported into *Polyworks* at grid intervals of 0.1 x 0.1 mm and maximum edge length of 0.75 mm, were aligned at exclusion thresholds of 0.07 to 0.015 mm. Alignment statistics appears in Table 8.11. As was the case with *DSMatch*, as the threshold decreased and more points were excluded from the solution the standard deviation value decreased. Standard deviations of the alignment translation did not change significantly.

Threshold (mm)	s.d. (µm)	% < threshold	s.d. on parameters (mm)
0.070	17.3	96.67	2.9×10^{-7}
0.050	16.7	95.99	4.5×10^{-7}
0.045	16.4	95.45	1.0×10^{-7}
0.040	15.8	93.81	4.7×10^{-7}
0.030	13.5	87.77	1.3×10^{-7}
0.020	10.2	73.49	4.6×10^{-7}
0.015	7.9	60.25	2.4×10^{-7}

Table 8.11. Alignment of DTM numbers 1 and 2 with *Polyworks*, 0.1 mm grid interval, maximum edge length of 0.75 mm; varying exclusion threshold: s.d. error, % points below the threshold, s.d. on alignment parameters.

The standard deviation point data from alignments with thresholds 0.03 to 0.07 mm were represented graphically in *Polyworks* (Figure 8.5). As with *DSMatch*, examination of the deviation maps shows that reducing the exclusion threshold from 0.07 to 0.03 mm has not affected the difference data and therefore the actual alignment result.

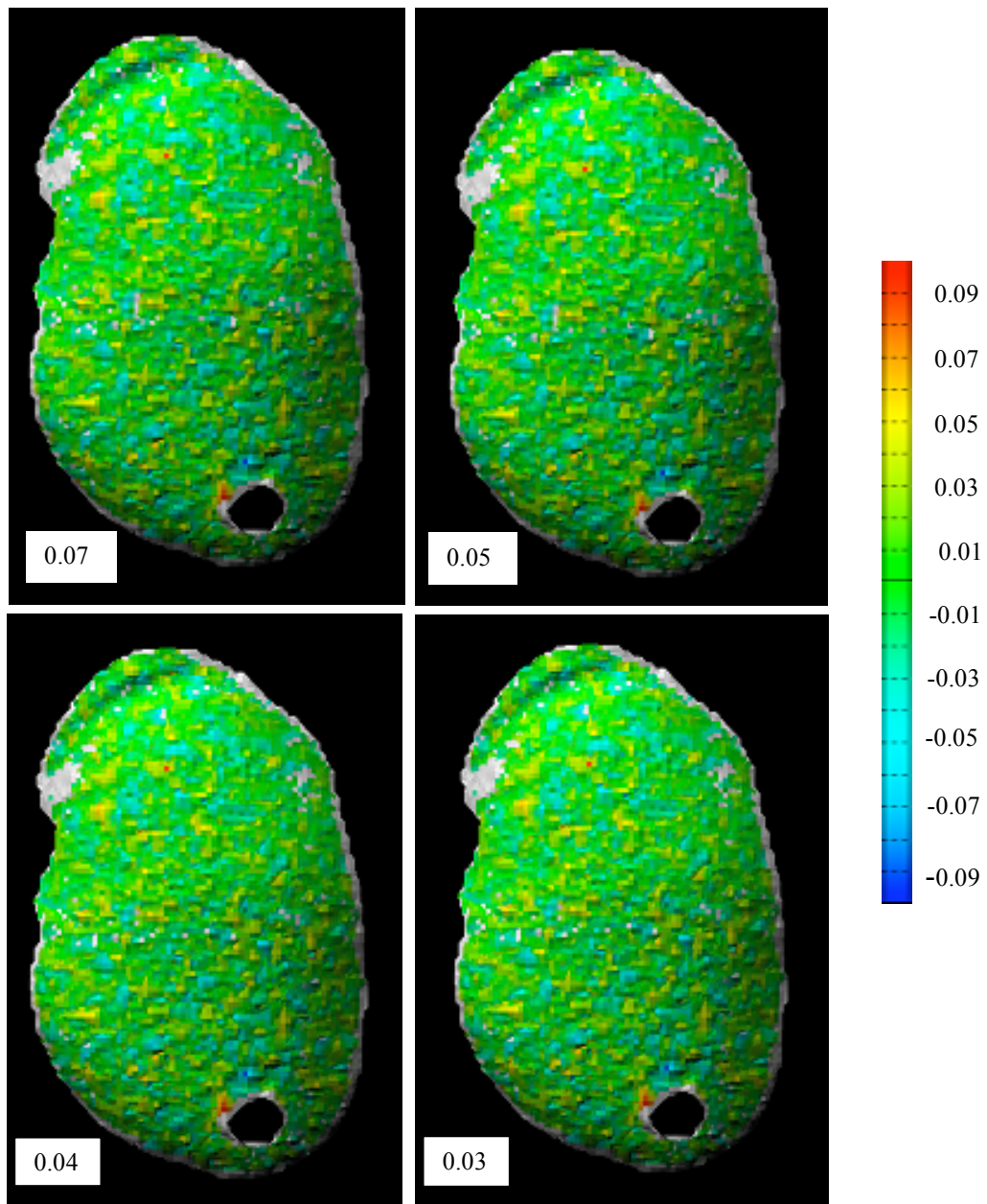


Figure 8.5. *Polyworks* standard deviation point data, DTM datasets 1 and 2, exclusion thresholds: 0.07, 0.05, 0.04 and 0.03 mm, Scale units: mm.

The difference data may also be displayed by rescaling the data to eliminate negative values or values below a threshold. Difference data from the alignment in Figure 8.5 (0.07 mm threshold) were rescaled to show only the positive differences with a minimum value of 0.00, 0.01, 0.02, 0.03 and 0.04 mm. As the lower limit of the display was increased, for example to 0.01 mm, the colour scale in *Polyworks* also changed. The 0.00 minimum value display shows all of the positive difference data, approximately half of all difference points. As the minimum value is increased more points are excluded from the display.

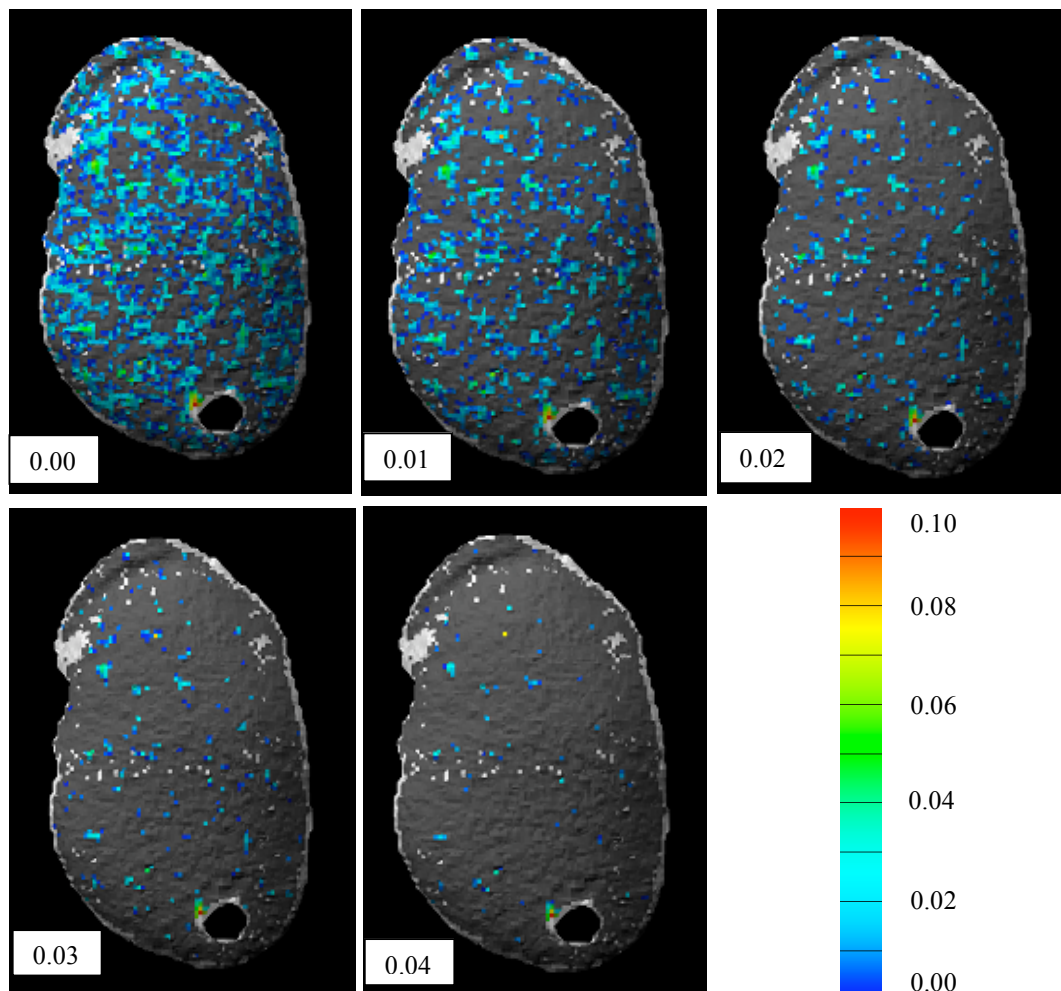


Figure 8.6. *Polyworks* standard deviation point data, positive data only. Minimum data values 0.00, 0.01, 0.02, 0.03 and 0.04 mm. Scale for 0.00 mm minimum value display, scale units: mm.

8.3.3 Alignment precision

8.3.3.1 DSMatch

The DTM for dataset number 1 was re-sampled at various grid intervals and various grid offsets with *3DM Analyst* and aligned using *DSMatch*. The results show that as grid interval and grid offset increased, alignment error increased (Table 8.12). For a grid interval of 0.07×0.07 mm, offsets of 0.02 and 0.05 mm gave a similar alignment error of approximately $5.6 \mu\text{m}$ for, in effect, they amounted to the same grid offset. The same was true of the 0.1×0.1 mm grid interval with offsets of 0.02 and 0.08 mm giving a similar result of approximately $6.5 \mu\text{m}$. It may be concluded that the magnitude of the alignment error was cyclic as the offset moved across the grid interval with the peak of the curve at half the grid interval (0.05 mm in the case of grid interval of 0.1 mm). In order to mimic an average offset likely to occur in a typical alignment exercise, the DTM dataset was sampled at 0.1×0.1 mm and 0.11×0.11 mm for the two surfaces to be aligned. This resulted in an rms of residuals of $7.6 \mu\text{m}$. This may be taken as the average alignment error associated with aligning tooth surfaces of the same grid intervals. A second tooth surface was sampled at 0.07 and 0.14 mm intervals and with offsets as above. Alignment errors were similar to the results above, indicating that they were not peculiar to that surface. When rotations were introduced to the dataset, the alignment error was $0 \mu\text{m}$ with 100 percent of points included in the solution. When rotations and offsets were both introduced, the alignment error varied in line with the results above where offsets were introduced.

Grid interval (mm)	Offsets (mm):	0.00	0.01	0.02	0.05	0.08
	No. of Points	rms (μm)	rms (μm)	rms (μm)	rms (μm)	rms (μm)
0.07 x 0.07	11039	x	3.4	5.6	5.7	x
0.08 x 0.08	8463	x	3.6	5.9	7.4	x
0.1 x 0.1	5036	x	3.7	6.5	10.2	6.7
0.12 x 0.12	3762	x	4.0	7.2	11.5	x
0.14 x 0.14	2758	x	4.4	7.2	12.5	x
0.1x 0.1 // 0.11x 0.11		7.6	x	x	x	x
Rotate (Om=0.3, Phi=0.2, Kap=0.1 radians)		0	4.0	6.7	10.1	x

Table 8.12. Alignment precision (rms) of single DEMs with *DSMatch*, threshold 0.07 mm. s.d. units: μm , x denotes test not performed.

The average alignment error of DEMs resulting from different grid intervals was also tested. These are tabulated below (Table 8.13). As grid interval decreases, alignment precision improves.

Grid interval (mm) Dataset: 1 , 2	Threshold (mm)	Precision (μm)
0.07 x 0.07, 0.08 x 0.08	0.07	5.3
0.10 x 0.10, 0.11 x 0.11	0.07	7.6
0.14 x 0.14, 0.15 x 0.15	0.07	10.0
0.20 x 0.20 , 0.21 x 0.21	0.07	14.6
0.30 x 0.30, 0.31 x 0.31	0.07	17.8
0.40 x 0.40, 0.41 x 0.41	0.07	19.6*

Table 8.13. Residual errors on average DEM alignment: *DSMatch*,

* denotes convergence criteria not met.

8.3.3.2 Polyworks

Grid offsets could not be provided to DTM datasets in *Polyworks*, and so DEM alignment with *DSMatch* (as in Table 8.12) could not be directly compared. DEM datasets prepared above were then processed with *Polyworks* (Table 8.14). Overall, alignment precision was improved over that with *DSMatch*, with average alignment error (0.1 mm interval data aligned to 0.11 mm interval data) being 5.4 μm compared to 7.6 μm for *DSMatch*. Processing a dataset with rotations included showed that typical alignment errors occurred even when a rotation and no offset was provided. This is in contrast to *DSMatch* and indicates that sampling into *Polyworks* does change the grid location if not the grid interval.

Grid interval (mm)	Offsets (mm):	0.00	0.01	0.02	0.05	0.08
	No. of Points	s.d. (μm)	s.d. (μm)	s.d. (μm)	s.d. (μm)	s.d. (μm)
0.07 x 0.07	11039	x	3.1	3.6	3.5	x
0.08 x 0.08	8463	x	3.6	4.0	4.4	x
0.1 x 0.1	5036	x	4.2	4.6	5.7	4.5
0.12 x 0.12	3762	x	5.0	5.6	6.8	x
0.14 x 0.14	2758	x	3.9	4.9	7.1	x
0.1x 0.1 // 0.11x 0.11		5.4				
Rotate (Om=0.3, Phi=0.2, Kap=0.1 radians)		4.0	4.2	4.7	5.7	4.7

Table 8.14. Alignment precision (s.d.) of single DEMs with *Polyworks*, threshold 0.07 mm. s.d. units: μm , x denotes test not performed.

To separate the influence of sampling by *Polyworks* of a DEM already sampled with *3DM Analyst*, DTMs were imported into *Polyworks* with grid intervals of 0.1 x 0.1 mm and 0.11 x 0.11 mm and then aligned with *Polyworks* using an exclusion threshold of 0.07 mm. The results below show alignment error of 6.5 μm compared with 5.4 μm for the *Polyworks* alignment of DEMs, and 7.6 μm for the *DSMatch* alignment of DEMs (Table 8.12). *Polyworks*

allows subsampling to speed up the alignment process (Table 8.15).

Subsampling, which reduces the number of points included in the alignment solution, resulted in a very small improvement in alignment precision. This effect was not investigated further.

Grid interval (mm)	Subsampling:	1/1	1/4	1/9	1/16	1/25
0.1x 0.1//0.11x 0.11	s.d. (µm):	6.5	6.4	6.6	6.2	5.9

Table 8.15. Alignment precision of single DTM: *Polyworks*, maximum edge length of 0.75 mm.

The average alignment error of DTMs resulting from different grid intervals was tested (Table 8.16). As grid interval decreased, alignment precision improved.

Grid interval (mm)	Threshold (mm)	Precision (µm)
0.07 x 0.07, 0.08 x 0.08	0.07	4.6
0.10 x 0.10, 0.11 x 0.11	0.07	6.4
0.14 x 0.14, 0.15 x 0.15	0.07	9.1
0.20 x 0.20, 0.21 x 0.21	0.07	11.7
0.30 x 0.30, 0.31 x 0.31	0.07	14.7
0.40 x 0.40, 0.41 x 0.41	0.07	16.5

Table 8.16. Average alignment precision of single DTM: *Polyworks*, maximum edge length of 0.75 mm.

8.4 Discussion

8.4.1 Data Acquisition

The lighting required for very close range stereo imaging remains problematic with areas of light scatter from the replica still occurring. Wide separation of lighting elements is usually used to overcome this problem. However the bulky nature of the experimental stereo camera places limitations on the placement of lighting, and the complex nature of the tooth

surfaces results in light reflection off different parts of the surface in a complex manner. This has resulted in some missing data on the surface models, although in non-critical areas. Combining surface data from two or more separate stereo views would reduce the amount of missing data and improve the fidelity of the surface models. The use of a digital image acquisition system does allow immediate review of images to check for any problems with alignment, depth of field and light scatter.

8.4.2 Data sampling

Datasets for the sequential alignment sections were sampled utilizing a grid interval of 0.1×0.1 mm. This represented a point spacing no smaller than around eighty-five percent of the underlying point cloud data. *3DM Analyst* generates a DEM from within a triangulated point cloud (e.g. Figure 8.2). The maximum edge length applied by *3DM Analyst* is not reported by the manufacturer and it is likely that there are additional variables involved during triangulation. *Polyworks* contains additional sampling features, which enable missing data to be interpolated to varying degrees. Interpolation of missing data has an influence on alignment statistics, however choice of threshold also influences the inclusion or exclusion of interpolated points (Tables 8.7 and 8.8). The importation into *Polyworks* of a DEM already sampled in *3DM Analyst* had an additive smoothing effect resulting in better alignment precision 'values' (Table 8.9).

8.4.3 Data alignment

Both *DSMatch* and *Polyworks* reported various alignment statistics, however none that coincided. *DSMatch* recorded an rms of residual Z-axis differences whereas *Polyworks* recorded a standard deviation of the difference vectors along the surface normal direction between this point and an overlapping surface. *DSMatch* also produced an output data file of difference data that could be analysed, and calculation of the standard deviation of residual data varied from rms values in the order of $0.1 \mu\text{m}$. That is, rms and s.d. measures yielded very similar values, although the two programs measure different

residual data parameters. In areas of steep relief, where *DSMatch* minimizes the Z-axis separations, it is likely the two surfaces will be drawn closer together than would be the case with *Polyworks* where minimization occurs along a normal to the surface.

8.4.4 Mapping and alignment precision

There was a small difference in mapping and alignment precision between the two software packages. DEM sampling in *3DM Analyst* and alignment with *DSMatch* yielded a mean rms residuals value of 21.8 μm . Default sampling and alignment with *Polyworks* yielded a mean standard deviation of residuals of 19.4 μm (0.07 mm exclusion threshold). *Polyworks* had the capability to limit interpolation in areas with missing data, using the *maximum edge length* option, reducing the standard deviation of residuals to 18.7 μm . The two unsampled datasets aligned with *DSMatch* were aligned with an rms residuals value 1.5 μm lower than the datasets that had been sampled to DEMs, suggesting that DEM generation in *3DM Analyst* may have introduced errors into the surface data.

8.4.5 Varying grid interval

The combination of mapping and alignment precision was insensitive to grid interval with the precision of alignments with *DSMatch* varying from 20.1 to 21.2 μm (exclusion threshold of 0.07 mm) for grid intervals from 0.07 to 0.4 mm (Tables 8.5). The precision of alignments with *Polyworks* varied from 17.1 μm to 18.2 μm (exclusion threshold of 0.07 mm) for grid intervals from 0.07 to 0.4 mm (Tables 8.10). Alignment was successful for all grid intervals and exclusion thresholds tested, except for the 0.4 mm interval and 0.03 mm threshold. Therefore, reducing the density of the data did not degrade the representation of the surface to an extent that it affected the alignment precision values.

Alignment of some surfaces at the largest grid intervals failed to meet the convergence criteria of *DSMatch*. Mitchell and Chadwick (1999) found for the

alignment of palatal surfaces of upper anterior teeth, that where solutions were weak, the rms of residuals and the percentage of points included in the solution were not significantly affected by whether the solution converged or not, provided they were close to convergence. Palatal surfaces of upper anterior tooth, particularly those affected by erosion, may be large and relatively flat and it was noted that surface measurement of the steep inclines leading to the interproximal area of the tooth surfaces was important for successful alignment. The facial surface of the two teeth examined in this case were very rounded with greater visual access into the interproximal areas such that mapping, using stereo imagery, captured sufficient of the steeper inclines into these areas to assist in alignment. Consequently, at grid intervals of 0.3 and 0.4 mm, while the convergence criteria of the software were not met, the solutions were accepted as valid.

8.4.6 Varying exclusion threshold

Reducing the exclusion threshold resulted in a reduction in precision values as outliers and surface noise was excluded from the alignment solutions (Tables 8.6 and 8.11). *Polyworks* excluded fewer data points than *DS Match* at and below thresholds of 0.04 mm, suggesting that *Polyworks* was more efficient at including more points in the alignment solution at lower thresholds. However, as noted in section 8.4.2, differences in data sampling using the two methods has meant direct comparisons are not totally reliable.

For both methods, as the threshold was reduced from 0.07 to 0.04 mm, more points were excluded. When the threshold was reduced to below 0.04 mm, the rate at which points were excluded accelerated. This supported the selection of 0.04 mm as an appropriate threshold for the exclusion of outliers and is consistent with Mehl et al., (1997) who recommended a threshold for exclusion of 3 times the precision of the mapping system. In the current case mapping precision was 13.0 μm . Applying this criteria to surface alignment and attempting to match other data sampling parameters produced alignment values for *DSMatch* and *Polyworks* of 17.2 and 15.6 μm respectively

(Tables 8.6 and 8.11). Graphical display of the difference data of both *DSMatch* and *Polyworks* showed that the actual alignment results were not sensitive to the exclusion threshold, whether it was above or below the '3 times mapping precision' criteria.

The accuracy of the mapping system has previously been shown to be 3 μm (previous chapter). The large number of points measured on the tooth replica provides several avenues for data sampling and smoothing so that the values for measurement precision (13 μm) and measurement and alignment precision ($\sim 16 \mu\text{m}$) do not represent the threshold of change detection possible with this system.

8.4.7 Alignment precision

To test the alignment method (alone), a single dataset may be transformed with translations and rotations then aligned to the original dataset. If the alignment algorithm operates with sufficient accuracy, then the two datasets should align without error. This is because merely translating and rotating a dataset does not alter the spatial relationship between each 3D coordinate. This was shown to be the case with *DSMatch* (Table 8.12, bottom line) where the alignment error was 0 μm when the dataset was rotated about the three axes and there was no offset to the grid intersection. When grid offsets were incorporated, alignment error was the same, as though no rotations had been included. The same was not true for *Polyworks*, suggesting that the importing of a regular array and conversion to another regular array of the same dimension resulted in altered grid location (Table 8.13). Alignment was not affected by the exclusion threshold as there were no outliers created when the same surface was resampled.

To test the alignment methods, a single data set was resampled with grid offsets to mimic real conditions where, as a surface is sampled, grid nodes may not intersect in a random fashion. The alignment error for the 0.1mm \times 0.1 mm grid data in the case of *DSMatch* was 7.6 μm and may be taken as the

average alignment error associated with aligning tooth surfaces of this grid interval. The average alignment error in the case of aligning DEM datasets with *Polyworks* was 5.4 μm . However, when DTM datasets were aligned with *Polyworks*, a better comparison, the average alignment error was 6.4 μm , a difference of 1.2 μm . This difference of 1.2 μm may be accounted for by the sampling method in *3DM Analyst* which interpolates missing data that may be present in the DTM when creating a DEM, leading to greater error in the DEM in these locations. *Polyworks* was able to align datasets that contained missing data, thus avoiding these potential errors.

In essence, this test evaluated the effectiveness of the alignment algorithms at sampling the surface as it had been sampled when the offsets were included. Alignment errors reduced as the grid interval was reduced (Tables 8.13 and 8.16). This shows that the smaller the grid interval, the lower the sampling error that was introduced by the inclusion of an offset. This would suggest that, for surface alignment applications, the smallest grid interval possible should be chosen. However this does not accord with the mapping *and* alignment results, where varying grid interval had no effect using *DSMatch* and only a small effect with *Polyworks*. On the basis of overall precision, there appears to be no advantage in the selection of a particular grid interval below a maximum threshold. This finding may be particular to tooth surfaces, which are relatively featureless and so relatively large grid intervals can be used to adequately represent the surface topography.

The final decision about grid interval should be determined by the particular application and the intended surface information required. In the case of change detection of non carious cervical lesions at annual intervals, if surface alignment and therefore change detection is not influenced by grid interval, then the choice of grid interval should be guided by the size of the lesions in the X and Y axes and the likely rate of change in these dimensions over time. The two most common wear measurements reported are volume loss and lesion depth, neither of which relate directly to X and Y dimensions. The

report of (Pintado et al., 2000) did not report on change in these dimensions. The size of lesions is very variable, with the height and depth of lesions in the order of millimetres (Aw et al., 2002). Because the spatial frequency of change in X and Y dimensions is unknown and, given the speed of modern desk top computers where there is not a significant penalty in computational time associated with any particular grid sampling interval, the maximum grid interval which reasonably represents the random point cloud should be chosen. As around eighty-five % of point spacings were less than 0.10 mm (Table 8.2), this grid interval was chosen for change detection work reported in the next chapter.

8.5 Conclusion

Both *DSMatch* and *Polyworks* successfully aligned the one tooth surface tested with an overall mapping and alignment error of 17.2 and 15.6 μm respectively, for an exclusion threshold of 0.04 mm. Alignment solutions appeared to be very stable, with the choice of grid interval and exclusion threshold having little or no effect on alignment. For alignment error (alone) *DSMatch* and *Polyworks* resulted in errors of 7.6 and 6.4 μm respectively. The measurement system produced point cloud data suitable for sampling on a 0.1 mm x 0.1 mm grid interval. Data sampling parameters used to interpolate areas of missing data did effect overall alignment precision. The choice of grid interval for a given application should be determined according to the spatial frequency of measurements desired in the grid axes.

8.6 References

- Aw, T., Lepe, X., Johnson, G. and Mancl, L., 2002. Characteristics of noncarious cervical lesions. *Journal of the American Dental Association*, 133: 725-733.
- Azzopardi, A., Bartlett, D., Watson, T. and Sherriff, M., 2001. The measurement and prevention of erosion and abrasion. *Journal of Dentistry*, 29 (6): 395-400.

- Azzopardi, A., Bartlett, D., Watson, T. and Smith, B., 2000. A Literature Review of the Techniques to Measure Tooth Wear and Erosion. *European Journal of Prosthodontics and Restorative Dentistry*, 8 (3): 93-97.
- Bartlett, D., Blunt, L. and Smith, B., 1997. Measurement of tooth wear in patients with palatal erosion. *British Dental Journal*, 182 (5): 179-184.
- Chadwick, R., Mitchell, H., Cameron, I., Hunter, B. and Tulley, M., 1997. Development of a novel system for assessing tooth and restoration wear. *Journal of Dentistry*, 25 (1): 41-47.
- DeLong, R. and Douglas, W., 1990. Quantitative assessment of anatomical change in the human dentition, 12th Annual International Conference of the IEEE in Medicine and Biology Society, pp. 2054-2055.
- DeLong, R., Pintado, M. and Douglas, W., 1985. Measurement of change in surface contour by computer graphics. *Dental Materials*, 1: 27-30.
- DeLong, R., Pintado, M., Ko, C., Hodges, J. and Douglas, W., 2001. Factors influencing optical 3D scanning of vinyl polysiloxane impression materials. *Journal of Prosthodontics*, 10 (2): 78-85.
- Evans, A., Harper, I. and Sanson, G., 2001. Confocal imaging, visualization and 3-D surface measurement of small mammalian teeth. *Journal of Microscopy*, 204 (2): 108-119.
- Lambrechts, P., Vanherle, G. and Davidson, C., 1981. An universal and accurate replica technique for scanning electron microscope study in clinical dentistry. *Microscopica Acta*, 85 (1): 45-48.
- Lee, I., DeLong, R., Pintado, M. and Malik, R., 1995. Evaluation of factors affecting the accuracy of impressions using quantitative surface analysis. *Operative Dentistry*, 20: 246-252.
- Leinfelder, K., Isenberg, B. and Essig, M., 1989. A new method for generating ceramic restorations: a CAD-CAM system. *Journal of the American Dental Association*, 118 (6): 703-707.

- Luthardt, R., Kuhmstedt, P. and Walter, M., 2003. A new method for the computer-aided evaluation of three-dimensional changes in gypsum materials. *Dental Materials*, 19 (1): 19-24.
- Mehl, A., Gloger, W., Kunzelmann, K.-H. and Hickel, R., 1997. A new optical 3D device for the detection of wear. *Journal of Dental Research*, 76 (11): 1799-1807.
- Mitchell, H. and Chadwick, R., 1998. Mathematical shape matching as a tool in tooth wear assessment - development and conduct. *Journal of Oral Rehabilitation*, 25: 921-928.
- Mitchell, H. and Chadwick, R., 1999. Digital photogrammetric concepts applied to surface deformation studies. *Geomatica*, 53 (4): 405-414.
- Persson, A., Andersson, M. and Bergman, B., 1995. The accuracy of a high-precision digitizer for CAD/CAM of crowns. *Journal of Prosthetic Dentistry*, 74: 223-229.
- Persson, A., Andersson, M., Oden, A. and Sandborgh-Englund, G., 2006. A three-dimensional evaluation of a laser scanner and a touch-probe scanner. *Journal of Prosthetic Dentistry*, 95 (3): 194-200.
- Peters, M., DeLong, R., Pintado, M., Pallesen, U., Qvist, V. and Douglas, W., 1999. Comparison of two measurement techniques for clinical wear. *Journal of Dentistry*, 27 (7): 479-485.
- Pilgrim, L., 1996. Surface matching and difference detection without the aid of control points. *Survey Review*, 33 (259): 291-304.
- Pintado, M., DeLong, R., Ko, C.-C., Sakaguchi, R. and Douglas, W., 2000. Correlation of non-carious cervical lesion size and occlusal wear in a single adult over a 14 year time span. *Journal of Prosthetic Dentistry*, 84 (4): 436 - 443.
- Price, R., Gerrow, J., Sutow, E. and MacSween, R., 1991. The dimensional accuracy of 12 impression material and die stone combinations. *International Journal of Prosthodontics*, 4 (2): 169-174.

- Roulet, J., 1985. In vivo wear measurement of composite resins. In: Vanherle G, DC., S. (Eds.), Posterior composite resin dental restorative materials, Peter Szulc Publishing Co, Netherlands, pp. 365-372.
- Ungar, P. and Williamson, M., 2000. Exploring the effects of toothwear on functional morphology: a preliminary study using dental topographic analysis. *Palaeontologia Electronica*, 3 (1): 18 pages.
- Van der Zel, J., Vlaar, S., de Ruiter, W. and Davidson, C., 2001 The CICERO system for CAD/CAM fabrication of full-ceramic crowns. *Journal of Prosthetic Dentistry*, 85 (3): 261-267.

Chapter 9

Change detection of non-carious cervical lesions from stereoimagery

9.1 Introduction

The non-carious cervical lesion (NCCL) is a generic term used to describe loss of hard tissue at the cemento-enamel junction (CEJ) in the cervical one-third of teeth (Figure 9.1). The major part of a tooth surface is covered with enamel, a very hard, relatively impervious mineralised tissue that, under 'normal' conditions, is resistant to wear, acid erosion and abrasion and changes very slowly. Where enamel is not present in the cervical part of the tooth, exposed dentine, a less heavily mineralised tissue, is more susceptible to an increase rate of surface loss by way of wear (attrition), acid erosion and abrasion. A fourth type of surface loss, the stress-induced cervical lesion (also known as abfraction), has also been described, in which stress originating at the occlusal surface results in micro-cracking, and subsequent loss of tooth material in the cervical region (Grippio, 1991). In a review of the biomechanics of abfraction, in addition to direct erosion and abrasion, Rees (2000) reported that one theory suggests that tooth loss is initiated in the cervical enamel as a result of micro-cracking associated with concentration of stresses originating at the occlusal surface. Another theory is that erosion preferentially removes cervical dentine, undermining the enamel, leaving it unsupported and more prone to failure. There may be more than one type of lesion, each possibly associated with a different aetiology, and factors associated with the initiation of lesions may be different from factors associated with their progression.



Figure 9.1. Intra-oral image of upper teeth with non-carious cervical lesions adjacent to the gum margin (arrows).

Lesions have a wide variety of size, shape, symmetry and location and are commonly encountered in clinical practice, with prevalence ranging from 5 to 85 % (Levitch et al., 1994). The height and depth of lesions is typically in the order of millimetres (Aw et al, 2002). Lesions may occupy anywhere from a few percent to over 30 percent of the area of a tooth surface. Quantitative studies of the progression of lesions are few in number and results vary widely, ranging from 10 $\mu\text{m}/\text{y}$ to 300 $\mu\text{m}/\text{y}$ (Bartlett et al., 1997; Pintado et al., 2000; Xhonga et al., 1972). The progression of NCCLs has been monitored using profile tracings of silicone replicas of teeth (Xhonga et al., 1972), profile tracings of lead foil (Xhonga and Sognnaes, 1973) and a contact stylus measurement system (Pintado et al., 2000). A lack of clear diagnostic criteria makes comparison of prevalence data difficult and may account for the wide range of data reported. The examination of stress patterns is complicated by their likely changing distribution as the occlusal contact areas on a tooth change as it wears over time.

9.1.1 Surface alignment and change detection

Change detection involves identifying common areas of a surface recorded at different times and measuring differences between those areas, most commonly as either volume or depth change. Common areas of a surface may be identified by using reference markers or, in their absence, by the super-imposition or alignment of part or all of the entire tooth surfaces. Reference free matching of surfaces recorded at different times has been reported (Chadwick and Mitchell, 2001; DeLong and Douglas, 1990; Mehl et al., 1997). There are two approaches to aligning surfaces in order to identify and measure areas of change:

The entire surface, including the area that is thought to have changed, may be aligned and a threshold value nominated for data, representing the area that has changed, to be excluded from the alignment (Chadwick and Mitchell, 2001). The difference data resulting from the alignment which exceeds the exclusion threshold represents the change between the two surfaces. In this case, data representing areas that have changed but are below the exclusion threshold will introduce some error into the alignment.

The area of the surface thought to have changed may be interactively excluded from the alignment process, then reintroduced before calculating the differences between the two surfaces (Pintado et al., 2000). In this case, the presence of change on the surfaces has no effect on alignment precision.

This chapter takes the tooth impression and replication method in Chapter 5, the digital cameras and lens system described in Chapters 6 and 7, and the tooth surface alignment findings from Chapter 8, and examines two specific examples of change detection of NCCLs. The two lesions, from two patients, are of significantly differing appearance and occupy a significantly different proportion of the surface area of their respective tooth surfaces.

9.2 Method

9.2.1 Replica preparation

Several patients attending a private dental practice were recruited for a long term study monitoring the progression of non carious cervical lesions. Patients were provided with an information sheet and provided their consent to participate in the study (see Chapter 4). Patients were selected for the presence of NCCLs that were judged at the time of selection not to warrant restoration, primarily because of perceived stability over an extended period. Tooth surface 1 was an upper right canine of a 62-year-old female with a heavily restored full dentition, some generalized gingival recession, and angular NCCLs affecting facial surfaces of the majority of her teeth. Over many years of regular dental attendance, no change was perceptible in these lesions. Tooth surface 2 was an upper right second premolar of a 45-year-male with a heavily restored dentition, moderate gingival recession and shallow, elongated NCCLs affecting up to a third of the facial surfaces of the majority of his posterior teeth.

Following polishing with polishing paste and a rubber cup, vinyl polysiloxane impressions (Reprosil; Dentsply International Inc., Milford, Delaware, USA) were taken in custom-made impression trays. Models were poured with an experimental material consisting of epoxy casting resin (Daystar Australia P/L, Dandenong, Victoria, Australia) modified with the addition of TiO₂ powder and coloured particles of various sizes up to 250 µm in diameter, and back filled with diestone. The tooth replicas had the same surface geometry as is usual for replicas poured from elastomeric impression materials, however the optical appearance of the replicas was speckled, which formed an essential part of automatic surface model generation referred to below (Figure 9.2). Impressions were taken of the tooth surfaces at baseline, one year and two year epochs.

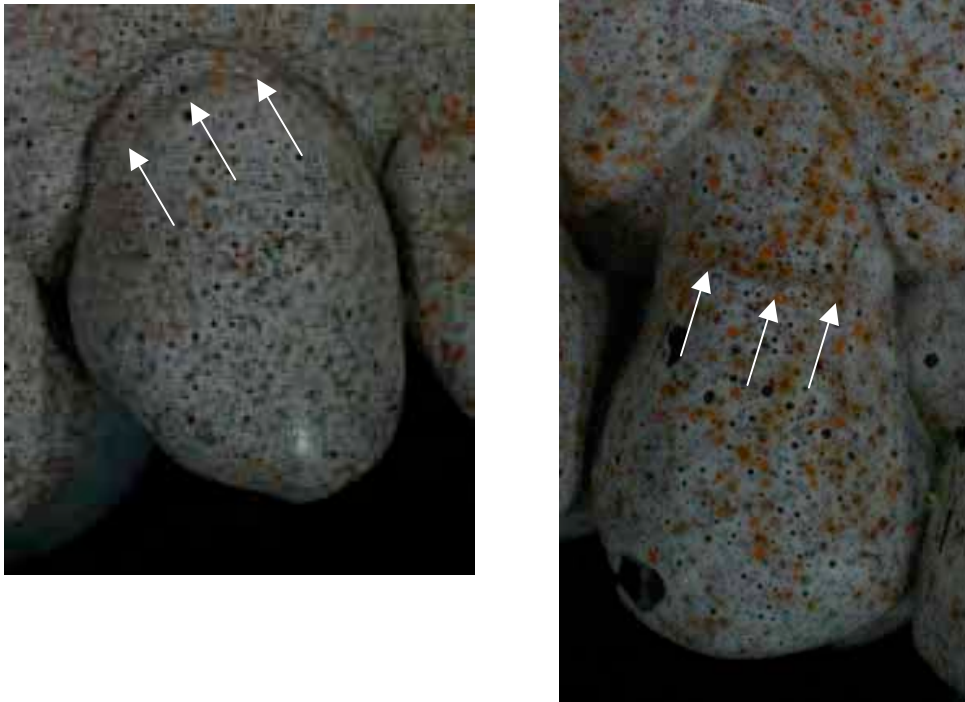


Figure 9.2. Tooth replicas with non-carious cervical lesions above CEJ (arrows). Left: surface 1, lesion accounts for approximately 6.5% of total surface; Right: surface 2, lesion accounts for approximately 27.0% of total surface.

9.2.2 Data acquisition

Stereoimages of the tooth surface replicas under study were taken with a fixed stereometric camera consisting of two 22.7 mm format digital cameras (Canon EOS 300D; Canon Inc., Tokyo, Japan) fitted with 80 mm enlarger lenses (Componon; Schneider-Kreuznach, Germany), fixed machined tubes and T-2 adapters, achieving a photoscale of 1:1. The camera and lens assemblies were mounted facing a front-silvered 90° mirror achieving a convergence angle of approximately 15° (Figure 9.3). Illumination was provided by four high-intensity LED units. A remote switch was used to expose both cameras simultaneously. The stereo camera was pre-calibrated with a composite artifact using multi-station convergent imaging and simultaneous bundle adjustment software (3DM Calib Cam v2.2a; Adams Technology P/L, Perth, Australia). A full description of the calibration

method is given in Chapter 7. Each pair of stereoimages was combined with the pre-calibration data and, utilising photogrammetry software (3DM Analyst v 2.2a; Adams Technology P/L, Perth, Australia), processed to automatically generate surface models.



Figure 9.3. Fixed base stereo camera, lens and mirror assembly with LED illumination. (also refer to Figure 7.2, pp. 124)

9.2.3 Accuracy and precision of the 3D data acquisition

A test object was fabricated from the experimental epoxy resin material, consisting of three circular planes of 4, 8 and 12 mm diameter with rises of 2 mm between each plane. Thirty-nine readily identifiable near circular targets were measured with a coordinate measurement machine (CMM) (Starlite 250/300; Optical Gauging Products Inc. Rochester, NY, USA) to a reported precision of 2.6 μm (X, Y, planimetric) over the measuring length, and 7 μm (Z, vertical) over the measuring height (section 7.2). The test object was imaged from 10 different positions and surface models generated with the photogrammetry software. Absolute accuracy was evaluated from automatic DTM data (0.1 mm x 0.1 mm grid) from the top and low tiers, which was used to compute a plane of best fit and height distance normal to the top and low plane of the tiered object. Height distances were compared

with the CMM data and height distances computed by the same method. Precision was evaluated from automatic DTM data from the top tier, cropped to 1 mm x 1 mm, and used to compute the standard deviation of the Z coordinate from the plane determined by the least-squares plane fit algorithm.

9.2.4 Precision of 3D data acquisition and alignment

One of the tooth replicas was imaged from 10 different positions and surface models generated with the photogrammetry software. Surface DTMs from these ten stereomodels were compared sequentially (1 compared with 2, 2 with 3, etc) using commercial point cloud analysis software (Polyworks v.9.1.7, Innovmetric Software Inc, Canada) to test relative accuracy and precision of the measurement system. Point cloud data was imported on a 0.1 mm x 0.1 mm grid interval, maximum edge length of 0.75 mm and a threshold for the exclusion of outliers that was approximately three times the precision of the measurement system.

9.2.5 Change detection of NCCLs

The two tooth surface models with NCCLs were analysed with point cloud analysis software and reverse engineering software (Polyworks v 9.1.7, Innovmetric Software Inc, Canada). Surfaces from the different epochs were aligned utilizing the full surface area and then with the area of the lesion excluded from the alignment. Lesion data, including a 0.5 mm border of enamel at the DEJ, was excluded from data sets interactively with *Polyworks*. The area of the lesions was calculated as a percentage of the full surface area. Difference (change) data were displayed with the z scale of the difference data altered to remove measurement noise from the display (i.e. differences less than a minimum magnitude were not displayed).

9.3 Results

9.3.1 Accuracy and precision of the 3D data acquisition

The test object was stereoimaged ten times from different positions, and models formed and DTMs generated. The mean precision of measurements, from a 1 x 1 mm section fitted to a plane, was 13.0 μm . This represented the precision of automatic DTM generation. The mean (s.d.) normal height from the top plane to the low plane of the object was 4.0045 (0.0034) mm (Table 9.1). This compares with the CMM height of 3.997 (0.006) mm. The mean height fell just outside one standard deviation of the mean CMM height. The standard deviation from the mean of 0.0034 mm indicates the precision of the automatic generation of stereomodels.

Dataset no.	Precision (μm)	Height (mm)
1	12.0	4.0080
2	13.0	4.0070
3	11.8	4.0005
4	13.4	4.0074
5	15.4	4.0058
6	13.1	4.0050
7	12.2	4.0063
8	14.6	3.9976
9	12.7	4.0021
10	11.8	4.0058
Mean	13.0	4.0045
s.d.		0.0034

Table 9.1. Accuracy and precision of 3D data acquisition: object space precision (μm) and DTM height (mm), mean, s.d.

9.3.2 Precision of 3D data acquisition and alignment

Tooth surface 1 replica was stereoimaged 10 times from different positions, and models formed and DTMs generated. The ten DTMs were aligned sequentially with an exclusion threshold of 40 μm (approximately 3 x

precision). The standard deviations of the differences from the alignments appear in Table 9.2 and their mean was 16.3 μm . This represents the overall precision of the combined measurement and alignment system.

Dataset nos.	s.d. of differences (μm)
2-1	15.5
3-2	15.5
4-3	15.9
5-4	16.8
6-5	16.7
7-6	15.5
8-7	17.4
9-8	16.7
10-9	16.4
Mean s.d.	16.3
s.d.	0.7

Table 9.2. Precision of alignment and 3D data acquisition: sequential alignment, mean and s.d. (μm).

9.3.3 Precision of replication, 3D data acquisition and alignment

The standard deviations of the difference data from the alignment of the tooth surface obtained at different time periods were typically around 18.5 μm . This represents the overall precision of the combined replication, measurement and alignment process. Errors associated with the impressions, replication and the quality of the optical texture could be expected to contribute an increased error over that of remeasuring the same replica. There may also be change in the tooth surface not related to the NCCLs.

9.3.4 Change detection of NCCLs

9.3.4.1 Tooth 1

The lesion on the upper right canine accounted for approximately 6.5% of the total area of the facial aspect of the tooth. The difference data, with the lesion excluded from the alignment, for the first one-year interval (2004 - 2005) are displayed in Figure 9.4.

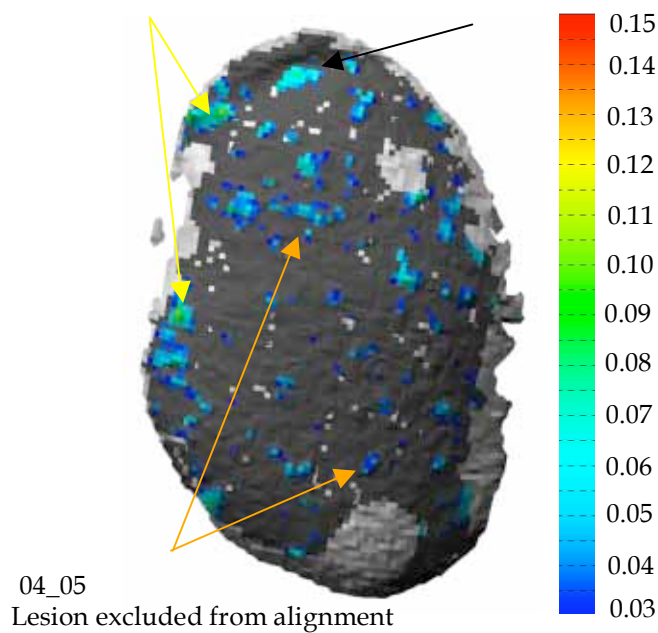


Figure 9.4. Tooth 1, change detection, first one-year interval; lesion excluded from alignment. Black arrow: area of surface loss; orange arrows: measurement noise; yellow arrows: measurement noise at margin of surface. X, Y pixels units: 0.1 x 0.1 mm, Z scale units: mm.

Each 'pixel' represents a 0.1 x 0.1 mm interval in X and Y axes. Areas of probable measurement 'noise' in the central area of the tooth surface are indicated with the orange arrows. These areas typically contain values in the range 0.03 to 0.05 mm and could be interpreted as the outer limits of measurement error. Areas of possible excessive measurement noise at the left side of the tooth surface are indicated with yellow arrows. These are typically in the range of 0.03 to 0.12 mm. The upper of the two areas indicated is within the body of the lesion and could be an area of genuine

change in the tooth surface; it could also be in an area of increased measurement noise associated with increasing relief at the left margin of the tooth. This is almost certainly the case with the lower of the two areas indicated by the yellow arrows. The area in the centre of the lesion indicated by the black arrow, which has a different distribution to either of the areas already discussed, is more likely to be change within the lesion. The depth variation in this area is around 0.04 to 0.09 mm. To investigate the validity of this conclusion, the surface model from a second yearly interval (2005 – 2006) was examined.

The difference data, with the lesion area excluded from the alignment, for a two-year interval (2004 - 2006) are displayed in Figure 9.5. Figure 9.5-left shows difference data generated with the lesion area excluded from the alignment and Figure 9.5-right shows difference data generated utilizing the full surface. The area of change, noted in the lesion in the 04-05 data, appears to have deepened with a maximum depth of 0.15 mm (black arrow), and enlarged with a further region of loss of 0.05 to 0.10 mm in depth (orange arrow). Areas at the left-hand side of the surfaces, noted in Figure 9.4 (yellow arrows), are smaller in size in Figure 9.5, supporting the interpretation that this is indeed measurement noise. The area adjacent to the area of change within the lesion, indicated by the upper blue arrow, may be change associated with the lesion. It may also be another phenomenon affecting the tooth surface generally, or it may be impression and replication defects. A repeat impression and replica from the same epoch or a further time interval would help clarify this issue. There is a small difference between the two alignment approaches in this case, visible in the region of the change.

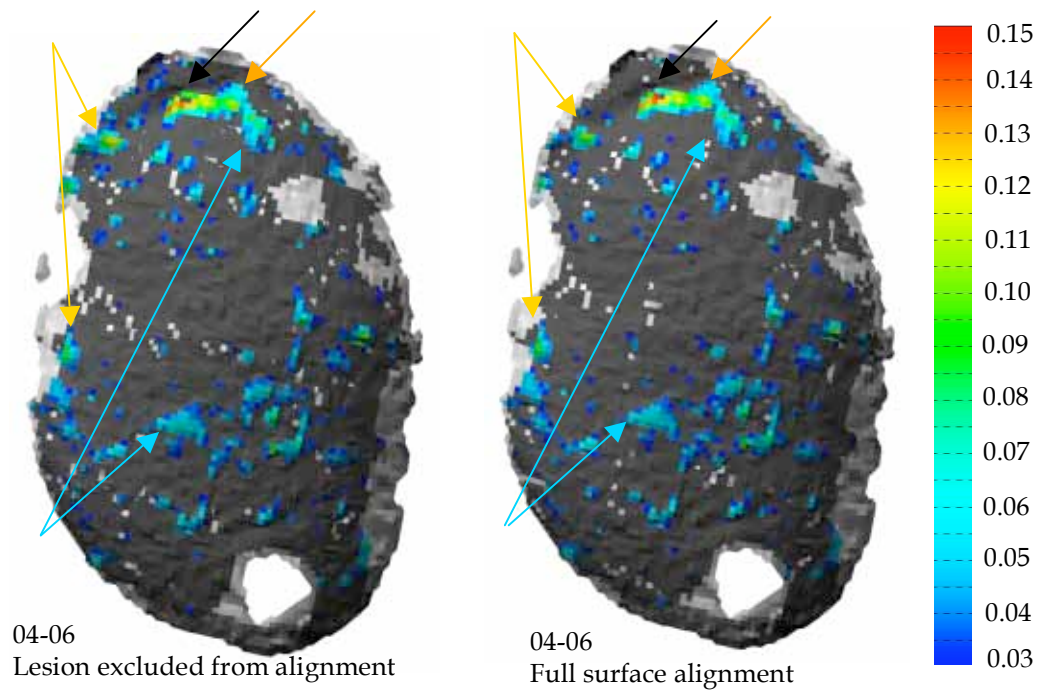


Figure 9.5. Tooth 1, change detection, two-year interval; lesion excluded from alignment (left), full area included in alignment (right). Black and orange arrows: areas of surface loss; blue arrows: possible area of surface loss; yellow arrows: measurement noise at left margin of surface. X, Y pixels units: 0.1 x 0.1 mm, Z scale units: mm.

In summary, in the first yearly interval (Figure 9.4) tooth 1 showed a small area of dentine loss immediately above the DEJ, measuring approximately 0.6 x 0.3 mm in area and 0.06 mm in depth. In the two-year interval (Figure 9.5) the change had extended to 1.4 x 0.4 mm in area and a maximum depth typically around 0.12 mm, with some loss in enamel of around 0.05 mm. This could be interpreted to suggest that loss of dentine immediately adjacent to the CEJ preceded the loss of enamel.

9.3.4.2 Tooth 2

The lesion on the upper right second premolar accounted for approximately 27% of total area of the facial area of the tooth. Difference data for the one-year interval (04-05) appear in Figure 9.6-left, middle, right. This change detection data shows surface loss of up to 0.320 mm. When viewed in relief, Figure 9.6-right, the area of maximum loss between 0.175 and 0.320 has occurred below the CEJ (orange arrow). The change detection data (Figure 9.6, left and middle) have been unaffected by the inclusion or exclusion of the change area. This may be due to the greater quantum of change when compared to the 2005 - 2006 data (Figure 9.7) leading to a greater delineation between the change area and the rest of the surface, or due to the absence of change at the majority of the circumference of the lesion (black arrow).

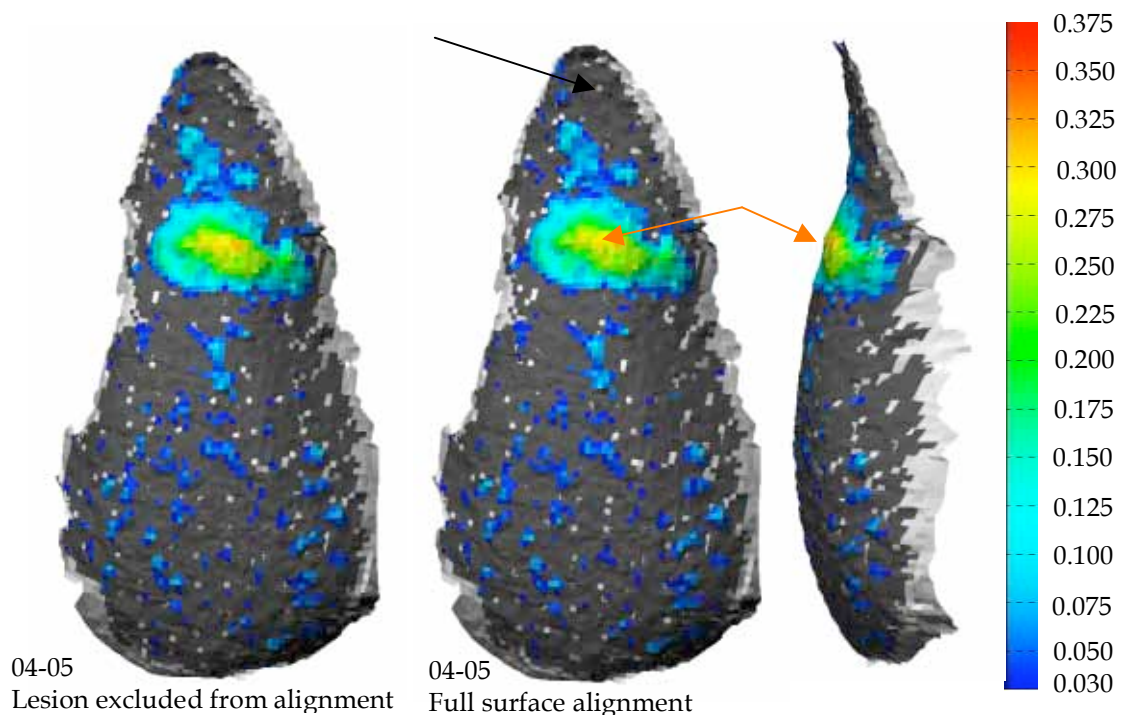


Figure 9.6. Tooth 2, change detection, one-year interval; lesion excluded from alignment (left), full area included in alignment (middle), surface rotated 90 degrees (right). Orange arrows: CEJ; black arrow: no change at gingival margin. X, Y pixels units: 0.1 x 0.1 mm, Z scale units: mm.

The difference data for the 2nd yearly time period (2005 – 2006), with the lesion excluded from the alignment, are displayed in Figure 9.7-left and middle. The entire lesion area has been affected by generalised substance loss from 0.03 to 0.10 mm (white arrow) and there is an area just above the CEJ (black arrow) with loss from 0.10 to 0.15 mm (yellow arrow). There is another area close to the occlusal surface which may be surface loss or impression and replication defects (orange arrow). A repeat impression and replica from the same epoch or a further time interval would help clarify this issue.

Figure 9.7-right shows the same surfaces aligned using the full surfaces. There is significant difference between the Figure 9.6-left and -right difference data. At the occlusal edge, in the region of the orange arrow, there is minimal difference between the two Figures. However most of the change in the 0.03 to 0.10 mm range, indicated by the white arrow, has not been detected and the quantum of change at the CEJ, in the range 0.10 to 0.15 mm, indicated by the yellow arrow, has been diminished. In this case, there is a significant difference in the ability of the two alignment methods to detect change, with the alignment utilizing the full surface being unreliable.

Difference data for the two-year interval (2004-2006) appear in Figure 9.8-left and right. This Figure is a summation of the change displayed in the previous two Figures, with some loss above and below the CEJ. The greater differentiation of the different rates of change in different areas is lost in the two year interval data.

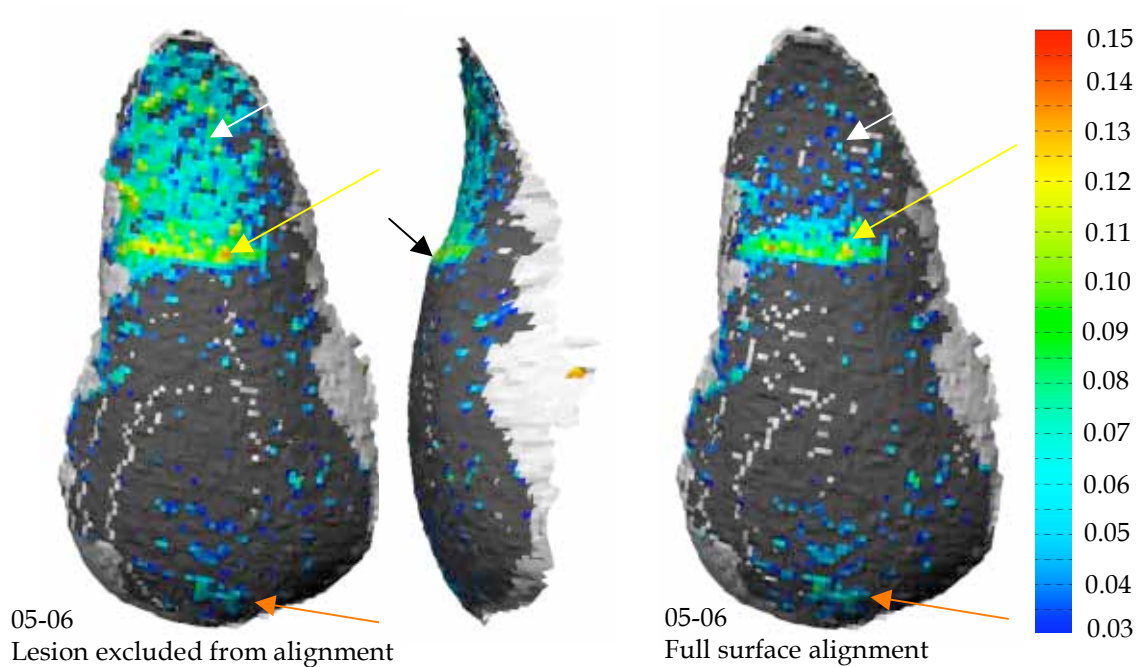


Figure 9.7. Tooth 2, change detection, one-year interval; lesion excluded from alignment (left); surface rotated 90 degrees (middle); full area included in alignment (right). Black arrow: CEJ; yellow arrows: area of maximum surface loss; white arrows: different difference data using different alignment methods; orange arrows: area of possible surface loss towards occlusal surface. X, Y pixels units: 0.1 x 0.1 mm, Z scale units: mm.

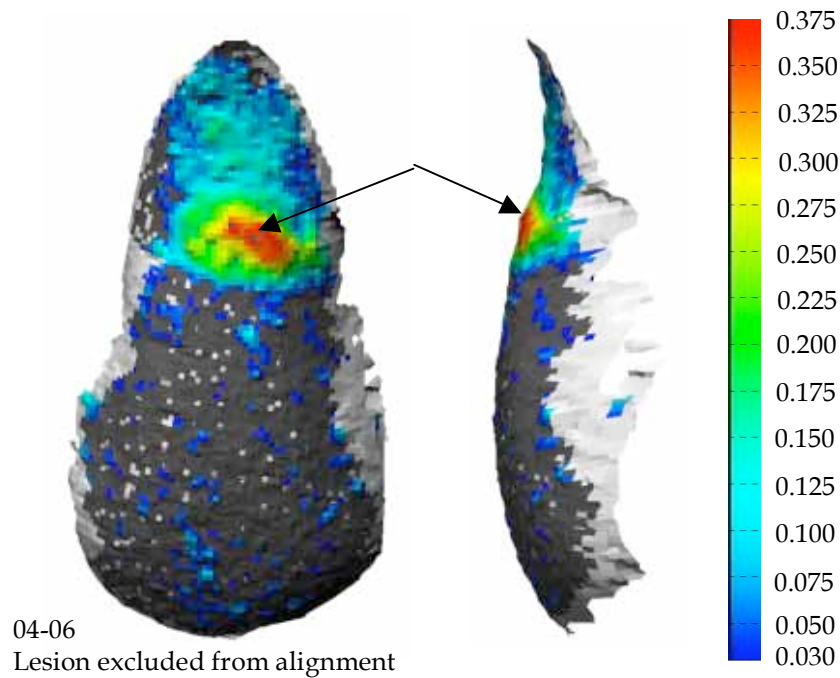


Figure 9.8. Tooth 2, change detection, two-year interval; lesion excluded from alignment (left); surface rotated 90 degrees (right). Black arrows: CEJ. X, Y pixels units: 0.1 x 0.1 mm, Z scale units: mm.

In summary, in the first yearly interval (Figure 9.6), tooth 2 showed an area of enamel loss at the DEJ approximately 1 mm sq. and 0.3 mm in depth. This area of loss appeared to extend to the full extent of enamel coverage in this particular area and suggests that the enamel in this area suffered catastrophic failure and was lost on bulk. Surrounding this area was a border of substance loss in both enamel and dentine in the order of 1 mm wide and 0.1 mm in depth. In the second yearly interval (Figure 9.6), there was generalised surface loss in the order of 0.05 mm over the entire lesion area, with a small band of increased loss at the DEJ. It is difficult to evaluate from the change detection images whether this band of surface loss has occurred in enamel or dentine. When reviewing the two yearly intervals combined (Figure 9.8), the picture obtained from the separate yearly intervals is less clear.

9.4 Discussion

9.4.1 Precision of replication, 3D data acquisition and alignment

The accuracy and precision data for the measurement system were consistent with earlier work reported in this thesis. Following the investigation in the previous chapter, an exclusion threshold of 0.04 mm was chosen for all alignments. However this exclusion threshold did not also serve as a change detection threshold. Change detection above 0.03 mm was found to be reliable with areas of measurement noise easily differentiated from areas of actual change. The precision of the 3D data acquisition did not quite match that of other high accuracy methods, however, the overall alignment precision of the entire replication, 3D data acquisition and alignment method was similar to that reported for contact stylus systems (Chadwick et al., 1997; Peters et al., 1999). The change detection data appeared stable and reliable and, in the two cases examined, were sufficient to draw meaningful conclusions about the spatial distribution and quantum of tooth hard tissue loss.

9.4.2 Change detection of NCCLs

Change detection studies for both occlusal and cervical tooth surface loss are rare. Such studies are not easy to conduct and the selection of cases that could be anticipated to show change is problematic. It could be regarded as unethical to monitor a patient while the condition 'deteriorated'. Aw et al. (2002) concluded that NCCL progression might be a slow process in many patients and that early restorative intervention might not be necessary, with monitoring and re-evaluation appropriate for small lesions. In the two cases reported here, both patients have been subject to long term visual monitoring for many years by the author without suspicion of significant change. For tooth 1, other teeth in the same quadrant have lesions much larger than the one reported here, and analysis of these tooth surfaces have not shown measurable change (i.e. less than 0.03 mm) over the period of this study. For tooth 2, other teeth in the same quadrant have shown measurable change,

but in an inconsistent manner, suggesting that replication error can be a significant confounding factor. These and other patients are currently being monitored as a part of a long term study and these results will be reported elsewhere.

Careful inspection of impressions under magnification would enable better identification of impression errors prior to replication. Occasionally, air bubbles were present in the replication material, however the majority was small and enhance the optical texture of the material.

Tooth 1 showed annual maximum depth loss of dentine of 60 μm for the two yearly periods, some loss of enamel and a doubling of the surface area of the loss. In the first yearly interval, tooth 2 appeared to show bulk loss of enamel, approximately 1 x 1 mm square, to a maximum depth of 0.3 mm at the CEJ with a surrounding border of loss of both enamel and dentine of 0.1 mm. It is surprising that both enamel and dentine should be lost at the same rate in this area. In the second yearly interval, the entire area affected by the lesion suffered generalised loss of 0.05 mm.

In a review of the biomechanics of abfraction, Rees (2000) reported one theory that suggests tooth loss is initiated in the cervical enamel as a result of micro-cracking associated with concentration of stresses originating at the occlusal surface. Another theory is that erosion preferentially removes cervical dentine, undermining the enamel, leaving it unsupported and more prone to failure. An additional factor may be the structural and physical properties of the enamel and the enamel-dentine junction in the cervical region, with reports that subsurface cervical enamel is inferior to coronal enamel with a lower mineral and higher protein content, and that the enamel-dentine junction is poorly developed with little scalloping. In the two cases examined here, tooth 1 showed loss of surface material in dentine only with the possibility that the enamel could be demineralised and undermined; tooth 2 showed bulk loss of enamel at the CEJ suggesting that mechanical failure of the enamel perhaps subsequent to micro-cracking had

occurred. However, surface data of the type reported here are not the most appropriate method of determining the type of tissue (enamel or dentine) from which surface loss has occurred. This is better performed via ultrastructural examination of tooth surface replicas, often poured in epoxy resin and examined with scanning electron microscopy (Khan et al, 1999).

Khan et al. (1999) concluded that the effects of acid demineralisation at the cervical margin may be amplified secondarily by cervical strains, and that toothbrush abrasion may exacerbate the formation of lesions; the site specificity of salivary protection offered the best explanation for the location of both shallow and deeper wedge shaped lesions. Saliva dilutes, buffers, neutralises and flushes acid from tooth surfaces and the presence of calcium and phosphate ions enable remineralisation tooth surface at normal saliva pH. Conclusions about the site specificity of saliva in the mouth have been based upon 'film velocity' work by Dawes and Macpherson (1993), salivary pellicle thickness by Amaechi et al (1999).

The apparently discreet nature of tooth substance loss in the case of tooth 1 suggests that there are very localised site specific factors influencing the loss, such as the local difference in the physico-chemical properties of the enamel and dentine and their junction, stress concentration or the piezoelectric effect. Factors of a more generalized nature such as acid erosion or toothbrush abrasion might be expected to have a more general effect over an entire tooth surface, as is more typical of tooth 2. The widely differing rates of change demonstrated in the two cases suggest different mechanisms are at play at the same time and that the concept of lesion initiation may not be a once-only effect, but a cyclic event which enhances the impact of variables affecting progression.

Much has been written and reported about the characterization of lesions and the contributions of strains, acid dissolution and toothbrush abrasion, however there have been no annual change detection studies. The results of this preliminary investigation suggest that annual change detection studies

will provide a clearer picture of the pattern of tooth surface loss and, in combination with other analytical techniques, a more detailed explanation of the natural history of these lesions.

Current methods for the research of NCCLs include the:

- i) qualitative characterization of shape and distribution of lesions within the dentition,
- ii) ultra structural characterization of tooth surfaces using scanning electron microscopy to identify the presence of demineralization and hard tissue defects such as enamel cracking and collagen degradation in dentine,
- iii) FEA modeling to study patterns of stress distribution within teeth,
- iv) cyclic occlusal loading of teeth in association with acid exposure,
- v) identifying the presence of lesions in association with other occlusal factors on the same tooth such as wear facets, occlusal attrition and erosion,
- vi) identifying the presence of extrinsic and intrinsic acid exposure and saliva quality, quantity and distribution, and
- vii) identifying the presence of patient behavioural factors such as diet, other occupational exposures and toothbrushing habits.

All the above methods contain spatial information as a core characteristic and an important element in the representation of data. Change detection from stereoimagery of replicas offers an important adjunct to existing methods of research and diagnosis. The provision of optical texture onto the surface of teeth intra-orally would increase the ease and speed of this approach, but will also introduce new challenges to understand what it is that is being measured, and what effect such a direct approach may have on the subject of study. It is by no means certain that a direct intra-oral approach to surface modelling and change detection will provide an easier, more practical solution.

9.5 Conclusion

The replication, stereoimagery and photogrammetric processing of tooth surfaces have been reliable and convenient, however errors in impression techniques can be problematic with a potential for inconsistency in the quality of change detection data. The change detection data appeared stable and reliable and, in the two cases examined, were of sufficient accuracy and resolution to draw meaningful conclusions about the spatial distribution and quantum of tooth hard tissue loss. Change detection of NCCLs in the cervical region of two teeth has been performed with a sensitivity of 0.03 mm, with change ranging from 0.03 to 0.32 mm per annum on one surface and 0.03 to 0.07 mm per annum for the second surface. Different rates of change were clearly evident in different areas of the surfaces. The results of this preliminary investigation suggest that annual change detection studies will provide a clearer picture of the pattern of tooth surface loss and, in combination with other analytical techniques, a more detailed explanation of the natural history of these lesions.

9.6 References

- Amaechi, B., Higham, S., Edgar, W. and Milosevic, A., 1999. Thickness of acquired salivary pellicle as a determinant of the sites of dental erosion. *Journal of Dental Research*, 78 (12): 1821-1828.
- Aw, T., Lepe, X., Johnson, G. and Mancl, L., 2002. Characteristics of noncarious cervical lesions. *Journal of the American Dental Association*, 133: 725-733.
- Bartlett, D., Blunt, L., Smith, B., 1997. Measurement of tooth wear in patients with palatal erosion. *British Dental Journal*, 182 (5): 179-184.
- Chadwick, R. and Mitchell, H., 2001. Conduct of an algorithm in quantifying simulated palatal surface tooth erosion. *Journal of Oral Rehabilitation*, 28: 450-456.

- Chadwick, R., Mitchell, H., Cameron, I., Hunter, B. and Tulley, M., 1997. Development of a novel system for assessing tooth and restoration wear. *Journal of Dentistry*, 25 (1): 41-47.
- DeLong, R. and Douglas, W., 1990. Quantitative assessment of anatomical change in the human dentition, 12th Annual International Conference of the IEEE in Medicine and Biology Society, pp. 2054-2055.
- Grippio, J., 1991. Abfractions: a new classification of hard tissue lesions of teeth. *Journal of Esthetic Dentistry*, 3 (1): 14-19.
- Khan, F., Young, W., Shahabi, S. and Daley, T., 1999. Dental cervical lesions associated with occlusal erosion and attrition. *Australian Dental Journal*, 44 (3): 176-186.
- Levitch, L., Bader, J., Shugars, D. and Heymann, H., 1994. Non-carious cervical lesions. *Journal of Dentistry*, 22 (4): 195-207.
- Mehl, A., Gloger, W., Kunzelmann, K.-H. and Hickel, R., 1997. A new optical 3D device for the detection of wear. *Journal of Dental Research*, 76 (11): 1799-1807.
- Peters, M., DeLong, R., Pintado, M., Pallesen, U., Qvist, V. and Douglas, W., 1999. Comparison of two measurement techniques for clinical wear. *Journal of Dentistry*, 27 (7): 479-485.
- Pintado, M., DeLong, R., Ko, C.-C., Sakaguchi, R. and Douglas, W., 2000. Correlation of noncarious cervical lesion size and occlusal wear in a single adult over a 14 year time span. *Journal of Prosthetic Dentistry*, 84 (4): 436 - 443.
- Rees, J., 2000. A review of the biomechanics of abfraction. *European Journal of Prosthodontics and Restorative Dentistry*, 8 (4): 139-144.
- Xhonga, F. and Sognnaes, R., 1973. Dental erosion: progress of erosion measured clinically after various fluoride applications. *Journal of the American Dental Association*, 87 (6): 1223-1973.
- Xhonga, F., Wolcott, R. and Sognnaes, R., 1972. Dental Erosion II. Clinical measurements of dental erosion progress. *Journal of the American Dental Association*, 84 (3): 577-582.

Chapter 10

Conclusion

The aim of the research applied in this thesis was to develop and implement a method for photogrammetric mapping of non-carious cervical lesions (NCCLs) that was sufficiently accurate and efficient to enhance the study of their rate and distribution of change. This aim has been met.

10.1 This thesis commenced with an examination of 3D coordinate data obtained using epoxy resin tooth replicas modified to incorporate optical texture, and stereoimagery from a single, commercially available, film-based semi-metric camera and macro lens on extension bellows. Model precision was within acceptable limits of 12 μm or better for manual image matching, however systematic errors resulted in unacceptably large model errors with the likely causes being the use of a semi-metric camera with unstable interior orientation and the reliability of the photogrammetric solutions formed by the photogrammetric workstation software.

10.2 A commercially available, moderately priced, digital SLR camera and customized, fixed camera lens was used to generate 3D coordinate data using a modified epoxy resin replica. Model precision was shown to be approximately 10 μm for convergences from 4 to 25 degrees. It was found that automatic image point measurement precision improved with decreasing convergence. A stereopair from the single camera did not prove sufficiently reliable at forming models of a tooth sized test object with model height error below a desired 10 μm .

10.3 A fixed base stereo camera and a composite calibration artifact were assembled. Manual image point measurement was used in combination with bundle adjustment calibration software to provide straightforward calibration and model generation. Variations in illumination and image clarity across the entire measurement volume restricted the use of automatic control point measurement. However manual point measurement proved satisfactory with precision in object space for individual point measurement shown to be approximately 13 μm , and accuracy of surfaces derived from automatic measurement of surface texture shown to be approximately 3 μm .

10.4 Surface alignment of one tooth surface was tested using two software packages. Both packages successfully aligned the tooth surface tested with an overall mapping and alignment error of 17.2 and 15.6 μm respectively, for an exclusion threshold of 0.04 mm. Alignment solutions appeared to be very stable with the choice of grid interval and exclusion threshold having little or no effect on alignment. For alignment error (alone) the software packages resulted in errors of 7.6 and 6.4 μm respectively. The measurement system produced point cloud data suitable for sampling on a 0.1 x 0.1 mm grid interval. Data sampling parameters used to fill in areas of missing data had an important effect on overall alignment precision. The choice of grid interval for a given application should be determined according to spatial frequency of measurements desired in the grid axes.

10.5 Two specific examples of change detection of NCCLs over a two-year period were examined. The two lesions, from two patients, were of significantly differing appearance and occupied a significantly different proportion of the surface area of their respective tooth surfaces. The replication, stereoimagery and photogrammetric processing of the tooth surfaces proved reliable and convenient, however errors in impression techniques were shown to be problematic with a potential for inconsistency in the quality of change detection data. Within this constraint, the change detection data appeared stable and reliable, and in the two cases examined were of sufficient accuracy and resolution to draw meaningful conclusions about the spatial distribution and quantum of tooth hard tissue loss. Change detection of NCCLs in the cervical region of the two teeth was performed, with a sensitivity of 0.03 mm, and with change ranging from 0.03 to 0.32 mm per annum on one surface and 0.03 to 0.07 mm per annum on the second surface. Different rates of change were clearly evident in different areas of the surfaces.

The results of this investigation suggest that annual change detection studies will provide a clearer picture of the rate of progression and the geometry of progression and, in combination with other analytical techniques, a more detailed explanation of the natural history of these lesions.